ANALYSIS OF BIOLOGICAL MOLECULES ON SURFACES USING STIMULATED DESORPTION PHOTOIONIZATION MASS SPECTROMETRY

A Dissertation
Presented to
The Academic Faculty

by

Yanfeng Chen

In Partial Fulfillment
of the Requirements for the Degree
Doctor of Philosophy in the
School of Chemistry and Biochemistry

Georgia Institute of Technology
May, 2006

ANALYSIS OF BIOLOGICAL MOLECULES ON SURFACES USING STIMULATED DESORPTION PHOTOIONIZATION MASS SPECTROMETRY

Approved by:

Dr. Thomas M. Orlando, Advisor
School of Chemistry and Biochemistry
Georgia Institute of Technology

Dr. Sheldon W. May
School of Chemistry and Biochemistry
Georgia Institute of Technology

Dr. Mostafa A. El-Sayed
School of Chemistry and Biochemistry
Georgia Institute of Technology

Dr. Facundo M. Fernandez
School of Chemistry and Biochemistry
Georgia Institute of Technology

Dr. Alfred Merrill, Jr.
School of Biology
Georgia Institute of Technology

Date Approved: March 31, 2006

To my family

for their unconditional love and support

ACKNOWLEDGEMENTS

First of all, I would like to thank my advisor, Dr. Thomas M. Orlando, for giving me the opportunity to join his research group and explore exciting fields of science. Without his encouragement, support, and guidance throughout my studies and research, I would never have achieved this goal. I want express my appreciation to Dr. Sheldon W. May, for his consideration, inspiration and support. I would also like to thank Dr. Facundo M. Fernandez, Dr. Mostafa A. El-Sayed, and Dr. Alfred Merrill, Jr. for serving on my committee. Their advice and encouragement have been greatly appreciated.

I would like to thank Dr. Cameron M. Sullards and David Bostwick for their valuable support and insightful comments in the field of mass spectrometry. My special thanks also go to Dr. Tiffany T. Hoang, Dr. Charlie Oldham, Dr. Shijun Zheng, Dr. Noriyuki Suzuki, Mike Foster, Di Wu and Veronica DeSilva for the suggestion and assistance on the analysis and synthesis of selenium compounds. I am grateful for the collaboration provided by Dr. Nicholas V. Hud and Catherine Santai in DNA damage studies. I also appreciate the assistances of Dr. Leslie Gelbaum for the NMR characterization and the SEM imaging help from Dr. Jian Dong.

I would like to thank Norman Scott and Sam Mize in the machine shop of college of science as well as Richard Bedell and Jack Hunt in the electronic shop of school of chemistry and biochemistry for their assistance on the development of the experimental setup.

I would like to thank my group members, past and present, Dr. Haiyan Chen, Dr. Alexandr Aleksandrov, Dr. Gregory Grieves, Dr. Janine Captain, Matthew Gilliland, Christopher Lane, Kristin Shepperd, Doogie Oh, Babajide Olanrewaru, Dr. Taishan Fan, Kenneth Kite, and Lan Sun, who have offered all kinds of help in every aspect during these years.

I owe gratitude to Dr. Richard F. Brower and his past group members, Dr. Tiffany T. Hoang, Dr. Christine Nolan, Dr. Victor DeJesus, and Dr. Catrina Higgins. Their courtesy, consideration and encouragement are precious and unforgettable.

Finally, I would like to thank my family from the bottom of my heart. My parents and sister made so many sacrifices for me and it is their unconditional support and encouragement that make me here now. Most of all, I must thank my wife Min Li, for her love and patience in this and every endeavor. She makes everything worthwhile!

TABLE OF CONTENTS

CHAPTER

LIST OF TABLES

LIST OF FIGURES

LIST OF SYMBOLS AND ABBREVIATIONS

A	Adenine
AAA	Amino acid analysis
Ac	Acetyl
amu	Atomic mass unit
API	Atmosphere photon ionization
Arg	Arginine
a. u.	Arbitrary units
B	Base
C	Cytosine
°C	Celsius
CCD	Charge-coupled detector
CE	Capillary electrophoresis
Da	Dalton
DEA	Dissociative electron attachment
DNA	Deoxyribonucleic acid
DSB	Double strand break
E_{des}	Desorption energy
EEL	Electron energy lose
EI	Electron impact ionization
ESD	Electron stimulated desorption
ESI	Electrospray ionization

Et	Ethyl
EtOH	Ethanol
eV	Electron volts
FTIR	Fourier transfer infrared spectroscopy
g	Grams
G	Guanine
GC	Gas chromatography
Gln	Glutamine
Gly	Glycine
h	Hour
HFBA	Heptafluorobutyric acid
His	Histidine
HPLC	High performance liquid chromatography
Hz	Hertz
ICP	Inductively coupled plasma
IP	Ionization potential
IR	Infrared
K	Kelvin
KJ	Kilojoules
kV	Kilovolts
LD	Laser desorption
LDI	Laser desorption/ionization
LEE	Low-energy electron

mA	Milliampere
MALDI	Matrix-assisted laser desorption/ionization
MeOH	Methanol
Met	Methionine
meV	Milli-electron volt
min	Minutes
ML	Monolayer
mm	Millimeter
Mo	Molybdenum
mol	Mole
m.p.	Melting point
MPI	Multi-photon ionization
MRM	Multiple reaction monitoring
MS	Mass spectrometry
N-Ac-SeGal	1β-methylseleno-N-acetyl-D-galactosamine
nm	Nanometer
NMR	Nuclear magnetic resonance
pA	Picoampere
ppb	Part-per-billion
PI	Photoionization
PS	Porous silicon
QMS	Quadrupole mass spectrometry
REMPI	Resonance enhanced multi-photon ionization

s	Second
SALDI	Surface-assisted laser desorption/ionization
SD	Stimulated desorption
Se	Selenium
SeEt	Selenoethionine
SeMet	Selenomethionine
SeGal	1β-methylseleno- D-galactosamine
SEM	Scanning electron microscopy
Si	Silicon
SIMS	Secondary ion mass spectrometry
SPI	Single photon ionization
SSB	Single strand break
R	Radicals
RC	Resistor-capacitor
T	Thymine
TMSe	Trimethylselenonium
THG	Third harmonic generation
TOF	Time-of-Flight
TPD	Temperature programmed desorption
Trp	Tryptophan
UD	Undamaged
UHV	Ultra-high vacuum
UV	Ultraviolet

V	Volts
vacuo	Vacuum
VUV	Vacuum ultraviolet
Xe	Xenon
μg	Microgram
μm	Micron
μs	Microsecond

SUMMARY

Mass spectrometry plays a pivotal role in the rapid advances of analytical and biological sciences. Improvements in sample preparation, instrumentation, desorption, and ionization methods are highly beneficial to the developments of mass spectrometric techniques for high-throughput analysis of biological molecules in complex systems.

Surface-assisted laser desorption/ionization mass spectrometry (SALDI MS) is a novel technique for direct analysis of organic and biological molecules. In this matrix-free method, specific surfaces are selected to trap analytes and to assist/enhance the laser desorption/ionization process. Amino acids, dipeptides, and organoselenium compounds were successfully detected by SALDI on carbon and silicon surfaces. Surface effects, solvent effects, temperature effects and pH effects were studied. A possible mechanism of SALDI is proposed based on observed results.

In general, stimulated desorption results in neutral yields that are much larger than ion yields. Thus, we have exploited and further developed laser desorption single photon ionization mass spectrometry (LD/SPI MS) as a means of examining biomolecules. LD/SPI MS uses one laser to desorb intact neutral molecules from the sample surface and another vacuum ultraviolet (VUV) laser to ionize the desorbed neutral molecules. The experimental results clearly demonstrate that LD/SPI MS is a very useful and fast analysis method with uniform selectivity and high sensitivity.

Selenium (Se) is an essential ultra-trace element in the human body. Se metabolites, especially organoselenium compounds, have been linked to toxicity, antioxidant enzymes, endocrine processes, and proper functioning of the immune system.

In efforts to obtain more useful information of Se-containing metabolites in human urine, exact mass determination of unknown organoselenium compounds in biological matrices using SALDI MS was investigated. In another approach, several selenium metabolites in human urine were successfully detected by LD/SPI MS. A HPLC-MS/MS method was also developed for a quantitative case study of selenium metabolites in human urine after ingestion of selenomethionine.

Low-energy electrons (LEE, 3-20 eV) have been shown to induce single and double strand breaks (SSB and DSB) in plasmid DNA. LEE-induced DNA strand breaks were related to the formation and decay of transient negative ion (TNI) states localized on various components of DNA (i.e. bases, phosphates, deoxyribose, hydration water, etc). To understand the genotoxic effects due to secondary species of high-energy radiation, we investigate the role of TNIs and the specificity in LEE-DNA damage by examining the neutral product yields using low electron stimulated dissociation SPI MS. The neutral yields as a function of incident electron energy are then correlated with the SSBs and DSBs measured using post-irradiation gel electrophoresis. The results provide further insight concerning the mechanisms of LEE-induced damage to DNA.

Overall, this research provided an in-depth understanding of non-thermal surface processes and the development of new mass spectrometric techniques for the analysis of biomolecules. It demonstrated that SD/PI MS is a uniquely advantageous tool for direct analysis of small molecules in complex biochemical systems and electron induced damage on large biological molecules. Furthermore, LD/SPI MS shows great potential for future work in the analysis of metabolites, drug discovery, and biomarker imaging.

CHAPTER 1

INTRODUCTION

Rapid growth of biological, environmental, clinical, pharmaceutical and material sciences have led to dramatically increased demands for chemical and structural information regarding organic/biological molecules from complex systems. Many analytical tools have been developed and utilized to characterize and analyze biomolecules.[1-6] Mass spectrometry (MS) is one of the most successful and popular techniques for the analysis of a broad range of analytes of interest. It uses different ionization methods to convert analytes into ions and separate them according to their mass-to-charge ratio (*m/z*) by various mass analyzers. Combined with separation techniques such as gas chromatography (GC), high performance liquid chromatography (HPLC) and capillary electrophoresis (CE), mass spectrometry is a very powerful tool to detect many compounds from relatively complicated systems. By employing proper ionization methods, mass spectrometry enables qualitative and quantitative analysis of many molecules with high sensitivity. By coupling high resolution mass analyzer with specific ionization sources, mass spectrometry provides accurate molecular mass and fragmentation data which allows the determination of elemental composition and chemical structure of analytes. Therefore, mass spectrometry is playing an increasing pivotal role in biological related research and applications. The further improvements of mass spectrometry in sample preparation, instrumentation, desorption, and ionization methods will be highly beneficial to high-throughput analysis of biological molecules in complex systems.

Stimulated desorption photoionization mass spectrometry (SD/PI MS) has been widely used in bimolecular analysis in recent years. This technique desorbs analyte molecules by photons or electrons and ionizes them by direct or indirect energy transfer. According to the different desorbing and ionizing sources, stimulated desorption photoionization mass spectrometry could be divided into three main categories: i) laser desorption/ionization mass spectrometry (LDI MS) in which both desorption and ionization are promoted by one laser; ii) laser desorption photoionization mass spectrometry (LD/PI MS) in which a laser desorbs the analytes and another laser ionizes the desorbed molecules by single photon ionization (SPI) or multiphoton ionization (MPI); iii) electron stimulated desorption photoionization mass spectrometry (ESD/PI MS) in which an electron beam is used to desorb molecules from the target surface and a laser beam is used to ionize the desorbed species.

The introduction of matrix-assisted laser desorption/ionization mass spectrometry (MALDI-MS) in the 1980s [7, 8] has dramatically improved the ability of stimulated desorption photon ionization mass spectrometry. In MALDI MS, samples are usually prepared by mixing with an excess amount (~10^4 fold) of matrix molecules that absorb laser energies. The use of matrix molecules is critical for success of the laser desorption/ionization. It serves to isolate analyte molecules from each other, to absorb the intense laser radiation, to vaporize and propel the analyte molecules into the gas phase, and subsequently to ionize the neutral analytes in the plume of the excited-state matrix immediately above the sample target.[9] By using a time-of-flight mass spectrometer with a nearly unlimited mass range, MALDI MS has successfully detected large biomolecules and synthetic polymers up to 1.5 million Daltons (Da).[10] In addition, MALDI MS also provides soft ionization (i.e. the parent ions dominate the mass spectrum with little or no fragmentation), high detection sensitivity and fast sample analysis. MALDI MS has become one of the cornerstones of the revolution in bioanalysis.[8, 11-13]

Although MALDI MS has been remarkably successful in making many advances in various fields, some the limitation still hinders its full development and application. A complete understanding of the MALDI phenomenon mechanism does not yet exist,[14] which greatly affects the optimization of MALDI. The effectiveness of the matrix material is also not always intuitively apparent. Thus, the matrix selection is often obtained after an exhaustive empirical search.[15] Poor shot-to-shot and sample-to sample reproducibility resulting from the crystalline matrix is another issue that must be dealt with for the improvement of MALDI performance. Finally and most importantly, MALDI produces a large amount of matrix background ions below *m/z* 600, which makes it impossible to analyze small molecules.

Increasing demands for high throughput methods in drug discovery, and biotechnology as well as analysis of complex mixtures in high salt matrices and buffers, has created great interest in utilizing the full power of LDI over the entire mass range of interest.[16]

In the studies presented in this dissertation, a versatile ultrahigh vacuum (UHV) analytical system was designed and constructed for the analysis of small organic/biological molecules using different forms of stimulated desorption photoionization mass spectrometry (details are described in chapter 2). The approach pursued in this thesis work is to carry out detailed studies which concentrate on the surface chemistry and physics governing non-thermal desorption. The combination of this approach with sensitive laser detection schemes developed by the atomic and molecular physics communities has provided the paths for advancing bioanalytical techniques. Specifically, surface-assisted desorption/ionization (SALDI MS), laser desorption single photon ionization mass spectrometry (LD/SPI MS) and electron stimulated desorption single photon ionization mass spectrometry (ESD/SPI MS) methods were developed to characterize small thermally labile molecules in different sample environments. The high sensitivities of SALDI MS, LD/SPI MS, as well as ESD/SPI MS and the generalities of their applications suggests that these techniques may be used as widespread tools for the detection of small analytes in complicated biological samples.

SALDI-MS has been newly developed as a supplemental technique for MALDI MS. It utilizes specific target substrates with porous structures and high photon absorptivity to retain samples and generate soft ionization. Because this method does not add matrix molecules, it produces a clean mass spectrum in the low-mass range for easy characterization of small molecules. In chapter 3, SALDI MS on three different surfaces were studied to provide useful guides to its applications. The effectiveness of SALDI MS in analysis of the amino acids, small peptides, and organoselenium metabolites were also investigated to explore its potential of analyzing various molecules in complex systems. The amino acids, dipeptides and organoselenium are typical small molecules with great significance in many aspects and the fast and sensitive analysis of these molecules has been very challenging. In addition, the analysis of these molecules usually involves great amounts of sample which require a high-throughput method. Therefore, traditional techniques such as HPLC-MS and GC-MS which suffer from time consuming operation and methods development that often can not provide satisfactory analysis. The good performance of SALDI MS on analyzing amino acids, dipeptides and organoselenium metabolites illustrate a potential approach for simple, fast and sensitive analysis of small molecules.

Although SALDI MS has been successfully applied in many applications, its mechanism is not clear. To fully understand the mechanisms of SALDI MS, the effects of surface morphology, sample solvent, surface storage, surface temperature, sample acidity have been investigated and discussed in chapter 4. A proposed mechanism is given and this could lead the optimization of SALDI MS.

Based on the fact that natural desorption yields are typically 1000~10,000 fold greater than the ion yields and two-step laser desorption photoionization technique could provide better control in both the desorption and ionization processes, the LD/SPI MS method was developed for sensitive analysis of metabolites in human urine. This approach uses an ultraviolet (UV) laser to desorb intact neutral molecules and a vacuum ultraviolet VUV laser to ionize the desorbed neutral molecules by single photon ionization. The details of LD/SPI MS are discussed in chapter 5. This technique provides more efficient detection than secondary ion mass spectrometry (SIMS), direct non-resonant laser ionization (LDI), MALDI and SALDI. An HPLC-MS/MS method was also created for the analysis of organoselenium metabolites and it provided results similar to those obtained using LD/SPI MS. This study demonstrates the viability of matrix free LD/SPI MS for molecular characterization and quantitive analysis of biological metabolites in the *m/z* 10 ~ 600 range that are present in complex biological fluids.

By taking advantage of high efficiency, high sensitivity and uniform selectivity of single photon ionization, deoxyribonucleic acid (DNA) damage induced by low-energy electrons was investigated by ESD/SPI MS. This is discussed in detail in chapter 6. DNA damage caused by irradiation is of great importance to the application of radiobiology, public health, and clinical treatments. To understand the genotoxic effects and cell damage due to secondary species of high-energy radiation, the role of transient negative ions (TNI) and the specificity in LEE-DNA damage were studied by examining the neutral product yields using ESD/SPI MS. The neutral yields as a function of incident electron energy were also correlated with the SSBs and DSBs measured using post-irradiation gel electrophoresis. The results indicate that resonances involving the oxygen of the phosphate-sugar linkages and the surrounding water molecules may contribute to the DNA damage. Careful measurements of the role of intrinsic water and any sequence dependences of the strand break probability are still underway.

CHAPTER 2

EXPERIMENTAL SETUP AND SYNTHESIS

2.1 EXPERIMENTAL SETUP

2.1.1 Overview

A versatile ultrahigh vacuum (UHV) analytical system was designed and built for the studies of laser stimulated desorption, electron stimulated desorption, photon ionization, low-energy electron induced DNA damage, temperature programmed desorption and post-irradiation DNA analysis. Figure 2-1 schematically shows the configuration of the experimental system. It essentially consists of a sample loading system, a sample dosing system, a sample transfer system, a main analytical chamber equipped with a sample positioning mount, a temperature control system, a focusing low-energy electron gun, a vacuum ultraviolet (VUV) conversion cell, a time-of-flight (TOF) mass spectrometer and a quadrupole mass spectrometer (QMS). The whole analytical chamber is pumped to 10^{-9}~10^{-10} torr by two turbo molecular pumps. Two ND:YAG laser systems, an electronic pulse control system and a post-irradiation gel electrophoresis system were also used outside the UHV chamber to maximize the functions of the whole analytical system.

2.1.2 Sample Loading System

The sample loading system was attached to the main analytical chamber for spray dosing and fast sample loading. The sample loading chamber was equipped with a view

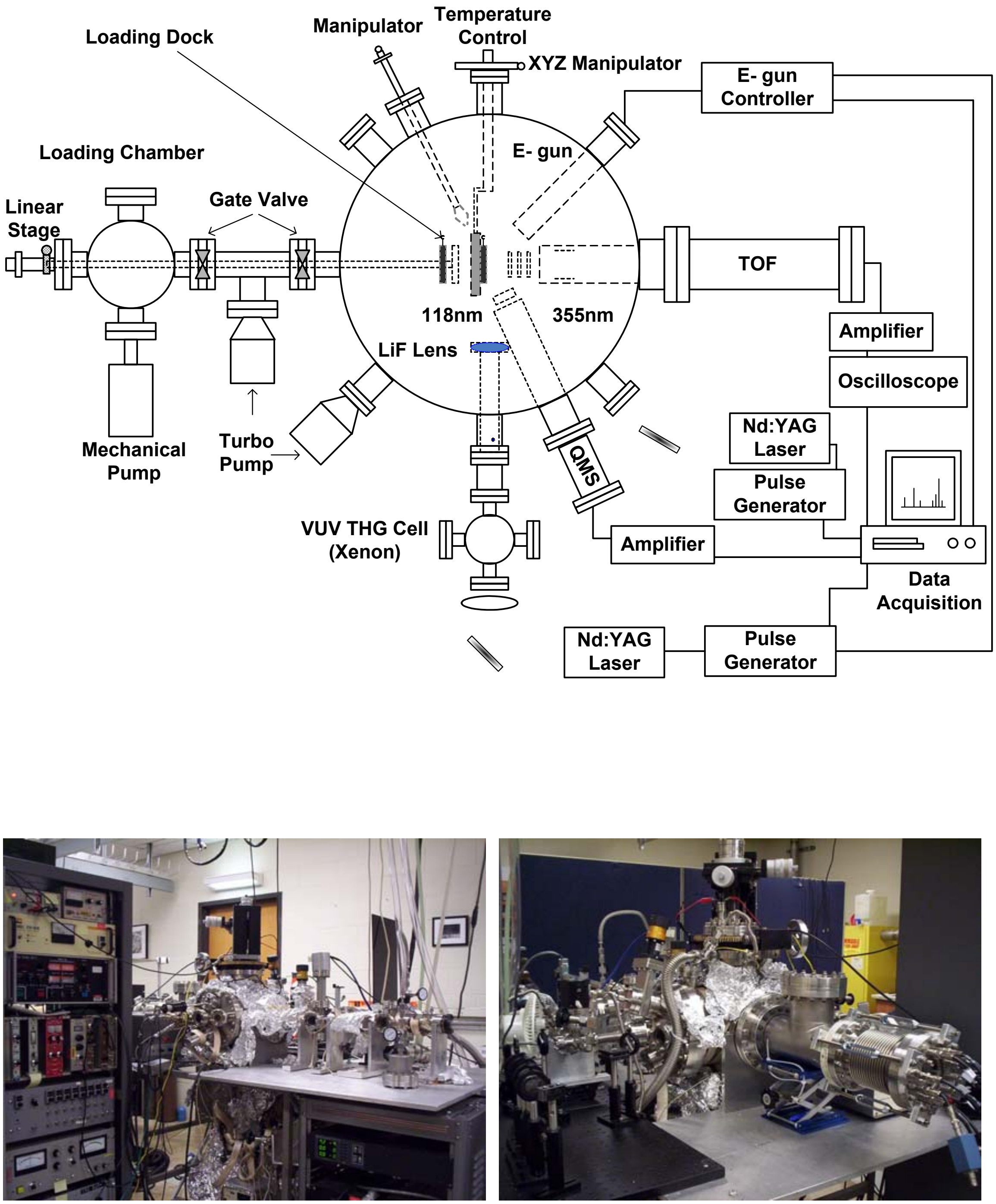

Figure 2-1. Schematic of UHV electron/laser stimulated desorption photon ionization chamber.

window, a dosing port, two gate valves, an angle valve (all from MDC, Inc., Hayward, CA, USA), a turbo molecular pump and a rotary vane pump (all from Pfeiffer Vacuum, Asslar, Germany). To load a sample, the gate valve between the dosing chamber and main analytical chamber was first closed. The other gate valve was then closed to separate the turbo molecular pump from the loading chamber. Finally, the angle valve was shut off to isolate the dosing chamber from the rotary vane pump. At that time, the dosing port could be opened for sample transfer. When samples or sample plates were in place, the dosing port was sealed and the angle valve was opened to the rotary vane pump to quickly reduce the pressure to 10^{-3} torr. At this pressure level, the gate valve to the turbo molecular pump was slowly opened by carefully monitoring the pressure change near the turbo molecular pump. After the pressure of the dosing chamber reached 10^{-8} torr, the dosing chamber was opened to the main analytical chamber and the sample plate was transferred to sample holder using a rotary-linear magnetic transporter.

2.1.3 Sample Dosing System

The sample dosing system had two major components: a sample dosing chamber and two sample dosing lines. The sample dosing chamber was used to spray liquid samples and facilitate the loading of clean substrates or air dried samples. Two sample dosing lines were connected to the main analytical chamber for gas phase dosing.

For sample spray dosing, the clean sample plate was transferred back to the dosing chamber from the main analytical chamber where annealing is performed. The samples were sprayed onto sample plates by a micro syringe or sprayer through the dosing port. During this process, the two gate valves were both closed to protect the turbo molecular pumps and prevent contamination.

Two dosing lines were connected to the main analytical chamber by different leak valves. The leak valves were mounted with ~ 0.25 inch diameter stainless steel tubes pointing to the sample. The distance between the steel tube tips and sample could be adjusted by moving the sample. This design effectively guided the molecules to the sample plate and decreased the background dosing to the chamber. To prevent cross contamination, one dosing line is kept for water vapor dosing only. The other one is used for other gas molecules (such as O_2, N_2, etc.). To dose water vapor onto the sample, nanopure water was contained in a glass tube and purified by several freeze-pump-thaw cycles to remove dissolved gas. The dosing line was passivated with water vapor by several cycles of saturating and evacuating before dosing. The relative exposure was controlled by vapor pressure and dosing time.

2.1.4 Sample Positioning Mount

The position of the sample in the main analytical chamber was precisely controlled by a XYZ translational manipulator (Mitutoyo, Plymouth, MI, USA) and a 360 degree rotation stage (Thermionics Inc., Port Townsend, WA, USA). The position resolution could be controlled as low as 50 μm and the finest angle resolution is about 0.5 degree. By moving the sample to different positions, various experiments such as surface-assisted laser desorption/ionization (SALDI), laser desorption single photon ionization (LD/SPI), electron stimulated desorption single photon ionization (ESD/SPI), temperature programmed desorption (TPD), sample dosing and sample loading could be performed. The highest dosing and detection efficiencies are obtained by carefully controlled sample manipulation.

2.1.5 Sample Transfer System

The sample transfer system is composed of two major parts: a customized 36-inch rotary-linear magnetic transporter (MDC, Inc., Hayward, CA, USA) and a customized 12-inch sample manipulator (MDC, Inc., Hayward, CA, USA).

The rotary-linear magnetic transporter was installed on the sample loading chamber. Two special designed U shape loading docks were mounted at the end of the rotary-linear magnetic transporter. Sample plates were special made with grooves by which they could be locked on the loading docks. The magnetic transporter was controlled outside the chamber to move across the whole system for sample delivery.

After sample plates were transferred into the main analytical chamber, an UHV multi-motion wobble stick modified with specifically designed tips was used to move the sample plates. The tips can pick up the sample plate from the loading dock and locate it onto the sample holder in the main chamber.

To take the sample out of the main chamber, the whole process was operated in reverse according to the sample transferring steps describes above.

2.1.6 Temperature Control System

The temperature control system utilized a cooling unit and a heating unit to precisely adjust the sample temperature. The sample holder is mounted to electrically isolated copper blocks of the cooling unit, which thermally contacted a liquid nitrogen reservoir. Two Molybdenum (Mo) clamps (~ 0.5 mm thick) were also bolted on the holder to fix the sample. A button heater thermally isolated from the cooling unit was placed at the back of the sample holder to heat the sample. The temperature increase was achieved by applying voltage increments to the button heater. Type K thermocouples are spot-welded on to the clamps and sample holder to monitor the temperature of sample. A LabVIEW computer program was developed to facilitate the temperature control. The sample could be cooled down to 85.0 K and heated up to 900.0 K by this system.

2.1.7 Electron Gun

A focusing low-energy electron gun (ELG-2; Kimball Physics, Wilton, OH, USA) was attached to the main analytical chamber for electron stimulated desorption (ESD) or electron bombardment experiments. The electron gun was capable of producing electrons in the range of 5 eV to 1000 eV. The full-width at half maximum (FWHM) of the electron energy distribution was less than 0.5 eV using a unipotential refractory cathode. The sizes of the focused beams were ~ 1 mm and were obtained by using the multistaging and electron zoom lensse to form a constant focal plane position at different electron energies. A high speed pulse grid allowed fast beam pulsing with an external pulse generator.

The electron gun was at a 45 degree angle relative to the sample surface and was positioned as close as possible alongside the TOF extractor. Irradiation of the sample (grounded or with an externally applied potential) was typically performed by pulse mode operated from 5 eV to 500 eV with 500 ns ~ 100 μs pulse widths.[17, 18] Variation of the electron flux was performed exclusively by changing the gun emission current. The electron flux was determined as 10^{12}~10^{14} electrons s^{-1} cm^{-2} by a picoammeter (Keithley Instruments Inc, Cleveland, OH, USA). The pulsed electron beam was focused on the target and controlled by x-y deflectors to scan the whole substrate surface. When electrons interacted with the substrate, the image of substrate could be obtained by monitoring the voltage or current on the substrate. The images provided the coordinates and settings for optimized electron focusing onto the sample surface. A LabVIEW programmed was used to control all the parameters for electron gun operation.

2.1.8 VUV Conversion System

The major part of the VUV conversion system was a 1.33 inch six-way cross cube equipped with a leak valve (MDC, Inc., Hayward, CA, USA), a pressure meter (Baratron 120; MKS, Wilmington, MA, USA), a needle valve (Swagelock, Solon OH, USA) connected to a rotary vane pump (Pfeiffer Vacuum, Asslar, Germany), a two-lens optic assembly (Almaz Optics, Marlton, NJ) and laser optics (CVI, Albuquerque, NM, USA) for incident laser (355 nm) alignment. The six-way cube was mounted on a XYZ stage (THORLABS, Inc., Newton, NJ, USA) and attached to the main analytical chamber with an adapter extended inside the main chamber toward the sample.

The VUV photons were produced by non-resonant third harmonic generation (THG). The power of VUV photons (118 nm) generated at the third harmonic frequency of incident 355 nm photons is determined by [19, 20]

$$P_{3\omega} = N^2 |\chi^{(3)}(3\omega)|^2 P_{\omega}^3 F(L, b, \Delta k) \qquad \text{(Equation 2-1)}$$

where P is the laser power density, N is the number density of the nonlinear medium, χ is the nonlinear susceptibility, ω is input angular frequency, F is phase matching function,

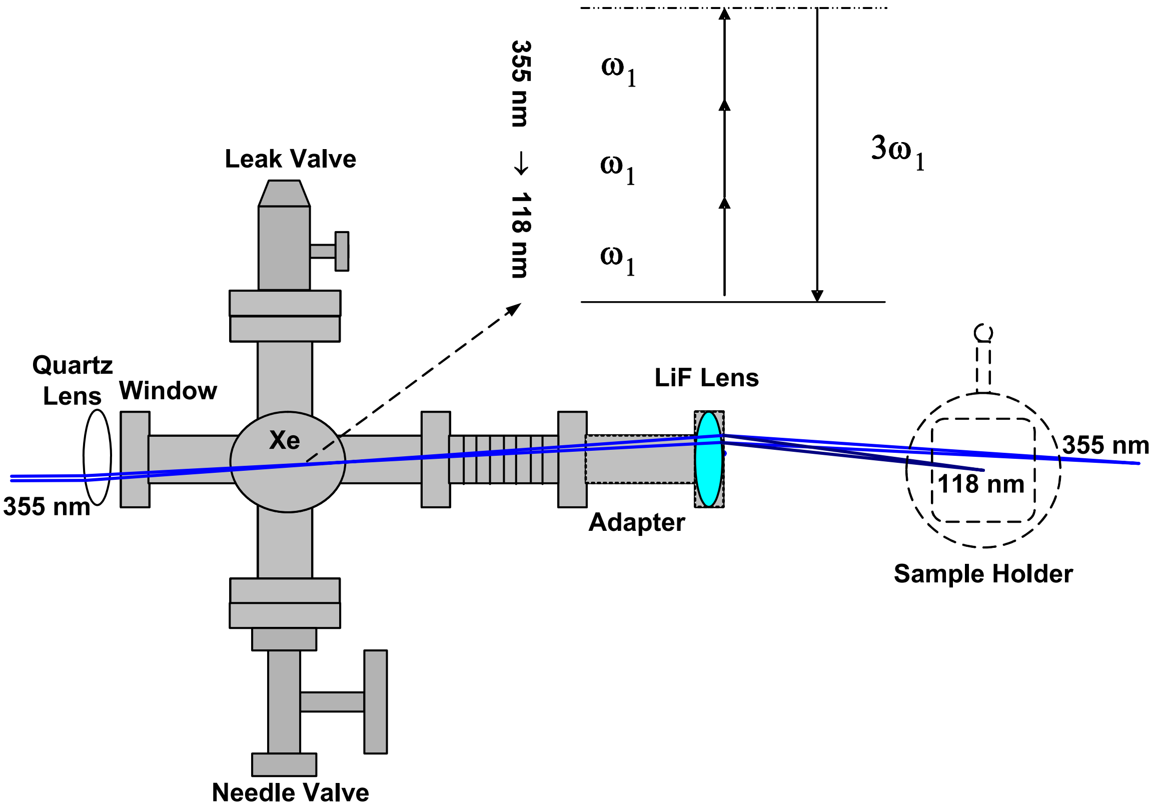

Figure 2-2. Schematic of third harmonic generation (THG) vacuum ultraviolet (VUV) conversion system and laser alignment to the sample. Approximately 0.1 μJ of 118 nm photons were generated by 25 mJ of 355 nm laser radiation.

L is the length of nonlinear medium, b is confocal beam parameter, and Δk is the wave-vector mismatch.

In all the studies of this thesis, xenon was selected as tripling medium because its simplicity and high conversation efficiency ($10^{-9} \sim 10^{-5}$) leading to intense coherent VUV outputs.[21,22] During the experiments, high purity xenon (>99.999%) was filled into the VUV conversion system and its pressure greatly influences the VUV conversion efficiency by affecting N, χ and F. The pressure of xenon was adjusted by using leak valve (filling) and needle valve (evacuating) together. To effectively generate VUV photons, 355 nm laser beam was focused in the xenon cell by a quartz lens (f = 200 mm) in front of the fused silica window. The 118 nm photons were separated from the 118 nm/355 nm beam by taking advantage of the chromatic aberration of a LiF (f = 75 mm) lens, which is installed on the adaptor inside the main chamber. This lens also functioned as the entry window to the main chamber and the spatially separated beams were focused in front of the sample surface (Figure 2-4). The distance between the sample surface and 118 nm beam was controlled in the range of 1~2 mm. The maximum VUV conversion was obtained by observing the highest ionization signals from neutral molecules. The highest VUV pulse energy was approximately 0.1 μJ with ~25 mJ of 355 nm radiation and ~ 7 torr of xenon.

2.1.9 Time-of-Flight (TOF) Mass Spectrometer

A linear TOF mass spectrometer was designed and constructed for ion detection (Figure 2-3). A specifically designed translation stage was placed at the end of the TOF. It enabled the movement of TOF in the main analytical chamber to obtain maximum ion signals, especially for stimulated desorption photon ionization experiments in which the electron gun was fixed and laser alignments were relatively difficult. The ion optics of the TOF consisted of a top-hat designed extractor and a series of focusing plates. The top-hat shape of the extractor allowed the e-gun to stay as close as possible to the sample. The focusing lenses could perform different space and time-lag focusing to improve the ion detection. Deflectors were also installed in the flight tube to maximize the collection efficiency. Various voltages were applied to the extractor, focusing lenses and deflectors to optimize the signal intensities. The ions were detected by drifting through the field free flight tube and reaching a pair of chevron configuration microchannel plates (MCPs) (Del Mar Ventures, San Diego, CA, USA) which magnified the signals by factors of 10^6 ~10^7. The output signal generated by the anode behind the MCPs was amplified, digitized, signal averaged and stored in computer. The TOF mass spectra were calibrated by alkali ions and standard molecules such as amino acids.

Another feature of this home-build TOF was its ability of obtaining mass spectrometric imaging of analyte ions by using a MCP/phosphor screen (MCP-IFP46/2; Del Mar Ventures, San Diego, CA, USA) as an imaging detector. The TOF was mounted on a special six-inch flange with a view port. A supporting plate was designed to hold the MCP/phosphor screen detector right above the window. A high-speed cooling CCD camera (Sensicam QE; Cook Corp., Auburn Hills, MI, USA) was focused on the P46 phosphor screen which emitted fluorescence (490 ~ 620 nm) with a fast 90%-to-10% decay (300 ns). By using proper pulse sequence and image collection parameters, the images of different ions could be recorded by the CCD camera. At the same time, the voltage change on the second MCP plate which reflected the flight time and intensity of detected ions could also be obtained by utilizing an oscilloscope through a RC circuit (Figure 2-3). Therefore, both of the whole mass spectrum and images of individual ions were able to be observed by this imaging TOF mass spectrometer (Figure 2-4).

2.1.10 Quadrupole Mass Spectrometer (QMS)

A quadrupole mass spectrometer (QMS) ((Extrel C50; ABB Analytical Instruments, Inc., Pittsburg, PA, USA) equipped with High-Q head was used to detect desorbed neutral molecules in TPD and ESD/SPI experiments.

In TPD experiments, the sample plate was turned toward the QMS by the sample positioning system. A LabVIEW program was designed to control the temperature increase and selected ion detection. The desorbed molecules were first ionized by 70 eV electrons in the electron ionization (EI) source of the QMS. The ions were then focused by ion optics behind the EI source and passed through four QMS rods upon which the High-Q head delivered an oscillating radio frequency (RF) and center trapped DC potential. At each specific RF frequency and DC voltage, only resonant ions with a specific mass to charge (*m/z*) ratio can reach the detector. By sweeping input DC voltages, a mass spectrum in the range of 1 ~ 200 amu could be obtained with a Model 13 High-Q head. The different applied voltages were calibrated to various specific masses of several residual gases (such as water and nitrogen). During TPD, the QMS could monitor up to six specific masses by applying corresponding voltages determined by calibration.

In ESD/SPI studies, the QMS was mounted perpendicular to the sample surface. An extraction plate was added to the ion optics region. To improve the signal, a pulsed

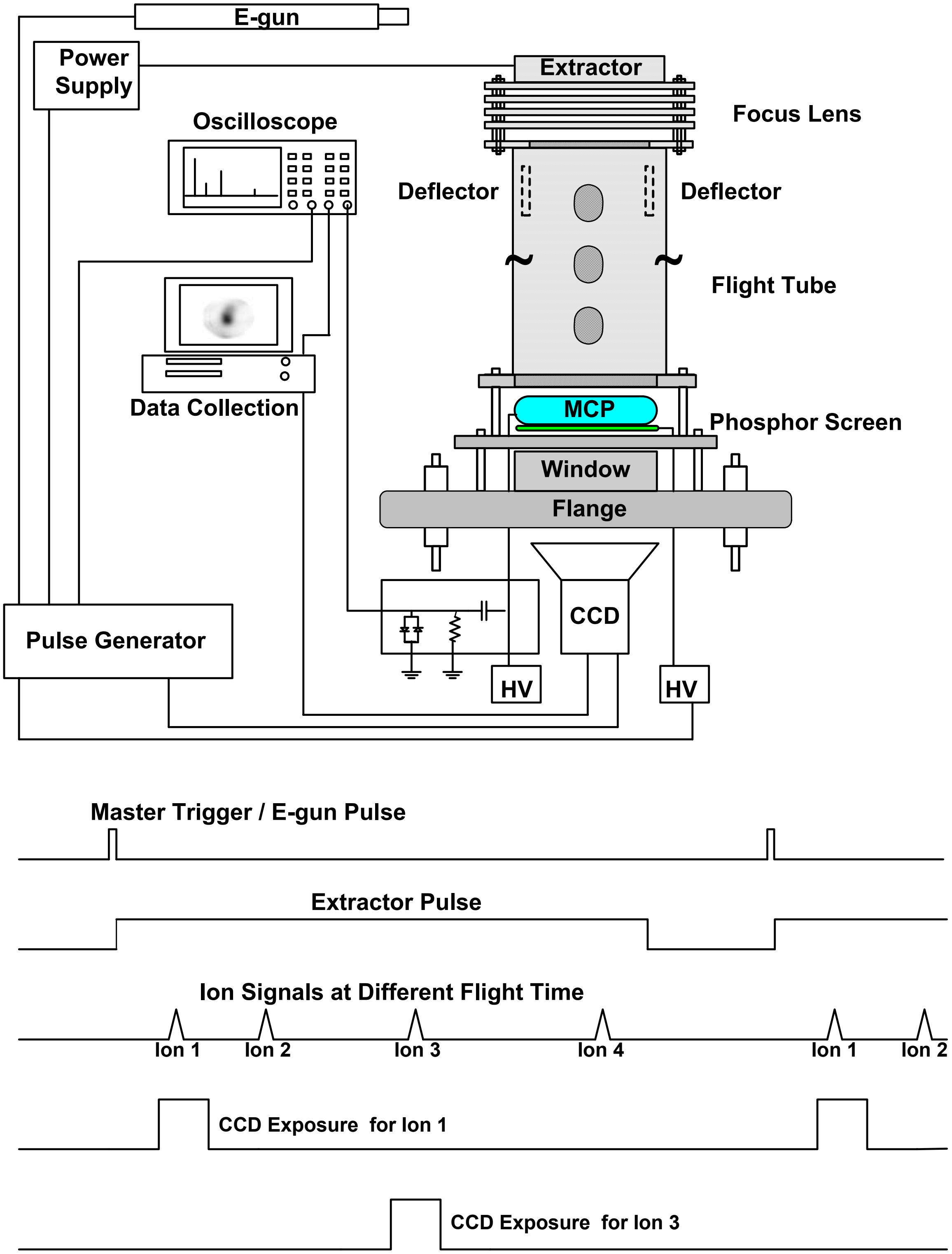

Figure 2-3. Schematic of Time-of-Flight (TOF) mass spectrometer (upper frame) and pulse sequence of imaging detection (lower frame).

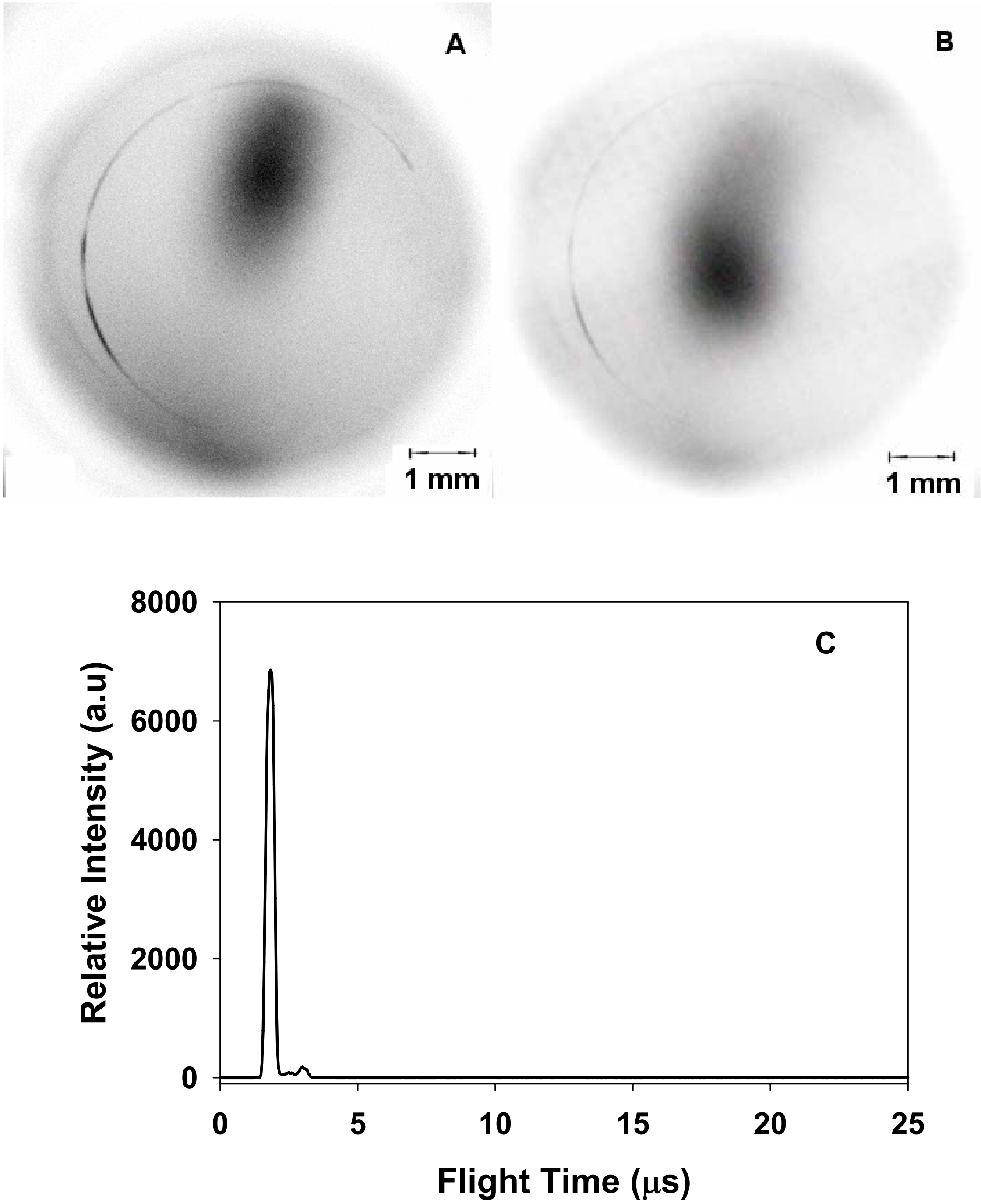

Figure 2-4. Images of H^+ generated by ESD (200 eV, 500 Hz, 500 ns) on graphite at different positions (A and B; 5 ms CCD camera exposure) and the ESD mass spectrum (C).

negative voltage was applied to extractor immediately after the pulsed electron beam irradiation. Because the VUV laser was used to ionize the neutral molecules during low-energy electron irradiation on DNA samples, the filament of the QMS electron ionizer was disconnected from the power supply to avoid further EI ionization and fragmentation. The QMS was then operated either in a voltage-sweeping mode to detect different ions or in a voltage-constant mode to monitor one specific mass, which was useful in increasing the intensity of ions of interest.

2.1.11 Laser Systems

Two Nd:YAG laser systems (Powerlite Precision II and Surelite I-20; Continuum, Santa Clara, CA, USA) were used in SALDI and LD/SPI investigations. Both of these laser systems were driven externally by pulse control systems in all the experiments.

The Surelite I-20 system was mainly utilized in SALDI studies. It was operated at 20 Hz with a pulse width of 3 - 5 ns. The highest power of this system could reach 120 mJ at 355 nm. A beam splitter (THORLABS, Inc., Newton, NJ, USA), a power attenuator made by glass slides and a series of irises (THORLABS, Inc., Newton, NJ, USA) were used to reduce the laser power to 200 ~ 500 μJ/pulse. The laser beam was focused on the sample plate at a 45° incident angle with a ~0.5 mm^2 spot area.

In LD/SPI experiments, the Surelite I-20 system was used as the desorption laser. The operational protocol was very close to the SALDI studies except the laser power was further reduced to 50 to 500 μJ/pulse. A Powerlite Precision II system was used to generate VUV photons for single photon ionization. It also had a 20 Hz repetition rate and 5 ~ 7 nm pulse width at 355 nm. The power of the 355 nm beam provided by the

Powerlite Precision II system was up to 300 mJ. Similar to the attenuation process of SALDI experiments, the laser beam was reduced to ~ 25 mJ/pulse and focused to the THG cell by a quartz lens with 200 mm focal length. The delays between the two 355 nm lasers were varied to obtain the velocity distribution of the desorbed neutral molecules and the optimization of neutral molecule ionization.

2.1.12 Pulse Control System

The electron gun, two 355 nm lasers, extraction grids of mass spectrometers and data collection are all controlled by pulse generators (PDG 2510; Direct Energy, Inc., Fort Collins, CO, USA). The pulsing system usually synchronized the desorption and ionization irradiation by generating pulses with controlled delay time. It also triggered the extraction and detection units. The pulse frequency, pulse width and pulsing sequences were varied in different experiments as needed. The detailed pulse sequences are described in the experimental sections of related chapters.

2.1.13 Post-ionization Gel Electrophoresis

Agarose gel electrophoresis is the easiest and most common way of separating and analyzing DNA. Supercoiled, single strand break (SSB) and double strand break (DSB) DNA could be separated by their various migrating abilities in agarose. The different positions of DNA can be visualized in the gel by adding ethidium bromide (Fisher Scientific, Pittsburg, PA, USA) or SYNR Gold nucleic acid gel stain (Molecular Probes, Eugene, Oregon, USA)(*Both these are mutagens which should be handled with care!*). The dye molecules typically bind strongly to DNA. By intercalating between the bases, they absorb invisible UV light and transmit the energy as visible light, which could be observed using an UV transilluminator or other appropriate device.

After electron irradiation, the DNA samples are removed from the main chamber and re-dissolved into water. The post-irradiated DNA samples are then analyzed by agarose gel electrophoresis. To make the agarose gel, ~0.4 g of molecular biology grade agarose (preparation of 0.8 % (w/v) agarose) was dissolved in 50 mL 1 × TBE (89 mM Tris base, 89 mM boric acid, and 1 mM EDTA, pH $\approx$ 8.0) solution by microwave heating. If using ethidium bromide as the dye, light protected stock solution was added to the agarose solution to make a 0.5 μg/mL concentration after the agarose solution was cooled to ~ 45°C. The gel solution was then poured into a gel tray (C.B.S. Scientific Inc., Del Mar, CA, USA) with a comb in the holder which was 1 mm above the bottom of the gel tray. After the gel had solidified, more of 1 × TBE running buffer was added to cover the whole gel surface by 5-10 mm. The walls of the gel tray and the comb were then removed for sample loading. Each DNA sample was mixed with a loading buffer (0.25 % (w/v) bromophenol blue, 0.25 % (w/v) xylene cyanol, and 30 % (v/v) glycerol in water) with volume ratio of 1:5 and pipetted into the gel lanes. The gel system was further connected to a power supply and run for approximately 35 minutes at 150 mV. Finally, the gel was removed from the gel box and placed in a plastic container. If the gel was not cast with ethidium bromide, 50 mL of 1 × TBE and 0.01% (v/v) SYBR stain was added into the container and stored in darkness for 20 minutes. The stained gel was visualized with an UV transilluminator and the picture was taken for quantitative analysis by gel-reading software.

2.2 SYNTHESIS OF 1B-METHYLSELENO-N-ACETYL-D-GALACTOSAMINE

1β-methylseleno-N-acetyl-D-galactosamine (N-Ac-SeGal) was obtained *via* a modified five-step synthesis procedure according to reference [23] (Figure 2-5).

2.2.1 1β-D-Galactosamine Pentaacetate (reaction step 1)

A solution of 2.0 g of D-galactosamine hydrochloride (1) in a mixture of 15 mL of anhydrous pyridine and 10 mL of acetic anhydride was mixed at room temperature under dry condition (reaction flask were equipped with a $CaCl_2$ tube as a drying agent and under N_2 atmosphere) for 48 h.

The reaction mixture was diluted with 300 mL of dichloromethane and washed at 0 ºC successively with 15 mL of water, two times with 10 mL of saturated sodium bicarbonate solution and then with 10 mL of a 10% solution of cupric sulfate until the disappearance of the deep blue pyridine-copper complex, and finally washed with water twice.

The organic layer was dried by dry Na_2SO_4, and evaporated *in vacuo*. The residual oil was crystallized by gradually adding dry EtOH to get 1β-D-galactosamine pentaacetate (product 2) (m.p. 227~229 °C). The total yield was about 60%.

2.2.2 1α-Chlorogalactosamine Tetraacetate (reaction step 2)

500 mg of 1β-D-galactosamine pentaacetate was suspended in 20 mL of dry dichloromethane and 2 mL of dry ethyl acetate equipped with a reflux condenser, under a N_2 atmosphere. 0.18 mL of $TiCl_4$ was added by a dry syringe. The reaction mixture was refluxed for 3.5 hours.

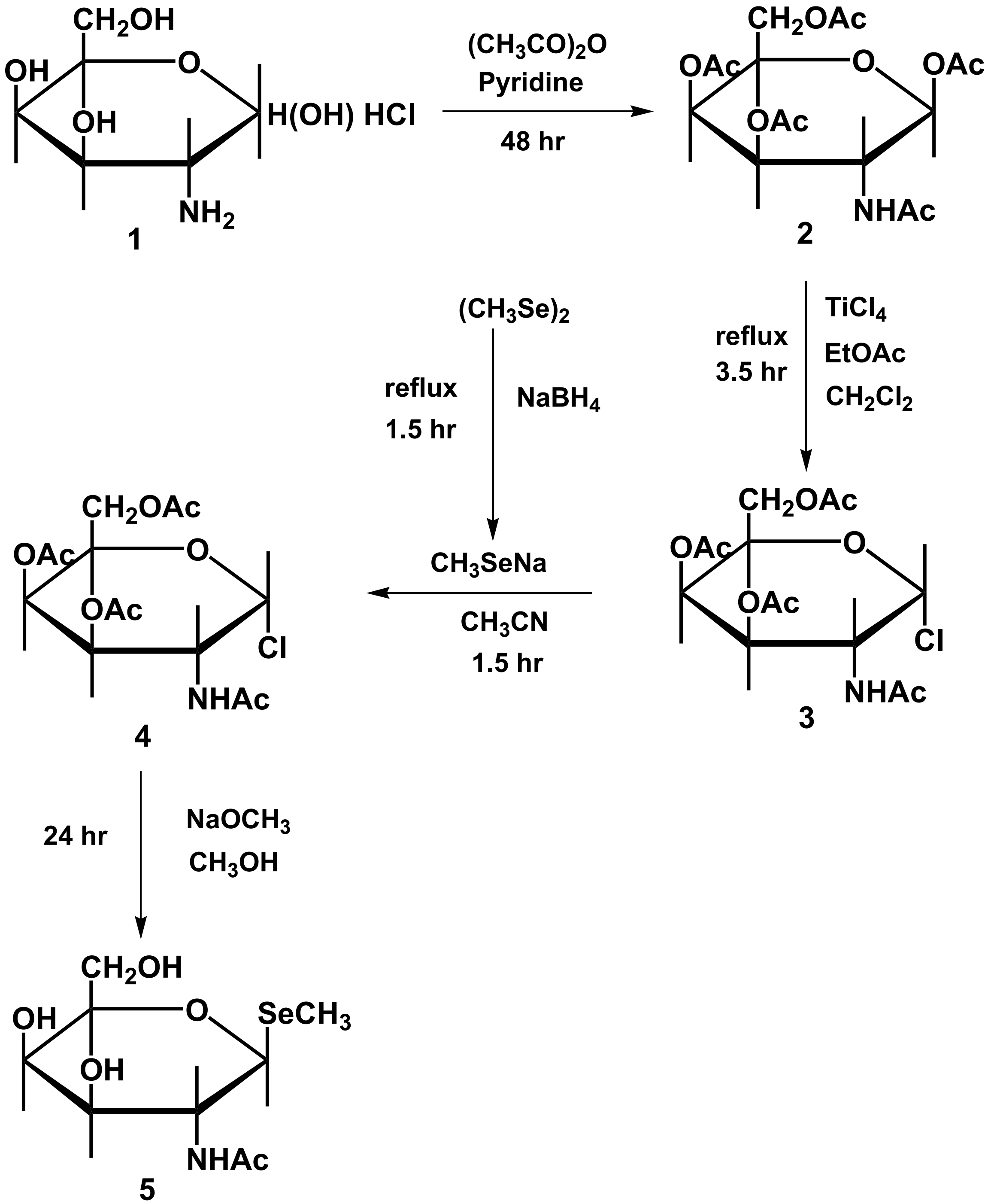

Figure 2-5. Chemical synthesis of 1β-methylseleno-N-acetyl-D-galactosamine.

The reaction mixture was cooled at room temperature and diluted by 40 mL of dichloromethane, then washed by 0 ºC water (50 mL twice) and cold saturated sodium bicarbonate solution (50 mL twice).

The organic layer was dried by dry Na_2SO_4 and evaporated *in vacuo*. The residue was purified by a silica gel column (eluted by CH_2Cl_2, 5% MeOH) to afford 1α-chlorogalactosamine tetraacetate (product 3) as white powders (55% yield, melting point 125~126 ºC). Product 3 can also be crystallized by gradual addition of dry Et_2O into the residue (~50% yield, m.p 123~127 ºC)

2.2.3 1β-Methylseleno-galactosamine Tetraacetate (reaction step 3&4)

136 µL of dimethyl diselenide was dissolved in 1.5 mL of dry acetonitrile and 55 mg of sodium borohydride was added. The reaction mixture was refluxed for 50 min. and cooled to room temperature.

260 mg of 1α-chloro-galactosamine tetraacetate was dissolved in 6 mL of acetonitrile, then gradually added to the reaction mixture and stirred for 1.5 hour at room temperature.

The reaction mixture was evaporated in vacuo and the residue was purified by silica gel column (eluted by CH_2Cl_2, 10% MeOH) to afford 1β-methylseleno-galactosamine tetraacetate (Product 4) as white-pink powders. The product 4 was characterized: melting point 218 ~ 220 ºC.

2.2.4 1β-Methylseleno-N-acetyl-D-galactosamine (reaction step 5)

100 mg of 1β-methylseleno-galactosamine tetraacetate was dissolved in 2 mL of

dry methanol and catalytic amount of sodium methoxide (240 μL 1 M methanol solution) was added. The reaction mixture was stirred at room temperature for 24 hours.

The reaction mixture was evaporated in vacuo and purified by a C_{18} semi-prep column (H_2O, 5% MeOH) to afford white powder (~ 40% yield) as 1β-methylseleno-N-acetyl-D-galactosamine (N-Ac-SeGal). The product was characterized: melting point 255~257 ºC (decomposition); ESI MS ($C_9H_{18}O_5NSe$ *m/z* 300.0) as shown in Figure 2-6; ^{1}H NMR (500MHz, D2O) δ 1.91(s, 3H), 2.00(t, 3H), 3.56(m,1H), 3.58(m,1H), 3.63(m,1H), 3.64(m,1H), 3.88(d,1H), 3.94(t,1H), 4.61 (d,1H) as shown in Figure 2-7 and Figure 2-8.

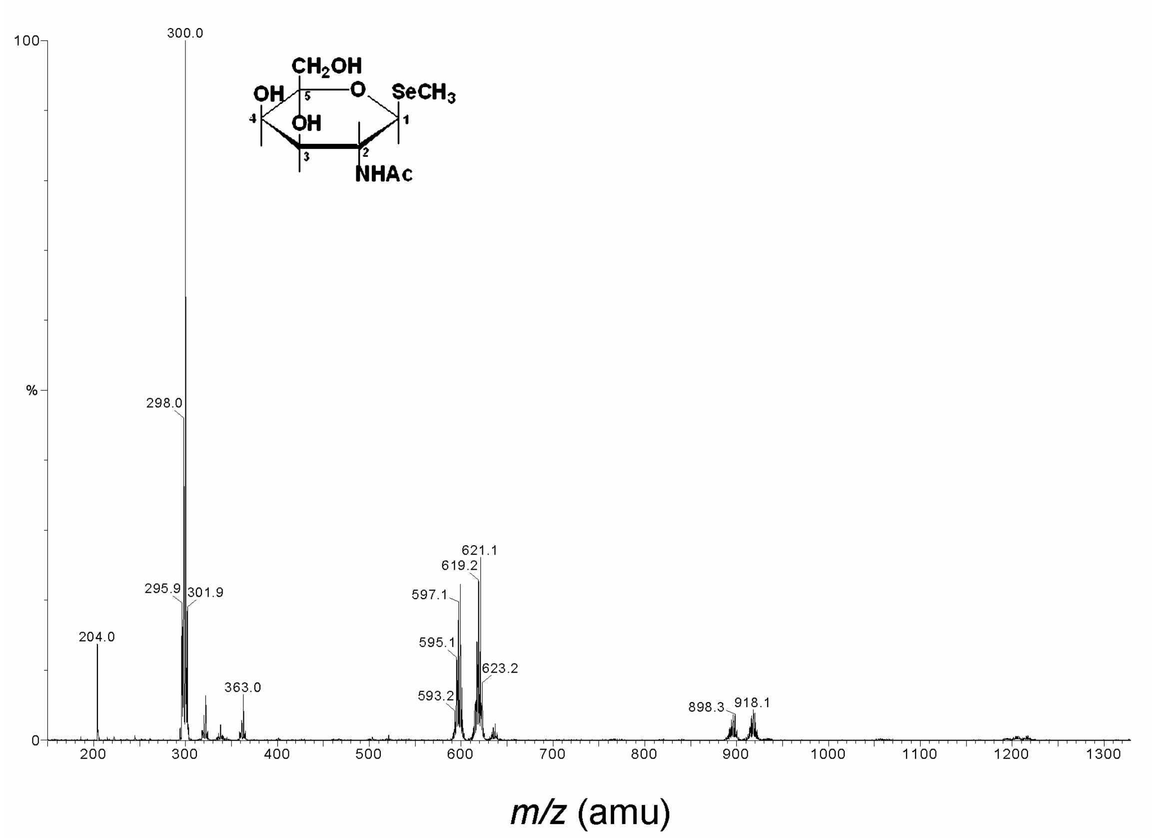

Figure 2-6. ESI mass spectrum of 1β-methylseleno-N-acetyl-D-galactosamine.

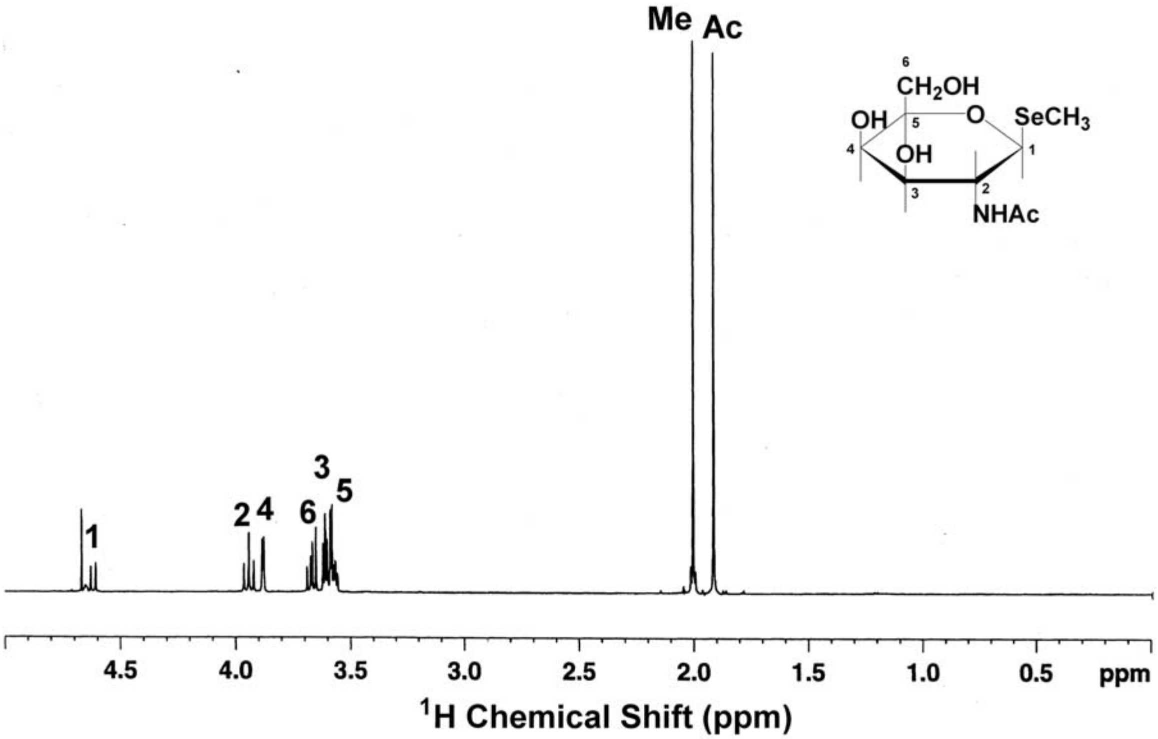

Figure 2-7. 1-D ^{1}H NMR spectrum of 1β-methylseleno-N-acetyl-D-galactosamine.

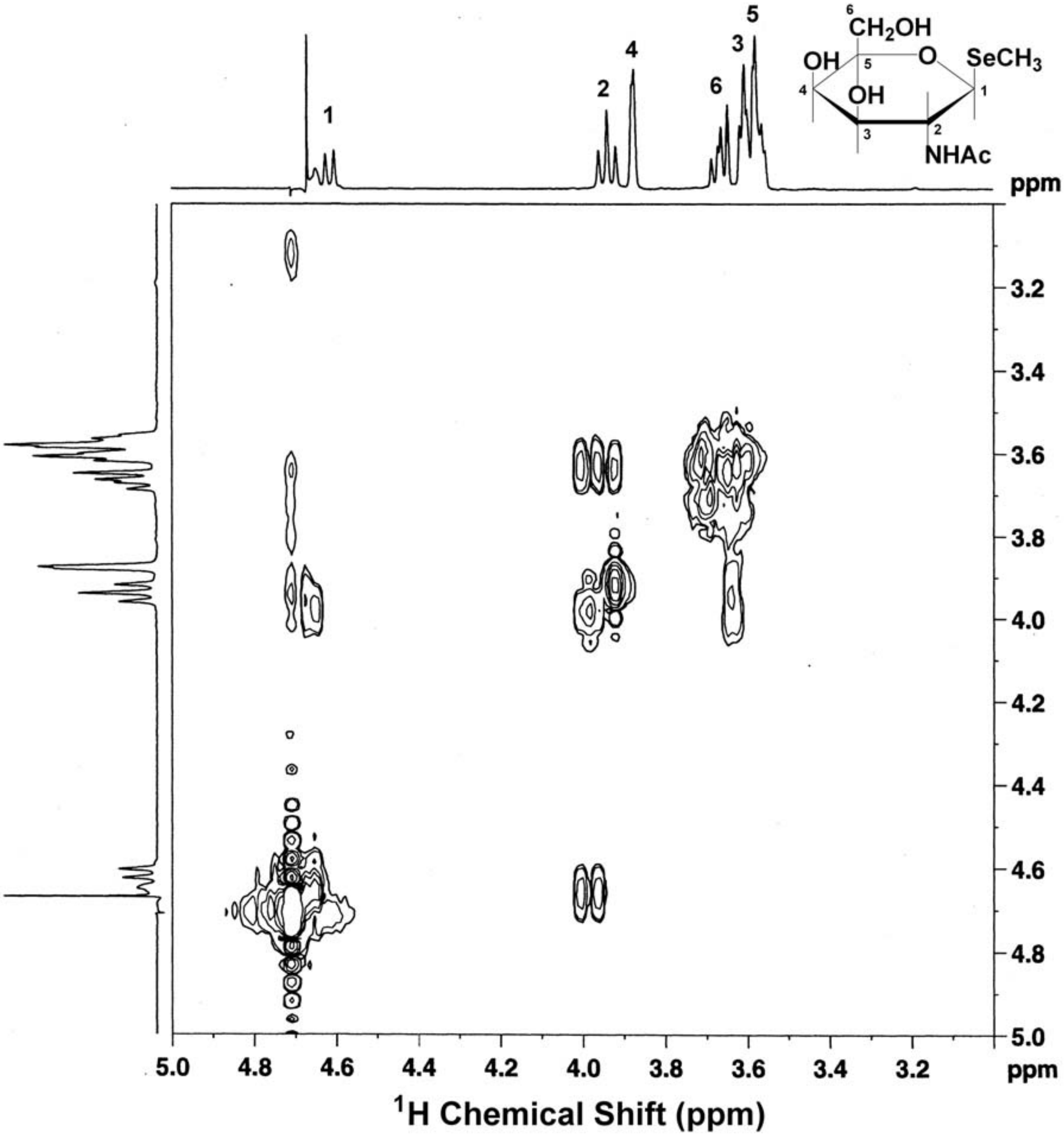

Figure 2-8. 2-D ^{1}H NMR spectrum of 1β-methylseleno-N-acetyl-D-galactosamine.

CHAPTER 3

ANALYSIS OF SMALL BIOLOGICAL MOLECULES USING SURFACE-ASSISTED LASER DESORPTION/IONIZATION MASS SPECTROMETRY

3.1 OVERVIEW

The introduction of matrix-assisted laser desorption/ionization (MALDI) less than two decades ago[7, 24] has dramatically improved the ability of laser mass spectrometry and gained broad successes in analytical, biological, environmental, clinical, pharmaceutical and material analysis.[8, 11-13] Direct laser desorption ionization (LDI) has been extensively studied since 1970,[25] but it usually exhibits severe molecular degradation for low mass analytes under laser irradiation. This greatly hindered LDI from being widely used. By simply adding energy-absorbing organic matrix molecules during sample preparation, MALDI overcomes the problems of LDI and generates intact large mass molecular ions. Coupled with time-of-flight (TOF) mass spectrometry, MALDI MS allows mass determination of large biomolecules and synthetic polymers of molar mass greater than 100,000 Daltons (Da).[10] Soft ionization, high detection sensitivity and relative simplicity have made MALDI a popular technique[14] and revolutionized the analysis of fragile or non-volatile molecules such as peptides/proteins,[26-29] carbohydrates,[30, 31] nucleic acids/oligonucleotides/DNA,[32-35] oligosaccharides,[36] toxins,[37, 38] and polymers.[39-42]

Although MALDI has been remarkably successful in analysis of large molecules, it has seldom been applied to low molecular weight compounds. One of the major reasons is that MALDI produces a large amount of matrix ions in the low mass range (*m/z* < 600). The signals of small molecules usually can not be separated and identified from the massive obscuring background signals of the matrix. As a result, MALDI is commonly considered inappropriate for analysis of low molecular weight compounds. However, increasing demands for high throughput methods in drug discovery and biotechnology as well as analysis of complex mixtures in high salt matrices and buffers, which could not be achieved by other techniques such as electrospray ionization (ESI) or atmospheric pressure ionization (API), has created great interests in utilizing the full power of LDI over the entire mass range of interest.[16]

Surface-assisted laser desorption/ionization (SALDI) has been recently developed to extend the ability of MALDI to detect small molecules. The instrumentation and operation of SALDI MS is similar to MALDI MS. However, SALDI uses materials or particles that are not ionized under laser irradiation but promote the desorption/ionization of analytes. This helps to avoid the noisy background of typical traditional organic matrix molecules while maintaining the advantages of MALDI. From this point of view, previous works using different active surfaces such as carbon suspended in solution,[15, 43] carbon nanotubes (CNTs),[44, 45] graphite,[46] and porous silicon (DIOS),[47, 48] were all defined as useful SALDI substates.[49] As a "matrix-free" method, SALDI circumvents most of the problems of MALDI since it involves simple sample preparation, low noise background, efficient soft ionization, high salt tolerance, even analyte distribution, and fast data collection. In the area of small molecule analysis, SALDI is a promising technique with many potential applications.

Despite the potential importance of SALDI, no systematic investigation has been reported to evaluate the performance of various SALDI substrates. In this chapter, three surfaces were studied to compare their ability in generating SALDI signals and provide useful guides to SALDI applications. The effectiveness of SALDI MS in the analysis of amino acids, peptides and organoselenium compounds were also tested in this work.

Amino acid analysis has been an integral part of analytical chemistry for more than 50 years.[50, 51] Free amino acids are routinely analyzed in complex matrices for numerous applications from basic research, nutritional labeling to patient diagnosis. However, the main technology of amino acid analysis still includes sample derivatization followed by chromatographic separation. Although many efforts have been carried out to reduce the analysis time, it still requires at least 15 to 30 minutes for a single sample.[52] The successful analysis of six amino acids (glycine, glutamine, histidine, methionine, arginine, and tryptophan) using SALDI MS provides a simple alternative method to complete the detection within several seconds, which will greatly benefit the high-workload routine analysis of amino acids.

Small peptide identification is one of the most difficult problems in MALDI MS characterization of complicated mixtures such as protein digests. A full mass spectrometric coverage of digest mixture components is rarely achieved partially because of the blindness of MALDI in low mass range. The easy detection of small peptides (H-Gly-Gln-OH and H-Gly-His-OH) using SALDI provides more useful information of small peptides as well as more reliable and faster protein identification.

Other compounds such as selenium containing metabolites are also amenable to SALDI MS analysis. Selenium deficiency in humans has been linked to numerous health problems[53] such as arthritis,[54, 55] heart disease,[56, 57] cancer,[58-61] and AIDS.[62] To fully understand the human metabolism of selenium, it is necessary to identify and analyze the selenium species present in biochemical samples. Historically, this has been a major experimental challenge because of the low levels of selenium species (*e.g.* ppb and sub-ppb), the thermally labile nature of the possible selenium species, and the complexity of analyte/matrix interactions. The readily interpretable mass spectra of organoselenium metabolites (selenomethionine and 1β-methylseleno-N-acetyl-D-galactosamine) using SALDI presented in this study provide a valuable means of analyzing selenium metabolites in biological samples (such as human urine) for the elucidation of selenium functions in the human body.

The general applicability and high sensitivity of SALDI MS demonstrated in this chapter suggests that this technique is indeed a promising and powerful technique which could be used as a widespread tool for the mass spectrometry of small to intermediate analytes in complex systems.

3.2 EXPERIMENTAL

3.2.1 SALDI Mass Spectrometry

The apparatus shown in Figure 3-1 is a custom designed ultra high vacuum (UHV) chamber (background pressure of ~ 10^{-9}-10^{-10} torr) equipped with a linear transfer antechamber, a sample holder with an XYZ controller mounted on a 360º rotation stage, a temperature control system and a home-built linear TOF mass spectrometer. The samples were loaded into the antechamber and then transferred into the analytical system by a rotary-linear magnetic transporter. The samples were located onto the UHV sample holder using a modified UHV compatible wobble stick. A 20 Hz Nd:YAG laser operated

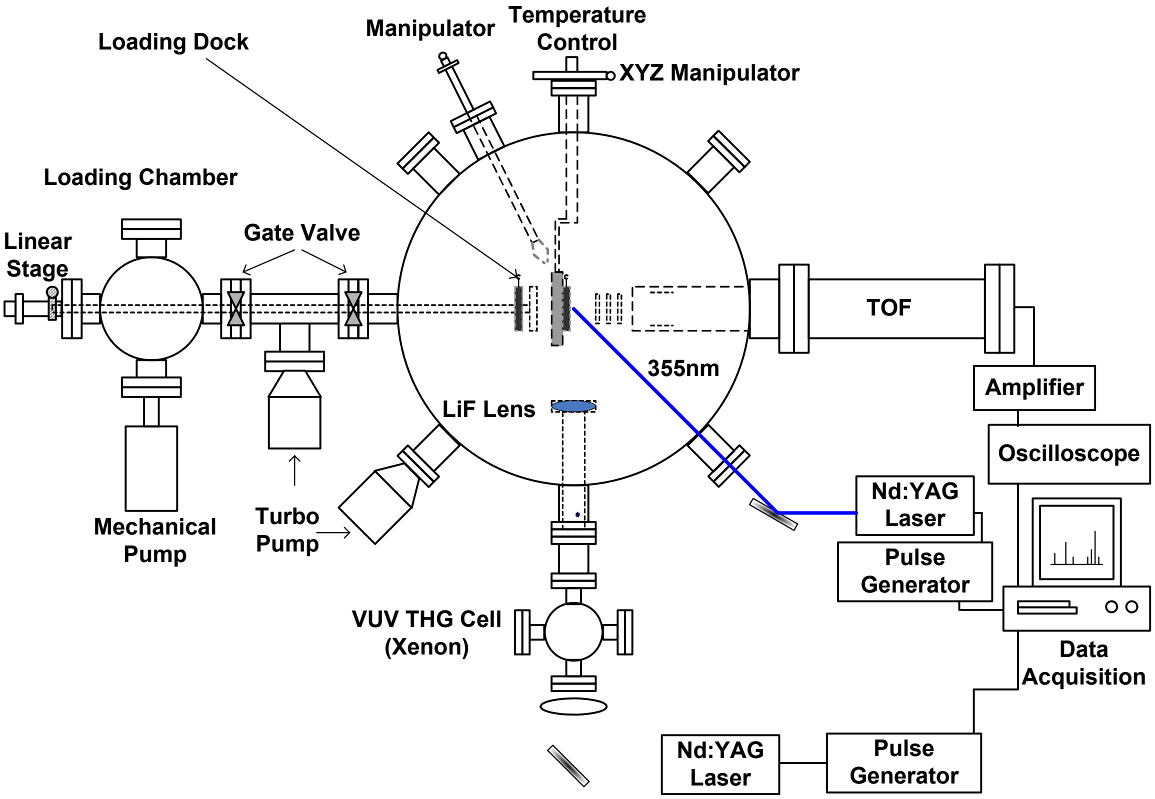

Figure 3-1. Schematic of surface-assisted laser desorption/ionization mass spectrometry (SALDI MS).

at the third harmonic (355 nm) impinged on the adsorbate covered surface at a 45° incident angle. The laser was focused to a ~ 0.5 mm^2 spot area and the pulse energy was controlled in the range of 200 to 500 μJ/pulse. A continuous positive potential (200 ~ 5000 V) was applied to the sample plate and a negative potential (-300 ~ 1300 V) was added to an extraction grid in the ion region. The potential of first grid was about 500 V less positive than that of second grid and the tube potential was -1.9 kV. Potentials in the range of -300 V were also applied across a pair of horizontal deflection plates for the optimization of signals. The ions were detected by the TOF mass spectrometer with a pair of chevron configuration microchannel plates and the output was amplified, digitized, signal averaged and stored in a computer. The number of required laser shots depends on the desorption laser energy and beam profile. For a pulse energy of 200 μJ, 1000 shots were typically used. The temperature control of samples was achieved by adding liquid nitrogen to the sample dewar and heating the sample by a button heater.

3.2.2 Chemicals and Reagents

All solvents were HPLC grade (Fisher Scientific, Atlanta, GA, USA). Other materials/chemicals used were: (i) graphite, 99.95% purity (Alfa Aesar, Ward Hill, MA, USA); (ii) Boron-doped (100) single-crystalline silicon wafer (1-20Ω·cm) (Wafer World Inc., West Palm Beach, FL, USA); (ii) hydrofluoric acid (48%) and nitric acid(70%) (Fisher Scientific, Pittsburg, PA, USA); (iii) glycine, glutamine, methionine, histidine, arginine, tryptophan, and seleno-DL-methionine (Sigma, St. Louis, MO, USA). (iv) H-Gly-Gln-OH and H-Gly-His-OH (BACHEM Inc., King of Prussia, PA, USA) (v)1β-methylseleno-N-acetyl-D-galactosamine (N-Ac-SeGal) (synthesized in a modified version according to reference [23], the details of the synthesis are given in chapter 2). Nanopure water of 18MΩ was used throughout the experiments.

3.2.3 Substrate Preparation

Graphite substrates were heated to 600 K in vacuum (10^{-8} torr**)** for 1 hour to remove organic contaminations and adjust the mean roughness of the surface. Porous silicon substrates were etched from p-type Si(100) using a $HF/HNO_3/H_2O$ (1:3:5) (*Caution! Hazardous and corrosive chemicals)* solution for 60 ~ 240 seconds according to reference [63] and cleaned by a 1:20 HF/H_2O solution as well as nanopure H_2O for three times. The pore size was in the range of 40 ~ 400 nm. The obtained porous silicon substrates were then sealed in nanopure water at 4 °C. Si(100) substrates were cleaned by a 1:20 HF/H_2O solution and nanopure H_2O for three tines and sealed in nanopure water at 4 °C.

3.2.4 Sample Preparation

Solutions of analytes were prepared by nanopure water and high purity methanol. 5 mm × 5 mm SALDI substrates were cleansed by sonicating in methanol or nanopure water for 30 minutes. 10 μL sample solutions were then directly deposited onto SALDI substrates. The sample plates were air-dried for 10 min. in desiccators and immediately transferred into the antechamber for further vacuum drying. Finally, the samples were transferred into the main UHV chamber for SALDI analysis.

3.3 RESULTS AND DISCUSSION

3.3.1 SALDI MS Analysis of Amino Acids Using Different Substrates

To test the applicability of SALDI MS to small biological molecules, six typical amino acids (glycine, glutamine, histidine, methionine, arginine, and tryptophan) (Figure 3-2) with various properties (such as polarity, proton affinity, etc.) were analyzed on three different substrates (graphite, porous silicon and, single crystalline silicon 100).

3.3.1.1 SALDI MS Analysis of Amino Acids on Graphite Substrates

The SALDI mass spectrum shown in Figure 3-3 was obtained by depositing 10 μL of aqueous solution of six amino acid mixtures (5 μg/mL for each) on a graphite surface at room temperature. Protonated molecular ions (MH^+) of all six amino acids were detected at m/z 76.1 (glycine), 147.2 (glutamine), 150.2 (histidine), 156.2 (methionine), 175.2 (arginine) and 205.2 (arginine). No obvious characteristic fragments of the amino acids were found, which confirms SALDI is a soft ionization method. It is consistent with a previous report[64] in which MH^+ of the amino acid (Lysine) was obtained by laser desorption/ionization mass spectrometry using active carbon and glycerol as mixed matrices. However, SALDI on graphite showed better performance than carbon/glycerol, since it did not produce adducts of Na^+ and K^+ and the intensive MH^+ peaks of analytes make the mass spectrum easily interpretable. The absence of molecular ions (M^+) in Figure 4-1(a) indicates that analyte molecules were not directly ionized by photons in the gas phase from the desorbing laser pulse. SALDI experiments on blank graphite were also performed. A relatively clean base line in the mass range of m/z > 50 was observed when laser power was controlled below 600 μJ/pulse. The unknown peaks marked by asterisk in Figure 3-3 were not detected from the blank graphite substrate.

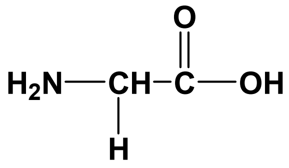

Glycine (Gly)

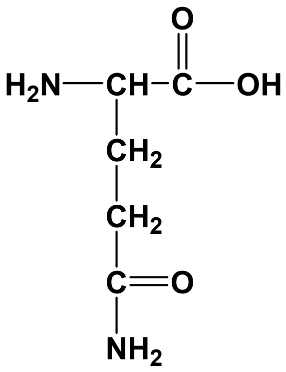

Glutamine (Gln)

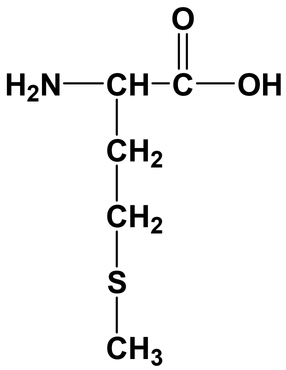

Methionine (Met)

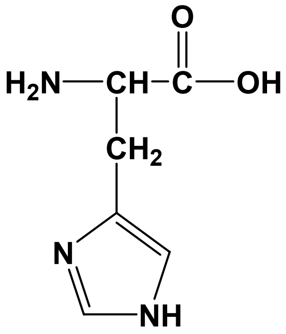

Histidine (His)

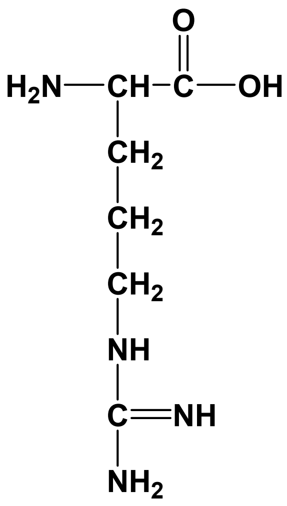

Arginine (Arg)

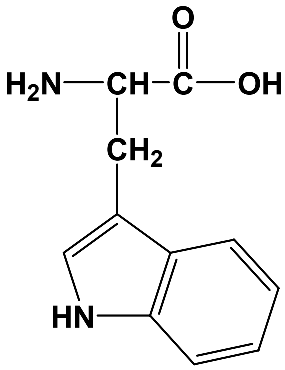

Tryptophan (Trp)

Figure 3-2. Structures of six amino acids studied by surface-assisted laser desorption/ionization (SALDI).

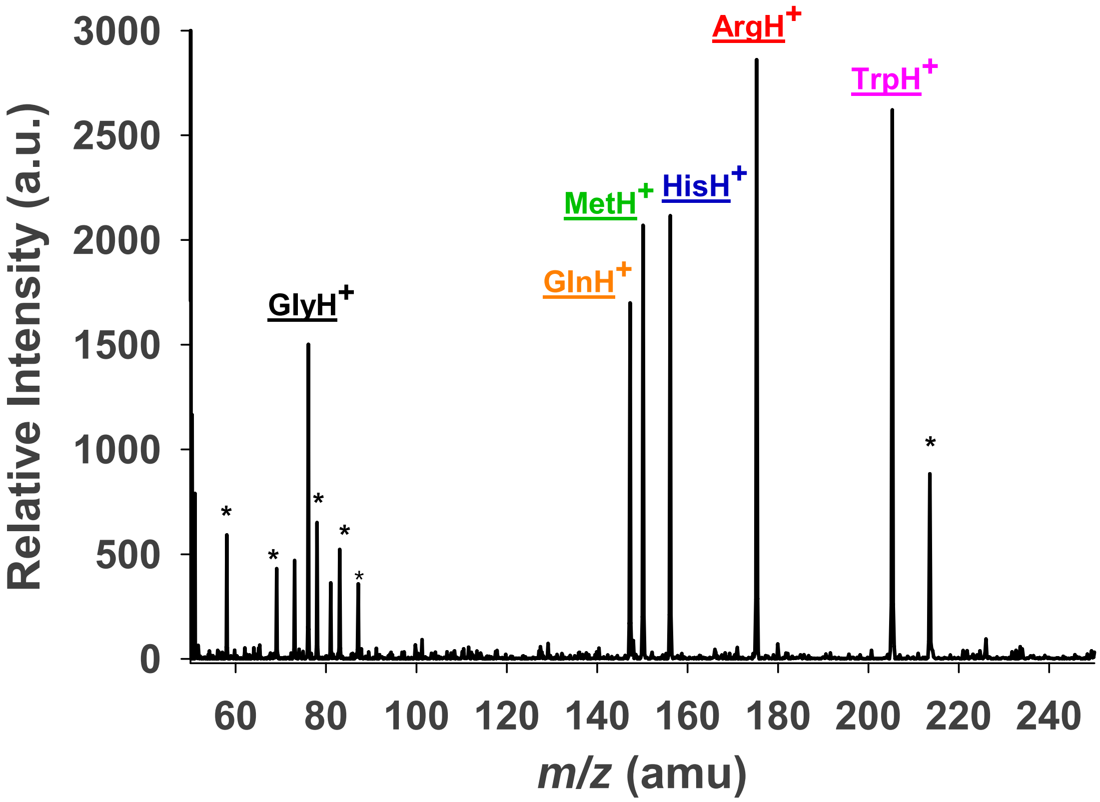

Figure 3-3. SALDI mass spectrum of amino acids on a graphite substrate at 300 K.

They are probably due to the impurities in the amino acid samples.

3.3.1.2 SALDI MS Analysis of Amino Acids on Porous Silicon Substrates

SALDI MS analysis of six amino acids on porous silicon was also investigated with standard solutions of amino acids (same as those in section 3.3.1.1) at room temperature. Figure 3-4 shows the representative mass spectrum, which is very similar to the results on graphite substrate. The most abundant ions were also MH^+ signals and fragmentation of the analytes did not occur. The ion intensities of amino acids from porous silicon were almost the same as those on graphite. It is also noticed that the noise level of base line in the mass range of $m/z > 50$ on blank porous silicon was about 2-3 times smaller than blank graphite. Some unknown peaks which probably come from impurities in the amino acid samples were also found and labeled with asterisks.

3.3.1.3 SALDI MS Analysis of Amino Acids on Si(100) Substrates

Si(100) was also used as a SALDI substrate to analyze the standard solution of six amino acids by laser desorption/ionization at 130 K (Figure 3-5). At room temperature, no analyte signal could be obtained. However, protonated molecular ions (MH^+) of all of six amino acids were easily detected by lowering the sample temperature lower to 170 K. The ion intensities on Si(100) at this temperature were about one half of those generated from graphite and porous silicon. Unknown peaks were also found and some of them are the same as those reported in Figure 3-3. These are considered as impurities in the amino acid samples and are labeled with asterisks as well. The other unknown peaks labeled by question marks could come from hydrocarbons frozen onto Si(100). To the best of my

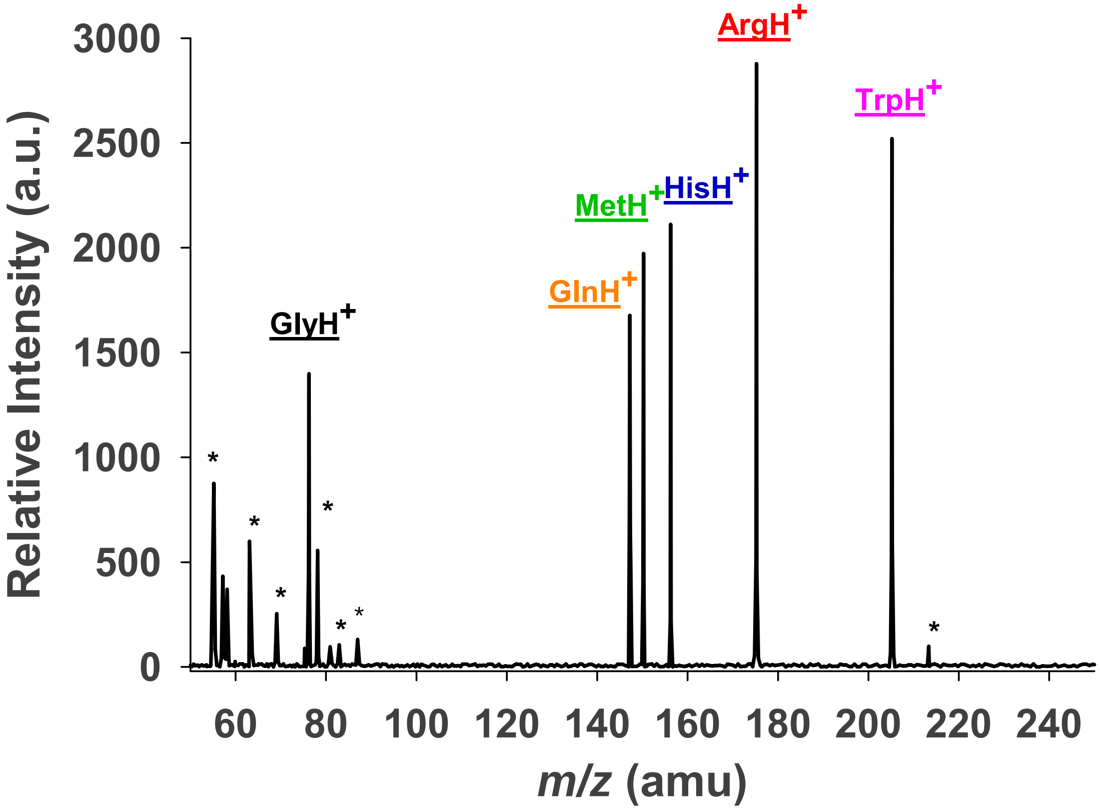

Figure 3-4. SALDI mass spectrum of amino acids on a porous silicon substrate at 300 K.

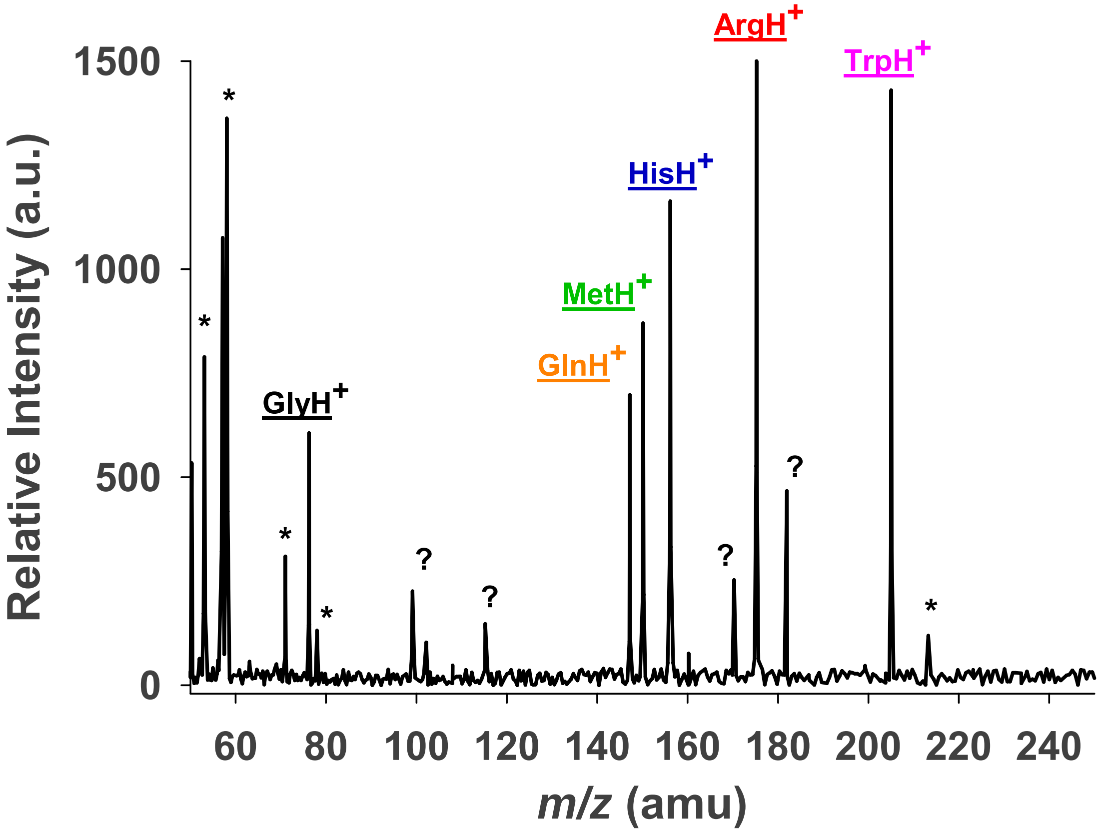

Figure 3-5. SALDI mass spectrum of amino acids on a Si(100) substrate at 130 K.

knowledge, this is the first time small biological molecules were detected on single crystalline silicon by SALDI MS using UV laser excitation. The possible mechanisms will be discussed in chapter 4.

3.3.1.4 Detection Limits of SALDI MS Analysis of Amino Acids on Three Substrates

The SALDI MS detection limit (S/R=3) of amino acids on graphite, porous silicon, and Si(100) were estimated to be 180 ~ 300 ng/mL (~ 1.5 μM), 70 ~ 150 ng/mL (~ 0.9 μM), and 300 ~ 800 ng/mL(4 μM) respectively. This is based on the observed signal-to-noise levels on each substrate. Quantitative analysis of amino acids is still under investigation. The laser power and stability are among the major factors that significantly affects the generation of SALDI signals. A better understanding of the desorption/ionization process and optimization of laser power stability should improve the quantitative performance of SALDI MS. In fact, an improved method based on single photon ionization has been developed with good performance on qualitative and quantitative analysis (see chapter 5)

3.3.1.5 Shot-to-shot Reproducibility of SALDI MS on Three Substrates

One of the most important advantages of SALDI MS is their high spot-to-spot reproducibility. It is found that graphite and porous silicon generate almost uniform SALDI mass spectra everywhere on these surfaces. Although the SALDI yields of amino acids had more variations on Si(100), it also produced mass spectra of all of six amino acids at different sample spots. The shot-to-shot reproducibility of arginine signals on these three substrates is shown in Figure 3-6. No “sweet spot” effects were found on

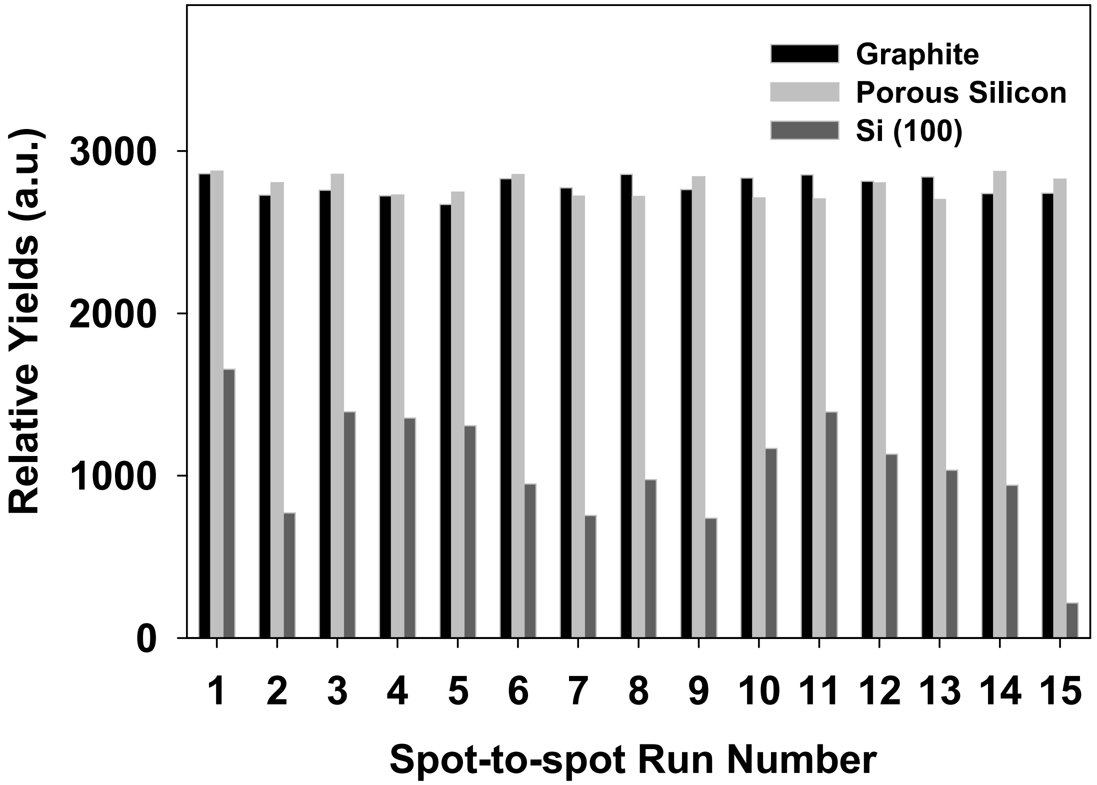

Figure 3-6 Spot-spot reproducibility of SALDI yields on graphite, porous silicon, and Si(100). The examined analyte was arginine.

graphite and porous silicon, indicating that analyte molecules were well distributed on these two surfaces. The absence of matrix molecules avoids the formation of matrix "co-crystallites", which often causes the problem of "sweet-spots". The rough and porous surfaces provide high surface areas, which may promote the uniform distribution of analyte molecules on the surface pores and prevent analyte aggregation. The high shot-to-shot reproducibility of SALDI MS greatly reduces the time and efforts of signal optimization. It demonstrates that SALDI MS is a faster and easier approach compared to traditional MALDI MS.

3.3.1.6 Potential of SALDI MS in Amino Acids Analysis

The successful analysis of amino acids by SALDI MS makes this technique very attractive for amino acid analysis (AAA), which is required in many fields from routine applications to basic research. The detection limits of this method (0.9~4 μM) are well below the normal values of plasma amino acids (~10 μM).[51] Combined with other advantages such as high yields of molecular ions and short data acquisition time (1-2 s), SALDI MS is a very promising AAA method by providing sensitive, simple, and fast analysis.

3.3.1.7 Comparison of SALDI MS Performance of Three Substrates

The SALDI results of amino acids proved that graphite, porous silicon and Si(100) are suitable substrates for analysis of small organic molecules. The three substrates have their specific advantages and limitations. The graphite substrate is easy to prepare and produces strong SALDI signals. Porous silicon has a clean base line and also produces satisfactory SALDI yields. However, porous silicon requires special etching techniques and its activity is usually variable depending on post-etching storage. The Si(100) substrates do not need any surface treatments and also have a clean background, but the signal intensities and spot-to-spot reproducibility are low. SALDI from Si(100) also needs to be operated at low temperature, which is not available in most instruments. Therefore, the appropriate SALDI substrate should be selected based on the application requirements.

SALDI on porous silicon (DIOS) has been reported as a potential platform on which a variety of molecules could be analyzed, such as small drug molecules, carbohydrates, peptides, glycolipids, polymers, and natural products etc.[47, 65, 66] In the following sections, the SALDI investigation of dipeptides and organoselenium metabolites is focused on graphite substrates, which have not been extensively studied before. It also demonstrates the promising ability of analyzing small molecules.

3.3.2 SALDI MS Analysis of Dipeptides Using Graphite Substrates

Two dipeptides (H-Gly-Gln-OH and H-Gly-His-OH, Figure 3-7) were used to study the effectiveness of peptide analysis using SALDI MS on graphite substrates. Figure 3-8 shows the SALDI mass spectrum of a standard solution of dipeptides (5 μg/mL for each). Protonated molecular ions of both analytes were easily identified at m/z 204.2 ($GlyGlnH^+$) and 213.2 ($GlyHisH^+$) with very clean background. The detection limit (S/R = 3) of the dipeptides were estimated to be 150 ~ 250 ng/mL based on the observed signal-to-noise levels. Small peptides are usually difficult to detect by laser ionization mass spectrometry. In direct laser desorption/ionization or multi-photon

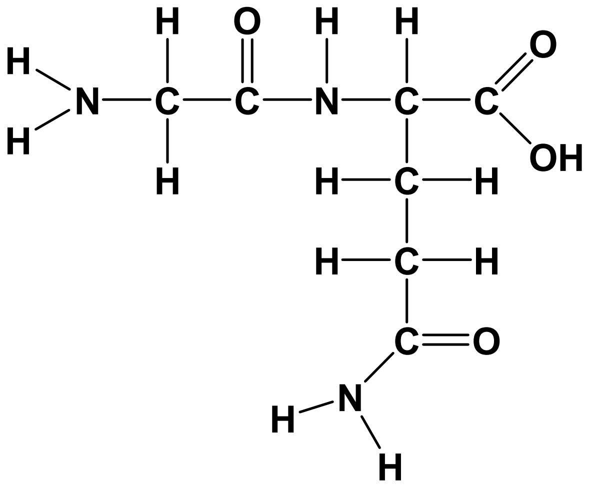

H-Gly-Gln-OH

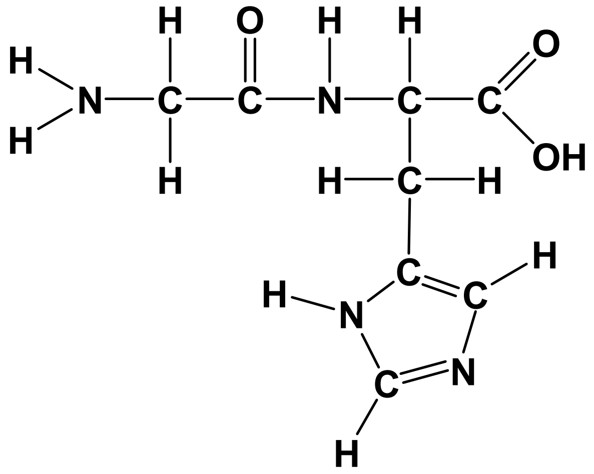

H-Gly-His-OH

Figure 3-7. Structures of H-Gly-Gln-OH and H-Gly-His-OH studied by surface-assisted laser desorption/ionization (SALDI).

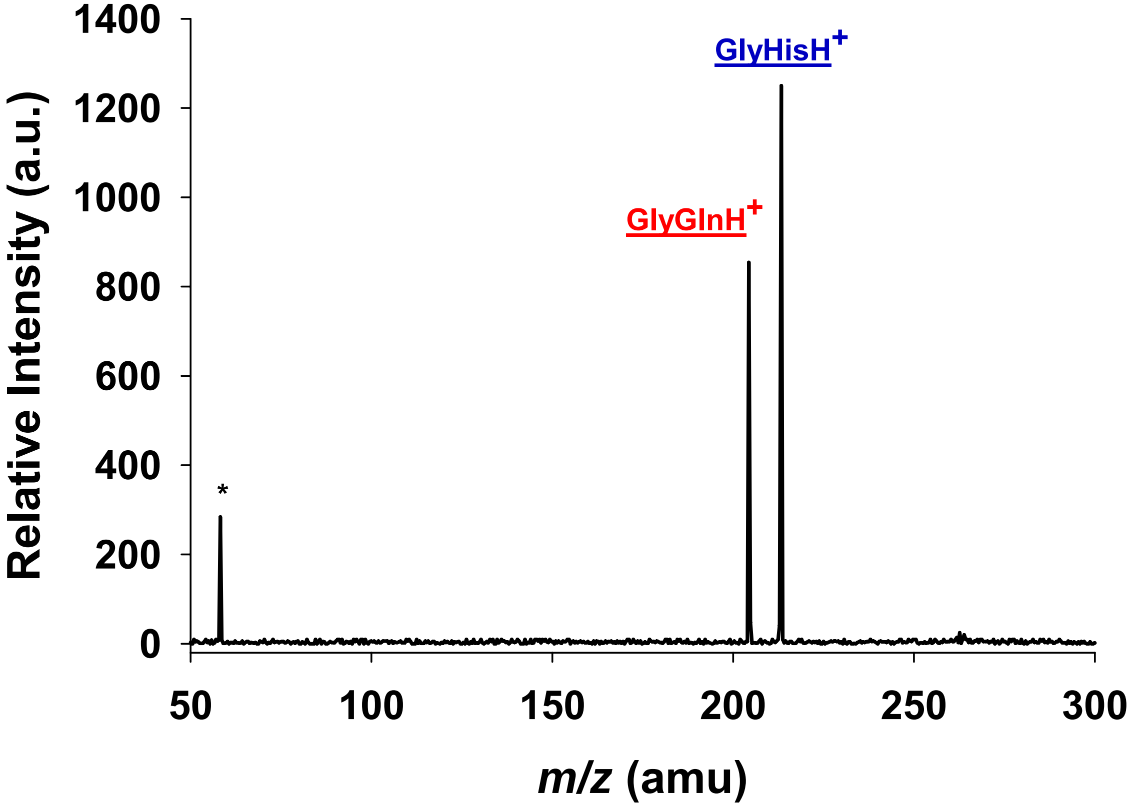

Figure 3-8. SALDI mass spectrum of dipeptides on a graphite substrate at 300 K.

ionization, they provide little or no molecular ions because of extensive fragmention.[67, 68] In MALDI MS, the signal of small dipeptides were often embedded in extensive matrix signals. The intense signal of protonated molecular ions and the interference-free background in Figure 3-8 suggests that SALDI on graphite is suitable for peptide analysis, especially for the challenging applications such as protein digest component identification.[14]

3.3.3 SALDI MS Analysis of Organoselenium Compounds Using Graphite Substrates

To evaluate the ability of SALDI MS for the analysis of organoselenium metabolites, selenomethionine (SeMet) and 1β-methylseleno-N-acetyl-D-galactosamine (N-Ac-SeGal), two of the major selenium metabolites in urine (Figure 3-9), were studied. The SALDI mass spectrum of two standard organoselenium compounds with the same concentration of 5 μg/mL is shown in Figure 3-10. Intense protonated ^{80}Se molecular ions of SeMet and N-Ac-SeGal at *m/z* 198.1 and 212.1 were observed. The selenium isotope patterns of the two MH^+ peaks match those expected from the natural abundances of the Se isotopes (*m/z* 74, 76, 77, 78, 80, and 82) ratios.[69] The good correlation is shown in Figure 3-11A and B for SeMet and N-Ac-SeGal. The detection limit (S/R = 3) of the two organoselenium metabolites were estimated to be 0.6 ~ 1 μg/mL (~ 3 μM) based on the observed signal-to-noise level. Coupling with high-resolution time-of-flight mass spectrometry, thermally labile organoselenium compounds were successfully identified in urine samples.[70] This approach opens a new route for the analysis of metabolites in biological samples.

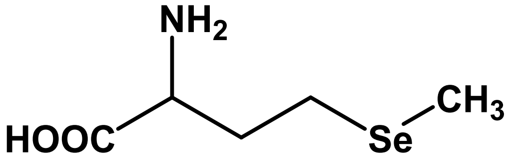

Selenomethionine
(SeMet)

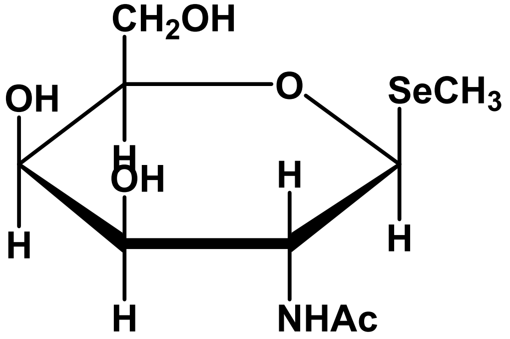

1β-methylseleno-N-acetyl-D-galactosamine
(N-Ac-SeGal)

Figure 3-9. Structures of selenomethionine and 1β-methylseleno-N-acetyl-D-galactosamine studied by surface-assisted laser desorption/ionization (SALDI).

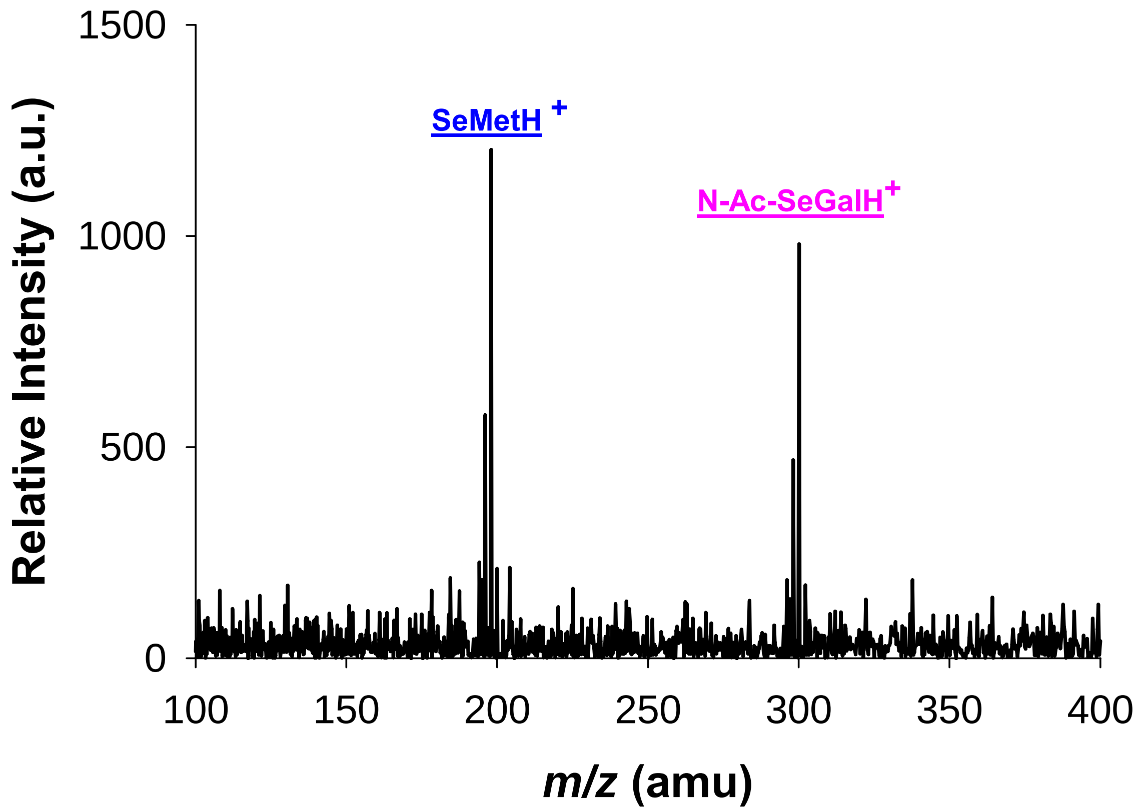

Figure 3-10. SALDI mass spectrum of organoselenium compounds on a graphite substrate at 300 K.

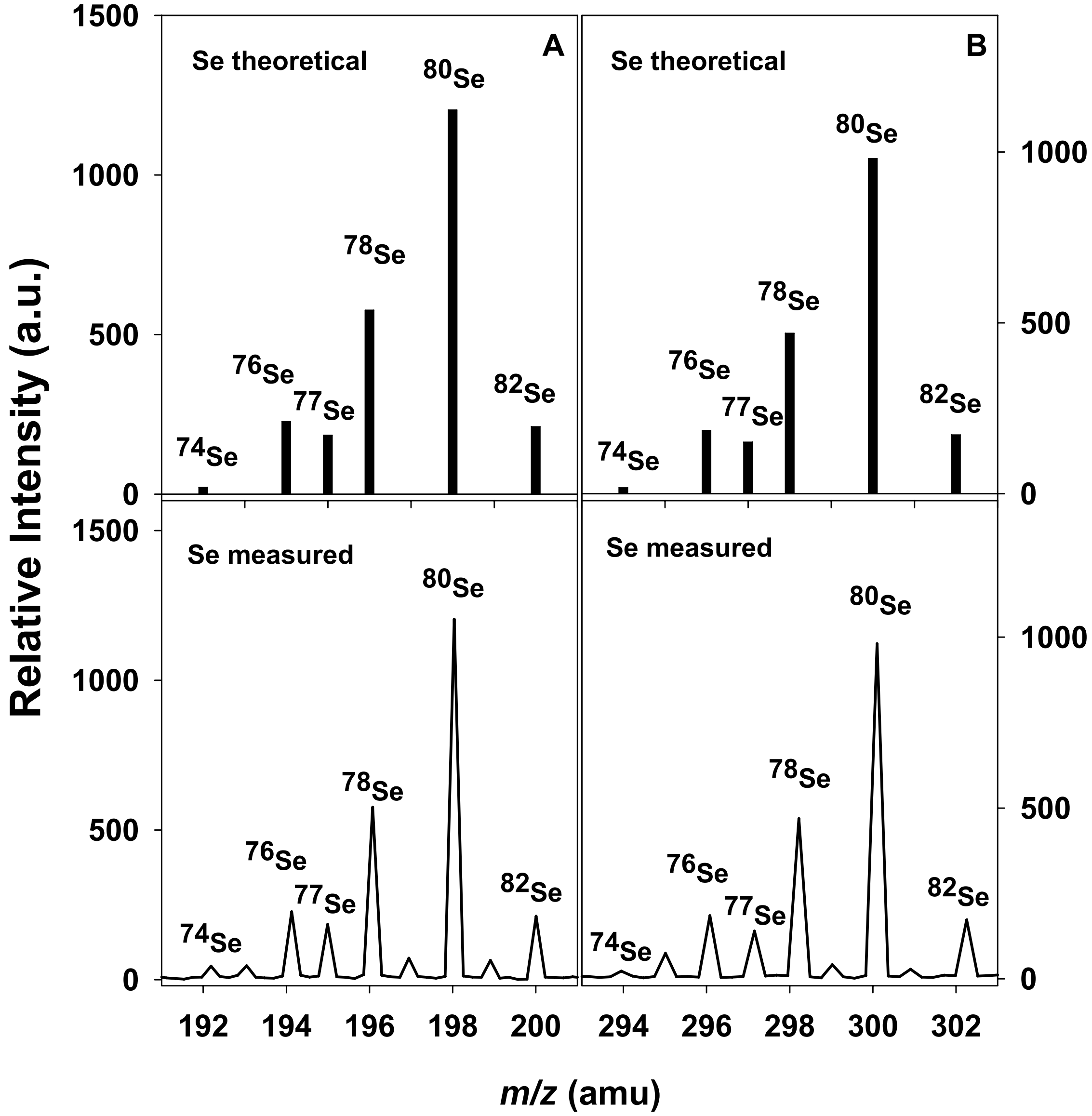

Figure 3-11 Comparison of masses corresponding to molecules containing selenium with the natural isotope abundance and measured ion signals of (A) SeMetH$^+$ and (B) N-Ac-SeGalH$^+$.

3.3.4 Sensitivity of SALDI MS

Considering that samples loaded in all SALDI MS experiments were 10 μL of 5 μg/mL standard solutions, the analyte signals were actually obtained for sample amounts as low as 50 ng (~ 250 fmol) and the detection limits were approximately in the range of 10 ~ 100 fmol (equivalent to ppb level) on various substrates. This is comparable with detection limits reported in conventional MALDI for the low molecular weight peptides and oligosaccharides.[15] Therefore, SALDI MS could be successfully applied to the analysis of small biological molecules in a variety of applications with sufficient sensitivity.

3.4 CONCLUSION

SALDI MS using graphite, porous silicon and Si(100) as substrates with simple sample preparation were investigated. Protonated molecular ions of amino acids were obtained on all three substrates without fragmentation. Background ion peaks were not found or were very limited at *m/z* > 50. The performance of SALDI on graphite and porous silicon were comparable, indicating both could be used in various applications. Thermally unstable molecules such as amino acids, peptides and metabolites were used to demonstrate the feasibility of SALDI analysis of small biological molecules. The readily interpretable mass spectra of all the tested molecules with high sensitivity and good spot-to-spot reproducibility proves that SALDI MS is a potential method for analyzing important small molecules in complex biological environments, such as free amino acid analysis in physiological fluids, peptide identification in protein digest component mapping, and metabolite detection in biological samples. SALDI MS also offers a platform with an endless range of chemical and structural modifications for proteomic, metabolic and drug screening studies. Coupling with assay technology and high resolution mass spectrometry, SALDI is a good candidate for a new generation analytical technique.

CHAPTER 4

STUDIES OF SUBSTATE, SOLVENT, ACIDITY, AND TEMPERATURE EFFECTS IN SURFACE-ASSISTED LASER DESORPTION IONIZATION/MASS SPECTROMETRY

4.1 OVERVIEW

Surface-assisted laser desorption/ionization mass spectrometry (SALDI MS) is a relatively new technique for direct analysis of low and intermediate weight molecules. This technique usually utilizes porous substrates with large surface area and high optical coefficients in the infrared, visible or ultraviolet regions to generate soft desorption/ionization. Since this method does not add matrix material to the analyte sample, it eliminates the significant matrix noise in the low-mass range which obscures or suppresses analyte ions below *m/z* 600. This also avoids the requirement of matrix selection, which is critical for signal optimization in matrix-assisted laser desorption/ionization mass spectrometry (MALDI MS), one of the most important methods for mass spectrometric analysis of large non-volatile molecules. Due to its simplified sample preparation and elimination of low-mass background signals, SALDI MS is becoming a strong candidate which may extend the limitations of MALDI MS.

As a straightforward and general approach, SALDI has demonstrated its great potential as a technique to analyze a variety of small/intermediate molecules in complex mixtures.[43, 47, 71-75] Although SALDI MS has proven valuable in many chemical, biochemical and environmental applications,[49, 65, 76] the detailed mechanisms leading to

SALDI remain unknown. It is very important to understand these mechanisms for the future development and application of SALDI MS.

Among numerous tested substrate materials[44, 70, 77-80], carbon and silicon are two of the most successful substances in SALDI analysis. Some factors controlling the ion generation on porous and graphitic surfaces have been specifically investigated in different references.[15, 81, 82] For example, various parameters such as surface morphology, optical absorption, thermal conductivity, storage condition, sample preparation, laser wavelength, and pH contributions have been emphasized or optimized. Correlations between the porous structure of silicon substrates and SALDI performance have been discussed.[81] and it has been suggested that surface morphology plays a pivotal role in the desorption/ionization process. Contrary to this hypothesis, similar experiments on porous oxide surfaces such as sol-gel, silica glass, and alumina films did not successfully generate SALDI signals.[70, 79, 80] Since SALDI applications typically use materials with proper band gaps and high absorption coefficients, electronic structure and optical properties may also be crucial. For example, the signals of SALDI on porous silicon (it is also called desorption/ionization on silicon, DIOS) has been attributed to the high UV absorptivity of silicon.[47, 66] However, no SALDI ions were obtained by UV irradiation on Si(100) crystals at room temperature.[82] In addition, surface modification,[83] substrate storage and sample solvents[81, 82] also seem to influence SALDI yields. Despite some arguments in the literatures over specific details, there are agreements that i) porous substrates provide frameworks to retain analyte molecules, ii) large optical absorption cross sections and high thermal conductivities promote the energy transfer between the substrate and analytes when irradiated by a laser.[81, 82, 84]

This chapter reports systematic studies of the fundamental processes governing SALDI. Specifically, 1) analyte molecules on three different SALDI substrates were characterized by scanning electron microscopy to reveal the states of sample molecules on surfaces, 2) temperature programmed desorption (TPD) of water on SALDI sample plates were investigated to confirm the importance of proton transfer solvents in the SALDI process, 3) SALDI MS of arginine at various temperatures (120K ~ 600K) were compared to the TPD of water and arginine to reveal the role of surface group and solvent in the desorption/ionization process, 4) substrate storage and acidity effects were further researched to understand the effect of the protonation to SALDI yields. Based on observed results, a possible mechanism of SALDI is proposed.

4.2 EXPERIMENTAL

4.2.1 Chemicals and Reagents

All solvents were HPLC grade (Fisher Scientific, Atlanta, GA, USA). Other materials/chemicals used were: (i) graphite, 99.95% purity (Alfa Aesar, Ward Hill, MA, USA); (ii) Boron-doped (100) single-crystalline silicon wafer (1-20Ω·cm) (Wafer World Inc., West Palm Beach, FL, USA); (iii) hydrofluoric acid (48%) and nitric acid (70%) (Fisher Scientific, Pittsburg, PA, USA); (iv) glycine, glutamine, histidine, arginine, and tryptophan (Sigma, St. Louis, MO, USA). Nanopure water of 18MΩ was used throughout the experiments.

4.2.2 Substrate Preparation

Graphite substrates were heated to 600 K in vacuum (10^{-8} torr) for 1 hour to remove organic contaminants and to anneal the surface. Porous silicon substrates were etched from p-type Si(100) using a $HF/HNO_3/H_2O$ (1:3:5) solution (*Caution! Hazardous and corrosive chemicals)* for 60 ~ 240 seconds according to reference [*63*] and cleaned by 1:20 HF/H_2O as well as nanopure H_2O for three times. The pore size was in the range of 40 ~ 400 nm. The obtained porous silicon substrates were then sealed in nanopure water at 4 °C before use. Si(100) substrates were cleaned by 1:20 HF/H_2O and nanopure H_2O three tines and sealed in nanopure water at 4 °C before use.

4.2.3 Sample Preparation

Solutions of amino acids (50 μg/mL for each) were prepared using nanopure water and high purity methanol. 5 mm × 5 mm SALDI substrates were cleansed by sonicating them in methanol or nanopure water for 30 minutes. 10 μL sample solutions were then directly deposited onto the SALDI substrates. The sample plates were air-dried for 10 min. in a desiccator and immediately transferred into the antechamber for further vacuum drying. Finally, the samples were transferred into the main UHV chamber for SALDI analysis. The vacuum-dried sample was also characterized by scanning electron microscopy (Hitachi S-800 SEM, Tarrytown, NY, USA).

4.2.4 Laser Desorption/Ionization Mass Spectrometry

The air-dried sample plate was loaded into the antechamber and then transferred into the analytical system by a rotary-linear magnetic transporter. The sample was positioned onto the UHV sample holder using a modified UHV compatible wobble stick.

A 20 Hz Nd:YAG laser operated at the third harmonic (355 nm) impinged on the adsorbate covered surface at a 45º incident angle. The laser was focused to a ~ 0.5 mm^2 spot area and the pulse energy was controlled in the range of 200 ~ 500 μJ/pulse. A continuous +5 kV potential was applied to the sample plate and a -1.3 kV potential was kept on the extraction grid in the ion region. The potential of first grid was about 500 V less positive than that of second grid and the tube potential is -1.9 kV. Potentials in the range of -200 V ~ -400 V were also applied across a pair of horizontal deflection plates for the optimization of signals. The SALDI ions were detected by a pair of chevron configured microchannel plates and the output was amplified, digitized, signal averaged and stored in a computer. The number of required laser shots depends on the energy of desorption laser and beam profile. For pulse energy of 200 μJ, 1000 shots were typically used.

4.2.5 Temperature Programmed Desorption

TPD measurements were made in an UHV analysis chamber, equipped with a homemade temperature control system and a quadrupole mass spectrometer (Extrel C50, ABB Analytical Instruments, Inc., Pittsburg, PA, USA). A LabVIEW program (TPD-QMS 6) with 6 mass channels was written to facilitate the experiments. The SALDI samples were heated using a button heater (HeatWave Labs, Inc., Watsonville, CA, USA) controlled by the TPD control program. The temperature increases were linear ($T=T_0+\beta T$) with β as 0.5 K/s. The H_2O (*m/z* 18) and arginine (*m/z* 174) signals were recorded using a quadrupole mass spectrometer normal to the sample surface.

4.3 RESULTS AND DISCUSSION

4.3.1 SEM Characterization of Analyte Molecules on SALDI Substrates

The analyte molecules on three different SALDI substrates i) graphite, ii) porous silicon, and iii) silicon (100) were characterized by scanning electron microscopy (Figure 4-1). The SEM images clearly showed that amino acid molecules distributed differently on these three surfaces. On rough graphite substrates, the analyte molecules localized in the big pores (2 ~ 10 μm) or the edges. On porous silicon, many small clusters (< 5 μm) of analyte molecules were observed. Because of the resolution limit of the SEM instrument, molecules in the pores (40 ~ 400 nm) of porous silicon were not visible in this study. However, the microstructure of porous silicon[85] and ordered silicon arrays[86] had been reported to confirm the sample trapping. In contrast to the sample distribution on graphite and porous silicon, the analyte molecules aggregate as spherical clusters (> 20 μm) on silicon (100) surfaces.

In chapter 3, the SALDI signals of amino acids on different substrates have been reported. Comparing those results with SEM images, an "apparent" link between surface morphology and SALDI yields were found. On rough surfaces such as graphite and porous silicon, molecular ions of analyte molecules could be easily obtained. *It is very clear that the porous structure plays an important role in promoting SALDI signals.* The SEM results were very useful on understanding how a rough surface facilitates the laser induced ion generation. On a single crystal, large clusters of analytes were formed and thus there was less interaction between the sample and the substrate. Whereas, the analyte molecules on porous surfaces were well distributed in pores or on specific

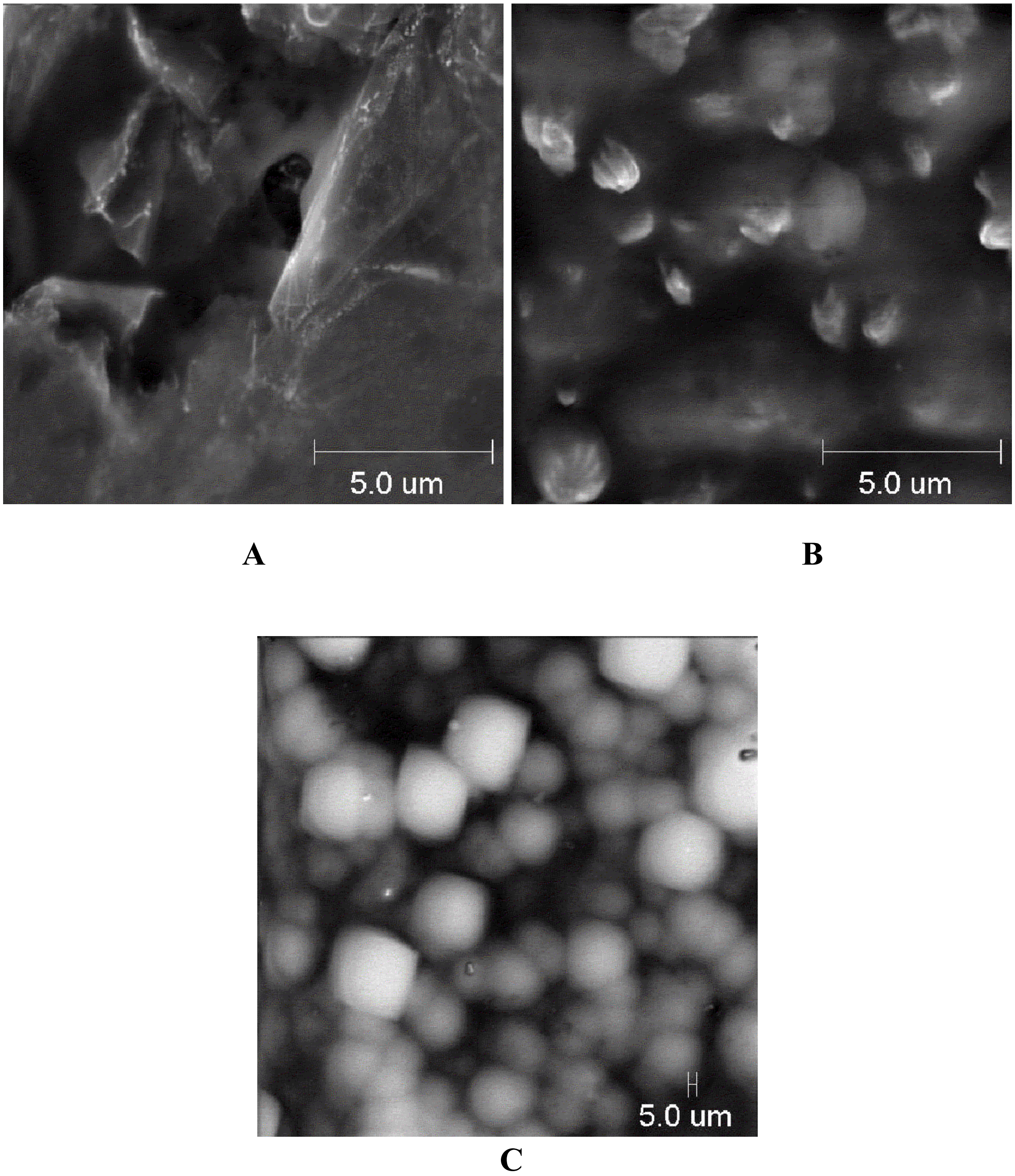

Figure 4-1. SEM images of 6 amino acids (5ug/mL) on (A) graphite (B) porous silicon, and (C) Si(100).

structures such as edges and terrace. This can greatly improve the sample-substrate interaction and energy transfer. Furthermore, the porous structure could contain more solvent to solvate, protonate, and stabilize analyte molecules, which is critical to enhance desorption and ionization in SALDI.

4.3.2 TPD of Water on SALDI Substrates

TPD of water on graphite, porous silicon, and Si(100) with sample depositions were investigated to confirm the importance of solvents in the SALDI process. Water molecules were found clearly on all of the three substrates. To quantitatively analyze the amounts of water on the different substrates, water was dosed onto clean Si(100) substrates and the TPD peak area for the coverage (monolayer, ML) was determined. A conversion constant was then obtained. By integrating the TPD peak areas shown in Figure 4-2, the numbers of water molecules on each substrate were estimated as 10^{18}, 10^{19}~10^{20}, and 10^{16} on graphite, porous silicon, and Si(100), respectively. Compared to the amount of analyte molecules (10^{15}), the numbers of solvent molecules were at least three orders of magnitudes higher on the porous surfaces.

The desorption energies of water on different substrates were also interpreted and calculated using the Polanyi-Winger equation.[87, 88] In equation 4-1, θ_M is the

$$-\frac{d\theta_M}{dT} = \frac{\upsilon \cdot \theta_M^n}{\beta} \cdot \exp\left(\frac{-E_{des}}{R \cdot T}\right) \qquad \text{(Equation 4-1)}$$

instantaneous coverage, n is the kinetic order (desorption order), E_{des} is the desorption energy, β is the heating rate, R is the gas constant and T is the temperature. Assuming a first order desorption (pre-factor $\nu = 10^{13}\ s^{-1}$) and a linear sample temperature increase (β= 0.5 K/s), TPD curves in Figure 4-2 were fit and the extracted desorption energies are listed in Table 4-1. The TPD of water on graphite and Si(100) were relative similar. The broad TPD peak on graphite indicates transport limits due to porous structure and the solvent molecules were mainly interacting with analyte molecules with a desorption energy of 105.1 kJ/mol, which was higher than the hydrogen bond energy in ice (~31 kJ/mol) and in liquid water (~ 28 kJ/mol).[84] Two shoulders in the TPD from Si(100) at high temperatures reveals different chemisorption states on Si terminal groups with stronger interaction. On porous silicon, the TPD of water is very complicated, due to the complex chemical and physical properties of silicon pores. It is also noticed that the major water desorption energies on porous silicon were much lower than on graphite and Si(100). Therefore, the water molecules in silicon pores should have weaker interactions with the surface and should provide solution-like environments, which may facilitate solvation, transportation and desorption of analytes.

Since solvent molecules could be involved in several steps of SALDI, such as sample diffusion, ion solvation, proton transfer, electron transfer, energy transfer, and thermal expansion, the analysis of solvent on substrates is very relevant to understanding the mechanism of SALDI. Although UV laser irradiation could not produce satisfactory SALDI results on silicon single crystals, infrared laser irradiation has been reported to successfully ionize target molecules (up to 6 kDa) on Si(100) wafers.[77] It has been postulated that IR photons were absorbed by the solvent and lead to the desorption and ionization of analyte molecules. The existence of water molecules on Si(100), graphite

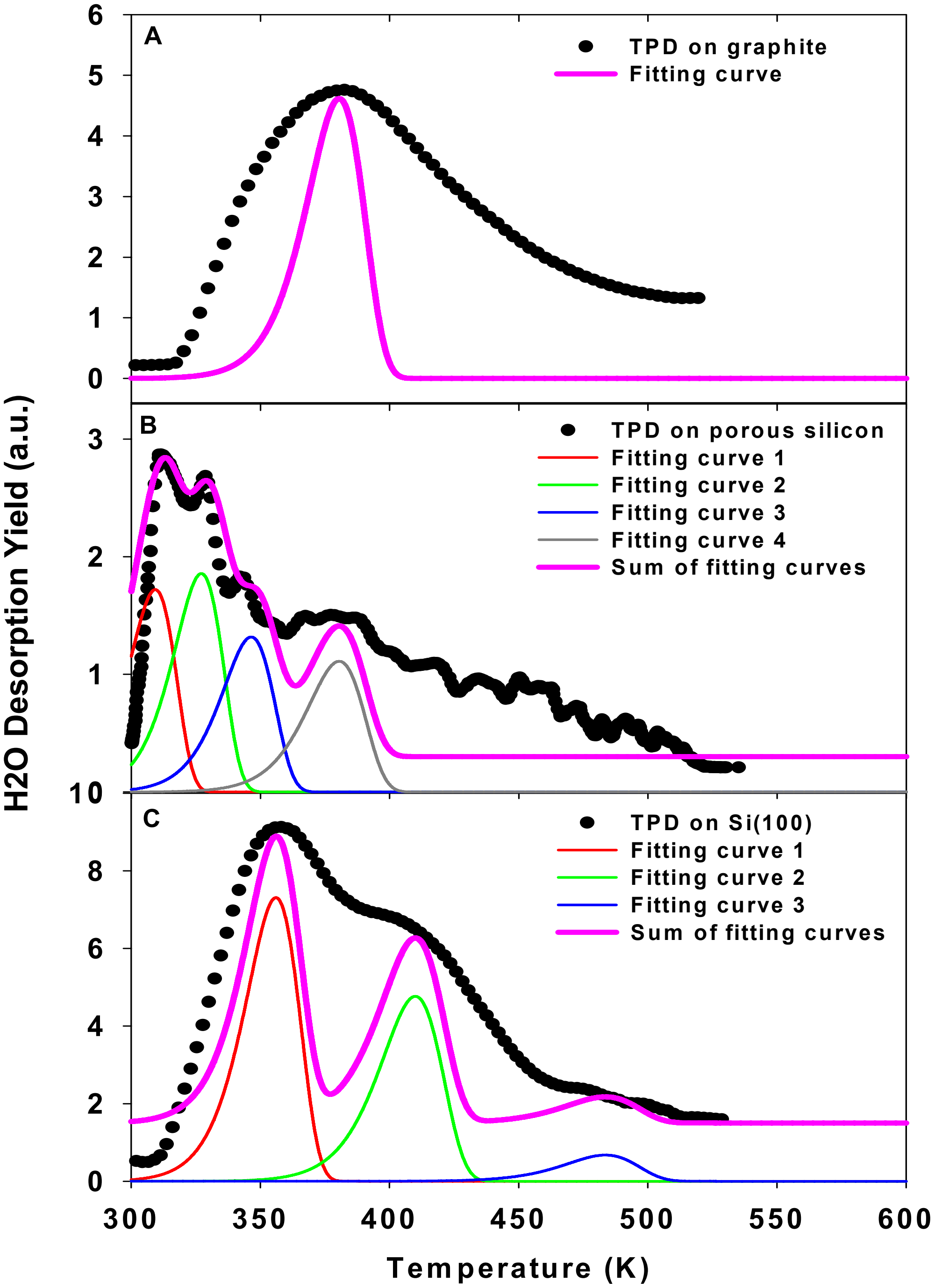

Figure 4-2 TPD of water on three SALDI substrates. (A) graphite; (B) porous silicon; (C) Si(100). The experimental data are given by the black dots; the fitting curves are shown by color lines, and the sums of fitting curves are represented by pink lines.

Table 4-1. Desorption temperatures and energies of water on three surfaces

Substrates	Desorption Temperature(K)	Desorption Energy(kJ/mol)
Graphite	392	105.1
Porous Silicon	315	84.84
Porous Silicon	328	89.88
Porous Silicon	349	95.34
Porous Silicon	375	102.9
Si(100)	352	98.07
Si(100)	410	113.4
Si(100)	480	134.4

and porous silicon could support this proposed mechanism. We have therefore examined the role of water and methanol in the SALDI process.

4.3.3 Solvent Effects in SALDI

Solvent effects on SALDI of amino acids were investigated by using pure water or pure methanol as solvents. The concentration of each amino acid is in both solutions was 5 µg/mL. The two different solutions were first deposited on graphite substrates to directly compare their SALDI yields. The same experiments were also carried out using porous silicon surfaces.

Fig 4-3 shows that SALDI yields on graphite were greatly enhanced by using water as the solvent. The protonated molecular ion (M+H) intensities of all five amino acids from water solutions were 7-15 time higher than those from methanol solutions. This sharp difference suggests that water molecules likely act as a matrix to assist the laser desorption and ionization on graphite. Based on the results of the water TPD (Figure 4-2), more than 10^{18} water molecules (100 ML) were co-adsorbed with amino acids (~10^{15} molecules) on the graphite surface. The excessive water molecules provide protons to the analytes and stabilize the protonated species to facilitate the soft ionization. The water molecules could also help the analyte diffuse and cover the substrate uniformly to improve the spot-to-spot reproducibility. During laser irradiation, the energy absorbed by the graphite could also be transferred to the water molecules to assist the thermal vaporization or explosive desorption. Therefore, SALDI on graphite is more likely to be a two-phase MALDI process. The graphite substrate is the solid matrix which serves to trap water and the analytes in its rough surface pores as well as an energy transfer

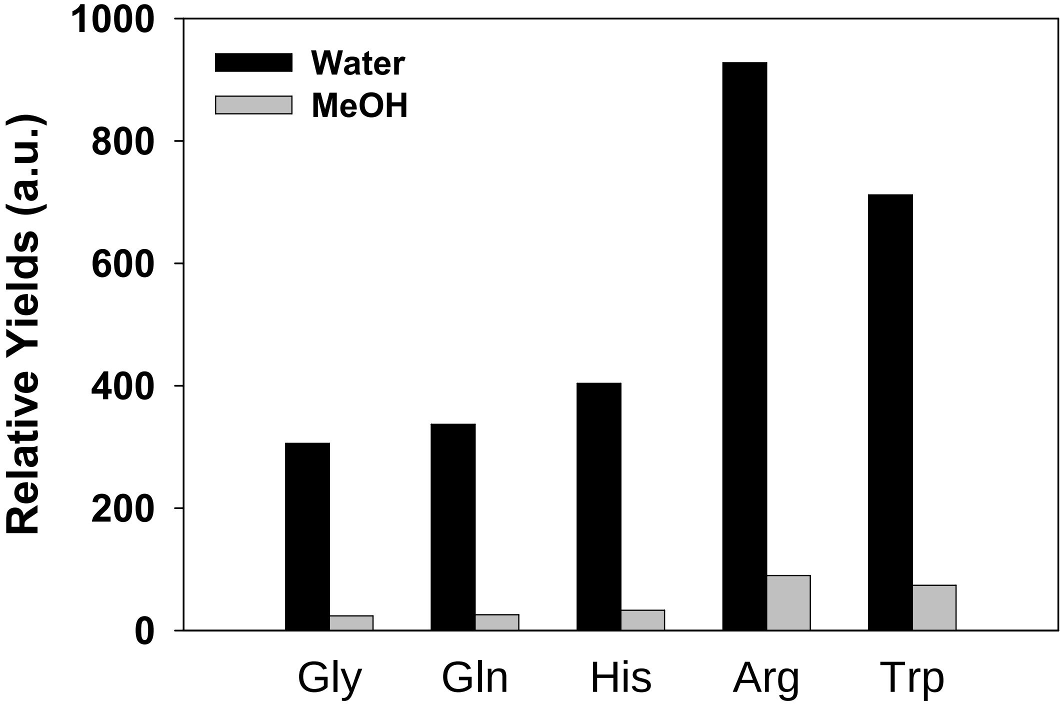

Figure 4-3. Solvent effects of SALDI MS on a graphite substrate

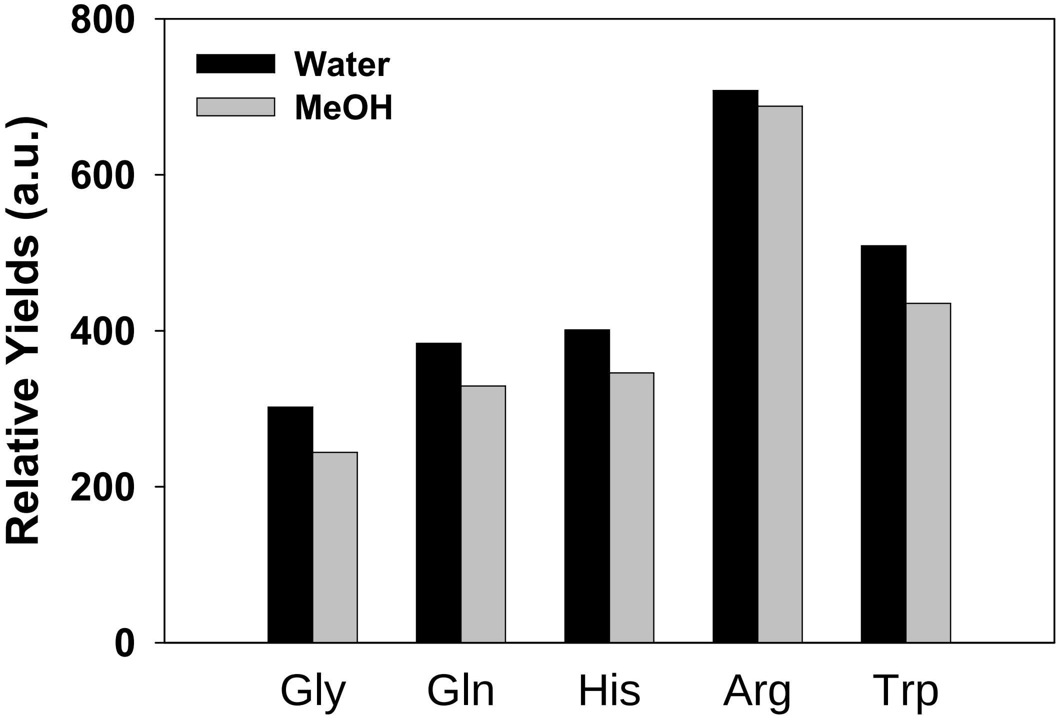

Figure 4-4. Solvent effects of SALDI MS on a porous silicon substrate.

medium. Water molecules are the liquid matrix, which can obviously assist proton transfer. Methanol is a relatively weaker proton source and a less-efficient matrix in the SALDI process. Compared to the previously reported two-phase matrix studies using fine graphite particles in liquid suspension,[15, 89] SALDI on graphite has more advantages, such as higher sample capacity, easier sample preparation and less ion source contamination.

Fig 4-4 shows the SALDI yields of 5 amino acids deposited on porous silicon substrates using water and methanol solutions. Interestingly, the ion yields of the amino acids on porous silicon substrates did not demonstrate obvious differences between the two solvents as observed on graphite. On porous silicon, the ion intensities generated by both solvent systems were close to the SALDI results from the water solution on graphite. This indicates that the SALDI mechanisms from graphite and porous silicon are probably similar, especially when water exists.

One of the major differences between graphite and porous silicon is the surface termination group. The surface groups on graphite are usually C-H, but porous silicon surfaces could be terminated by Si-H, Si-OH or Si-O_x at different post-etching conditions. It is has been suggested that specific termination groups (such as Si-OH) on porous silicon could serve as proton sources[83] and directly transfer energy to analyte molecules leading to ionization and desorption. Thus, porous silicon does not have a strict requirement of proton source in the SALDI process as graphite does. That is why samples prepared by methanol were also able to generate similar ion yields as aqueous solutions on porous silicon, but have much weaker signals on graphite.

4.3.4 Storage of SALDI Substrates

The important roles of the surface terminating group in SALDI on porous silicon are further supported by results and discussions in the sections on substrate storage (section 4.3.5) as well as SALDI at different temperatures (section 4.3.5).

It has been found that DIOS chips stored in methanol solution produced higher ion yields compared to those kept in dry air storage.[81] The effect of surface wetting was mentioned as a possible explanation for preserving SALDI efficiency. Under dry air, the porous silicon could be rapidly oxidized by O_2 to form Si-O_X terminated surfaces. The oxidation layer may dramatically decrease the energy or proton transfer between the silicon substrate and analyte molecules, which is necessary for the SALDI process. In addition, the thermal conductivity of the porous silicon surface is also drastically altered by the formation of oxidation layers. Since thermal contact is critical to desorption, it is reasonable that the signal generation was reduced by exposing porous silicon to dry air for a longer period of time. In contrast, the porous substrates stored in methanol solution could keep the surface terminated by Si-OH groups. Therefore, these substrates should show better SALDI activity.

It was also reported that porous silicon chips could maintain their SALDI activity over longer periods of time at low storage temperatures.[14] This result might also be related to surface groups. At low temperature, solvents have lower evaporation and oxidation rates. The residual solvent in the porous structure could keep the surface terminated by Si-OH. The Si-OH groups change the surface from hydrophobic (Si-H terminated surface after HF etching) to hydrophilic, which greatly facilitates the uniform distribution of analyte molecules and energy transfer during laser desorption/ionization.

The Si-OH groups on the surface may also act as proton sources during the SALDI process to enhance the molecular ion signals.

The porous silicon substrates used in the experiments discussed in this thesis were stored in water at 4 °C right after etching. The SALDI activity could be kept for more that four weeks. If the porous substrates were exposed to air, the SALDI signal declined ~ 95% after 7 days. This observation is consistent with previous references[14, 81] and discussions above.

4.3.5 SALDI Yields at Different Temperatures

To fully understand the solvent effects, a series of SALDI experiments were performed on porous silicon at different temperatures. Figure 4-5A shows protonated arginine molecular ion yields from 120 K to 600 K. The dependence of SALDI signals on temperatures was compared to the TPD of arginine (Figure 4-5B) and the TPD of water (Figure 4-5C).

The role of solvent (water) was clearly demonstrated in the low temperature region below 200K. When the substrate temperature exceeds 150 K, the SALDI signal decreased dramatically as water molecules began to desorb from the surface. Most of the physisorbed arginine molecules also desorbed together with the water solvent. This result firmly proves that a physisorbed water layer is necessary for the generation of SALDI signals. It is important to note that Si(100) surfaces could only produce molecular ion signals at low temperature. This indicates that a minimum number of water molecules are required to facilitate the SALDI. Another important feature in Figure 4-5 is that the SALDI yield dropped to a relative low level when the thermal desorption of arginine reached its maximum, but did not disappear. Rather, it remained at a fixed level until the terminated OH groups were desorbed. In the high temperature region, the SALDI yields showed a strong dependence on the surface terminal group Si-OH. When the surface temperature was high, the Si-OH groups on silicon could decompose and release H_2 and H_2O via recombinative desorption.[90] This is shown in Figure 4-4C as the H_2O TPD signal increased from 560 K. Along with the decreasing of Si-OH groups on the porous silicon surface, chemisorbed arginine also showed a desorption peak at 560 K. This peak demonstrates that some arginine molecules had relatively strong adsorption on the silicon surface groups. The disappearance of SALDI signals beyond 560K proved that Si-OH was closely related to the SALDI process. It also demonstrates that the existence of Si-OH facilitates the high SALDI signals from methanol solutions on porous silicon.

In the temperature range between 200 ~ 550 K, the SALDI results and TPD results were not comparable because of their different initial states. However, both chemisorbed solvent and arginine were observed at room temperature. The SALDI yield around 300 K confirmed the solvent acts as a matrix to assist the ionization and desorption.

4.3.6 Acidity Effects in SALDI

Acidity effects in SALDI were studied by adding HCl to adjust the acidity of sample solution from pH = 6 to pH = 1. In figure 4-6, the SALDI signal on graphite and porous silicon showed similar trends at these two pH values. The protonated molecular ion yields were enhanced by 20 to 30 times when acid was added. This observation is in

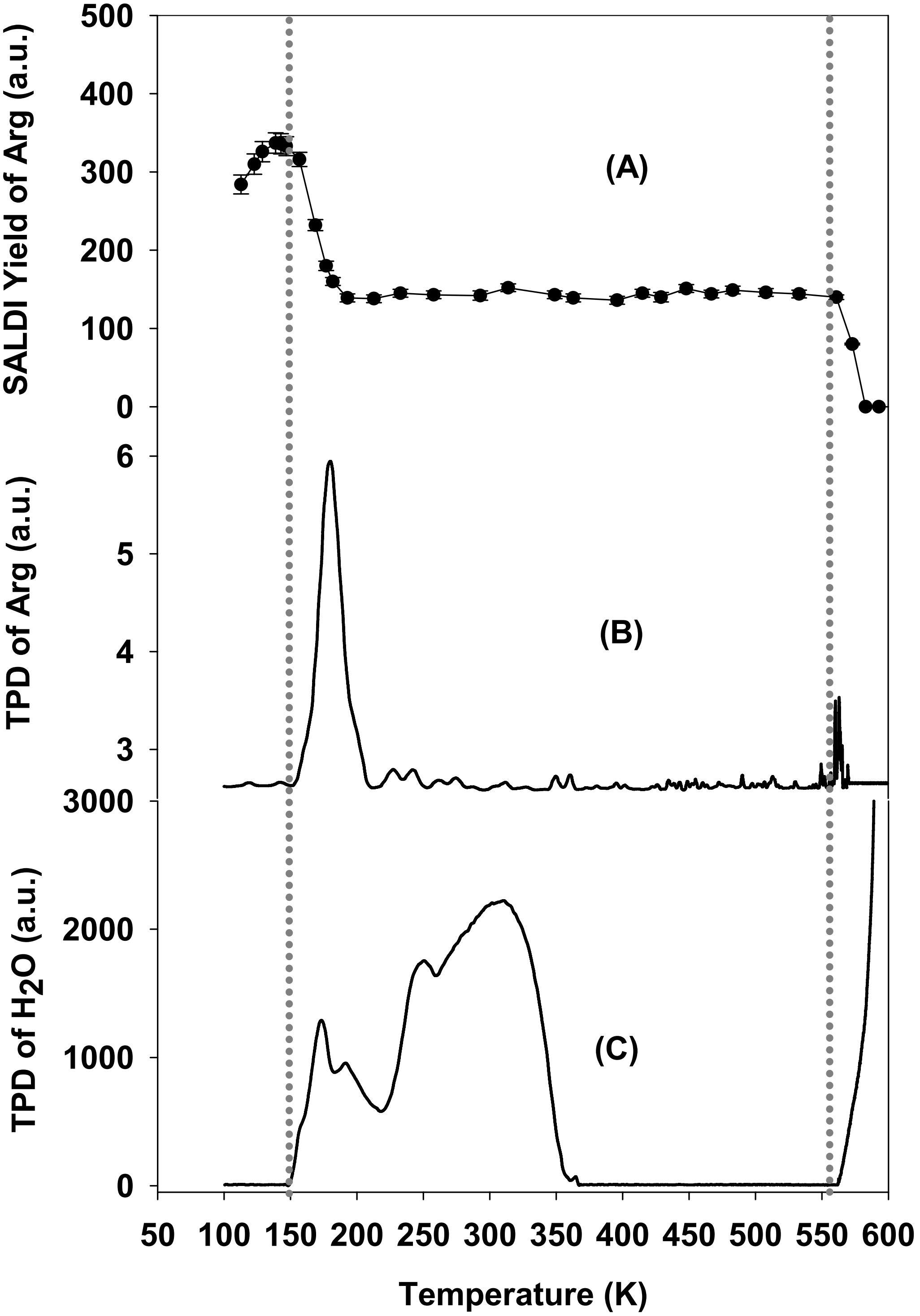

Figure 4-5. A comparison of (A) Arg SALDI at different substrate temperatures, (B) Arg TPD, and (C) water TPD from aqueous solution of arginine on porous silicon.

agreement with the previous discussion, as the addition of acid promotes the protonation of analyte molecules. The proton affinities of five amino acids[91] were compared with their SALDI yields on graphite and porous silicon in Table 4-2. The good correlation of the yields with proton affinities demonstrates that protonation, either before or during laser excitation, is critical to the SALDI process.

4.3.7 Mechanism of SALDI on Graphite and Porous Silicon

Based on the results of solvent, temperature, and pH effects on different substrates, possible mechanisms of SALDI on graphite and porous silicon were proposed. When water is used as the solvent to deposit samples, the SALDI process could be described as two-phase MALDI. Graphite or porous silicon could be considered as a solid "matrix". In this case, the substrate (i.e. solid "matrix") absorbs the photon energy and transfers the energy and protons to the water and analytes. The solvent molecules, such as water, act as a liquid "matrix" to transport protons and energy to the analyte molecules. The energy exchange and Coulomb force associated with hole production and protonation facilitate desorption. Similar to MALDI, certain amounts of matrix molecules were necessary for effective ionization and desorption. The porous structure is favorable because it could contain more solvent molecules and enhance solvation and proton transfer. Since Si(100) is not able to provide enough co-adsorbed water at room temperature, it requires low temperature to freeze physisorbed water layers. Si-OH groups also seem to be required for SALDI on porous silicon and this likely enhances the energy exchange at the interface. It could also protonate and stabilize analyte molecules to accomplish SALDI when the

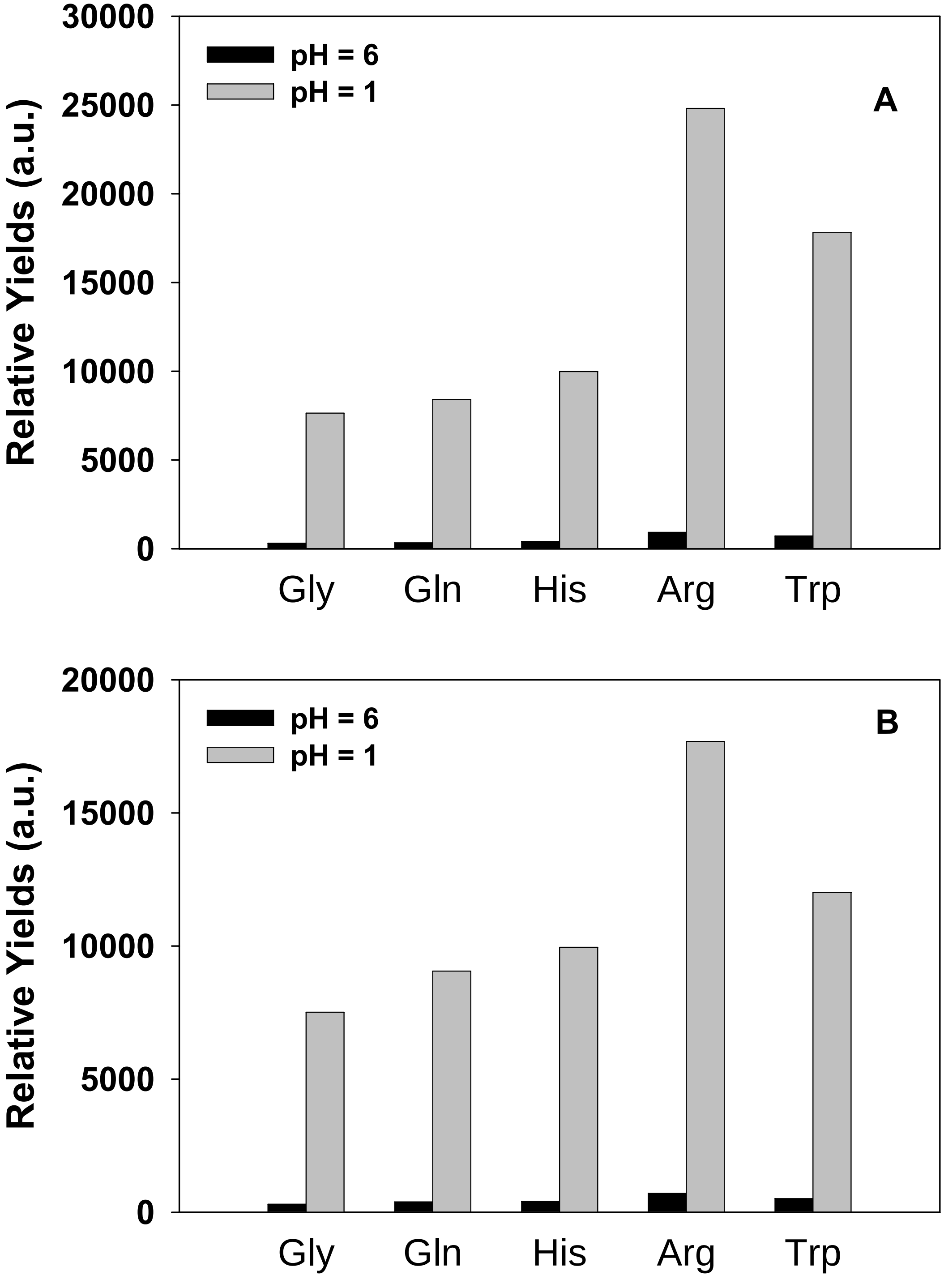

Figure 4-6. pH effects in SALDI of amino acids on (A) graphite and (B) porous silicon

Table 4-2. Comparison of proton affinities of amino acids with their SALDI yields

Proton Affinity[91]	Arg	>	Trp	>	His	>	Gln	>	Gly
(kcal/mol)	243.2	>	231.0	>	228.5	>	222.0	>	211.7
SALDI on graphite	Arg	>	Trp	>	His	>	Gln	>	Gly
SALDI on porous silicon	Arg	>	Trp	>	His	>	Gln	>	Gly

solvent was not an effective liquid matrix. The loss of Si-OH groups by oxidation would directly lead to the deactivation of the silicon substrate.

In view of the observations discussed in this chapter, graphite substrates, which are relatively easy to prepare, are recommend for SALDI of aqueous samples. Porous silicon substrates, which are also called DIOS chips, must be stored properly and require the presence of terminal hydroxyl groups to generate SALDI signals.

4.4 CONCLUSIONS

Surface morphology, TPD of solvent molecules, post-etching storage, solvent, temperature, and pH effects on graphite and porous silicon have been investigated and discussed to optimize SALDI MS performance and to explore the mechanisms of this laser desorption/ionization technique. The SEM analysis of analyte molecules on different SALDI substrates indicates that surface morphology is important to SALDI by trapping both the analyte and the solvent. This can facilitate sample distribution and assist efficient energy transfer. The existence of water molecules as an important solvent for SALDI from graphite and silicon was demonstrated by the TPD studies. Relative desorption energies of water molecules were obtained for elucidating the interactions among analyte, solvent, and substrates. Post-etching storage conditions and possible reasons of surface degradation were also discussed to improve the lifetime of porous silicon substrates. Mechanisms of SALDI on graphite and porous silicon were speculated based on reference works and results reported in this chapter. The crucial function of Si-OH in SALDI on porous silicon (DIOS) was revealed. Finally, it is stated that matrices (solvent and substrate) are actually present and critical to the SALDI technique, even though no traditional MALDI matrix is added.

CHAPTER 5

ANALYSIS OF ORGANOSELENIUM AND ORGANIC ACID METABOLITES USING LASER DESORPTION SINGLE PHOTON IONIZATION MASS SPECTROMETRY

5.1 OVERVIEW

Laser desorption techniques have been used for decades by the surface physics and chemistry communities to analyze adsorbate geometries and surface reactions. Currently, these types of experiments are yielding site specific information with unprecedented sensitivity, particularly for semiconducting[92, 93] and ionic materials.[94, 95] Chemists have also exploited laser desorption techniques to examine the removal of analytes which are often in the form of an adsorbate[88, 96] or embedded within a complicated matrix. In the latter case, the technique known as matrix-assisted laser desorption ionization (MALDI) has been developed and effectively utilized.[7, 13, 35, 97-100] In addition, when certain substrates are irradiated with relatively high fluxes, the stimulated desorption of ions can occur. In general, the formation of ions in the absence of a matrix is thought to be related to the electronic properties of the surface and thus this technique is sometimes referred to as surface-assisted laser desorption/ionization mass spectrometry (SALDI MS).[43, 72, 86, 101, 102] In reality, the process typically involves i) formation of an electron-hole plasma within the material, ii) a proton plasma at the interface, and iii) a hole or proton transfer event. In fact, our recent work in this area indicates that two of the most important parameters in SALDI are the inherent porosity and presence of a proton source such as water.[103]

SALDI MS is particularly valuable in the identification of small organic molecules because of the low level of background chemical noise in the mass region of *m/z* < 600. In previous work, ultraviolet laser induced SALDI MS was used to simplify sample identification by desorbing and ionizing analytes from carbon and sol-gel substrates.[72] The small background noise enabled reliable molecular mass determination using a high resolution mass spectrometer for correct speciation. However, this approach requires specific procedures to prepare substrates with optimum properties for reproducible results.

Two step laser desorption photoionization mass spectrometry has proven to be a powerful analytical technique for characterizing a wide range of molecular systems. This technique uses one laser to stimulate desorption of intact neutral molecules, and a second laser to ionize the desorbed molecules.[21, 104-111] Typically, photoionization is achieved via laser resonance enhanced multiphoton ionization (REMPI) or vacuum ultraviolet single photon ionization (VUV-SPI). REMPI is a highly sensitive and selective method for ionizing molecules via resonant rovibronic transitions with typical detection sensitivities as low as 10^5 molecules/cm^2/quantum state.[94, 95, 112] REMPI is also an excellent method for detecting small aromatic molecules or biomolecules with aromatic groups, such as polycyclic aromatic hydrocarbons (PAHs), ambient aerosols, serotonin, tryptamine, indole, and small peptides containing tyrosine, tryptophan, or phenylalanine.[15, 111, 113-120] However, REMPI is less suitable for aliphatic compounds, which represent the majority of small organic and biological molecules. In contrast, SPI is amenable for both aliphatic and aromatic compounds. Most SPI experiments use pulsed or continuous VUV radiation with a photon energy higher than 10 eV.[108] One of the most commonly used SPI wavelengths is 118 nm (10.5 eV) and this is produced from the 355 nm output of a pulsed YAG via non-linear third harmonic generation in xenon gas mixtures.[19, 68] Since the ionization potentials (IP) of most organic species range from 7 to 10 eV,[88] SPI deposits less excess energy into the resultant ion and reduces fragmentation of molecular ions. This makes SPI a soft ionization method with nearly uniform sensitivity for most neutrals. Combined with laser desorption, single photon ionization provides more efficient ionization than secondary ion mass spectrometry (SIMS), direct non-resonant laser ionization (LDI), MALDI and SALDI. This is largely due to the fact that the neutral desorption yields are typically 3 to 4 orders of magnitude greater than the ion yields.[121, 122] Laser desorption with single photon ionization mass spectrometry (LD/SPI MS) has reported detection limits in the low ppb (fmol) range.[21, 123] In addition, SPI also greatly reduces the solvent ion suppression and adductive ions from sodium and potassium in biological samples.

Although LD/SPI MS has been used to investigate some standard biological molecules and ambient particles such as aerosols, there are no reports on the direct analysis of metabolites from complex biological samples using this technique. Selenium (Se) is an essential ultra-trace element in the human body.[23] Although it is indispensable for human health, Se has been found to have both toxic and beneficial effects, which are concentration and species dependent.[124] Se metabolites, especially organoselenium compounds (Figure 5-1), have been linked to toxicity, antioxidant enzymes, endocrine processes, and proper functioning of the immune system.[49, 56, 61, 125-129] Therefore, there is

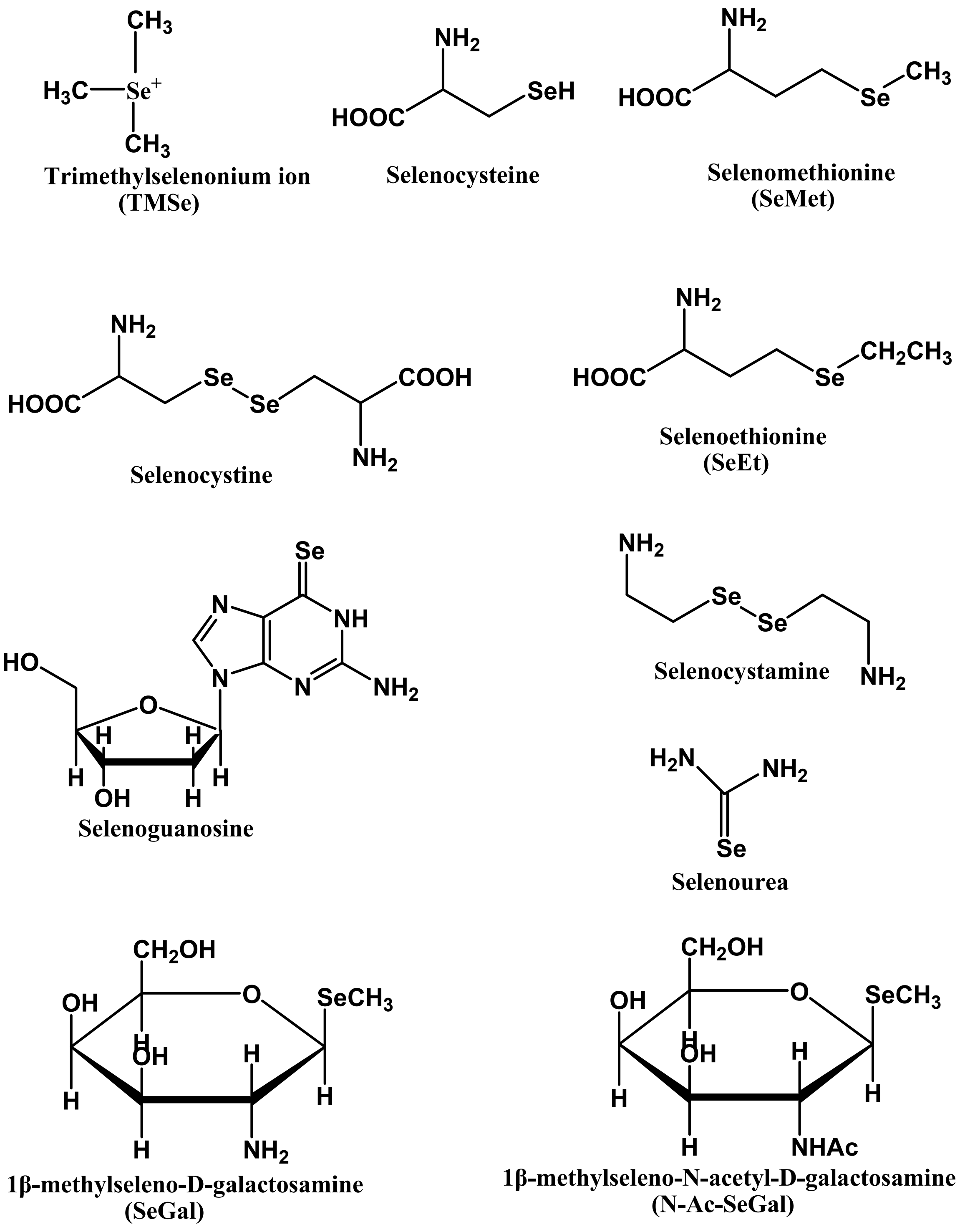

Trimethylselenonium ion (TMSe)

Selenocysteine

Selenomethionine (SeMet)

Selenocystine

Selenoethionine (SeEt)

Selenoguanosine

Selenocystamine

Selenourea

1β-methylseleno-D-galactosamine (SeGal)

1β-methylseleno-N-acetyl-D-galactosamine (N-Ac-SeGal)

Figure 5-1. Structures of possible organoselenium metabolites.

intense interest in these compounds in the biochemical, biological and pharmaceutical communities.

Although high performance liquid chromatography coupled with inductively coupled plasma mass spectrometry (HPLC-ICP MS) is among the more popular techniques used to detect Se metabolites in urine, it has many drawbacks associated with retention time issues, loss of structural/molecular information and interferences from overlapping masses.[130-132] Recently, HPLC-ICP MS has been combined with HPLC-ESI MS/MS and CE-nano-ESI MS^n to provide good quantitative results and reliable speciation for metabolites.[133-135] However, this approach is feasible only when authentic selenium metabolite standards are available, which is not often the case in many real applications.

In this work, laser desorption single photon ionization mass spectrometry is developed for the analysis of low molecular weight organoselenium compounds and organic acids within complex biological fluids such as human urine. This demonstrates the utility of this approach in the detection of metabolites in biological samples. In following sections, the apparatus and experimental protocol are first illustrated. The calibration data, detection sensitivities, time-of-flight distributions and analysis of standard as well as urine samples are then described. Finally, discussions of the biochemical relevance of trace detection of selenium metabolites and conclusions are presented.

5.2 EXPERIMENTAL

5.2.1 SPI MS Instrumentation

The schematic diagram of the experimental setup is similar to those typically used in quantum-resolved electron- and photon-stimulated desorption studies.[112, 136, 137] The apparatus shown in Figure 5-2 is a custom designed ultra high vacuum (UHV) chamber (background pressure of ~ 10^{-9}-10^{-10} torr) equipped with a linear transfer antechamber, a sample holder with an XYZ controller mounted on a 360º rotation stage, a third harmonic generation (THG) cell and a home-built linear TOF mass spectrometer. The sample plate was loaded into the antechamber and then transferred into the analytical system by a rotary-linear magnetic transporter. The sample was positioned onto the UHV sample holder using a modified UHV compatible wobble stick. A 20 Hz Nd:YAG laser operated at the third harmonic (355 nm) impinged on the adsorbate covered surface at a 45º incident angle. The laser was focused to a ~0.5 mm^2 spot area and the pulse energy was controlled in the range of 50 to 500 μJ/pulse. The VUV photons (118 nm, 10.5 eV) were obtained by frequency tripling another 355 nm ND:YAG laser using a THG cell filled with high purity xenon gas. The 118 nm photon intensity was optimized by increasing the 355 nm laser power and adjusting the pressure of xenon. In this work, the 20 Hz 355nm laser II (~ 25 mJ) was focused in the THG cell by a quartz lens (200mm) and the xenon pressure was adjusted to ~ 7 torr by observing the highest ionization signals from neutral molecules. The VUV pulse energy was not measured but is expected to be approximately 0.1μJ based on an approximate conversion efficiency of 10^{-5} reported in literature.[21,22] To avoid multiphoton ionization from the 355nm laser, the 118 nm photons were separated from the 118nm/355nm beam by taking advantage of the chromatic aberration of a LiF (f = 75 mm) lens. This lens also functioned as the entry

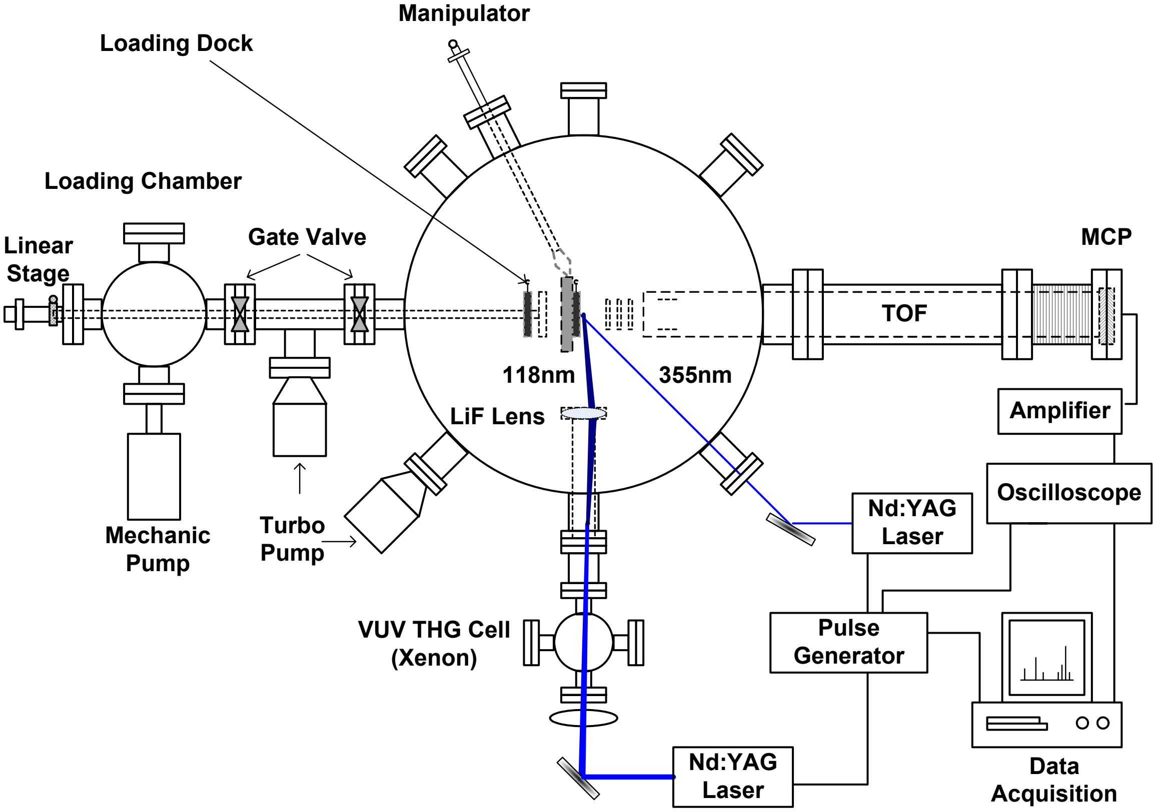

Figure 5-2. Schematic of laser desorption single photon ionization mass spectrometry.

window and the spatially separated beams were focused in front of the sample surface. The distance between the sample surface and 118 nm beam is about 1 ~ 2 mm. The delay time between the desorption laser (355 nm) and ionization beam (118 nm) was controlled by pulse generators and the optimal delay time varies from different substrate and sample molecules (Figure 5-3). In this work, a delay time from 7 μs to 15 μs was optimal for the analysis of selenium metabolites on graphite surfaces. By applying a continuous +5 kV potential to the sample plate and -1.3 kV potential to an extraction grid in the ion region, the ions generated by the desorption laser were quickly removed from the source region. The neutral molecules were then ionized by 118 nm photons at a proper delay time and analyzed by TOF mass spectrometer. The potential of first grid is about 500 V less positive than that of second grid and the tube potential is -1.9 kV. Potentials in the range of -300 V were also applied across a pair of horizontal deflection plates for the optimization of signals. The ions were detected by a pair of chevron configuration microchannel plates and the output was amplified, digitized, signal averaged and stored in computer. The number of required laser shots depends on the desorption laser energy and beam profile. For pulse energy of 50 μJ, 500 shots were typically used.

5.2.2 Chemicals and Reagents

All solvents used were of HPLC grade and (Fisher Scientific) OPTIMA trace metal grade water (Fisher Scientific) was used to prepare all standard aqueous solutions. Other chemicals used were as follows: (1) graphite substrate (Alfa Aesar), (2) glycine, glutamine, methionine, histidine, arginine, tryptophan, seleno-DL-methionine, Selenoethionine, selenocystamine, selenocystine, selenourea, selenoguanosine, and heptafluorobutyric acid (HFBA) (Sigma Chemicals) and (3) trimethylselenonium iodide

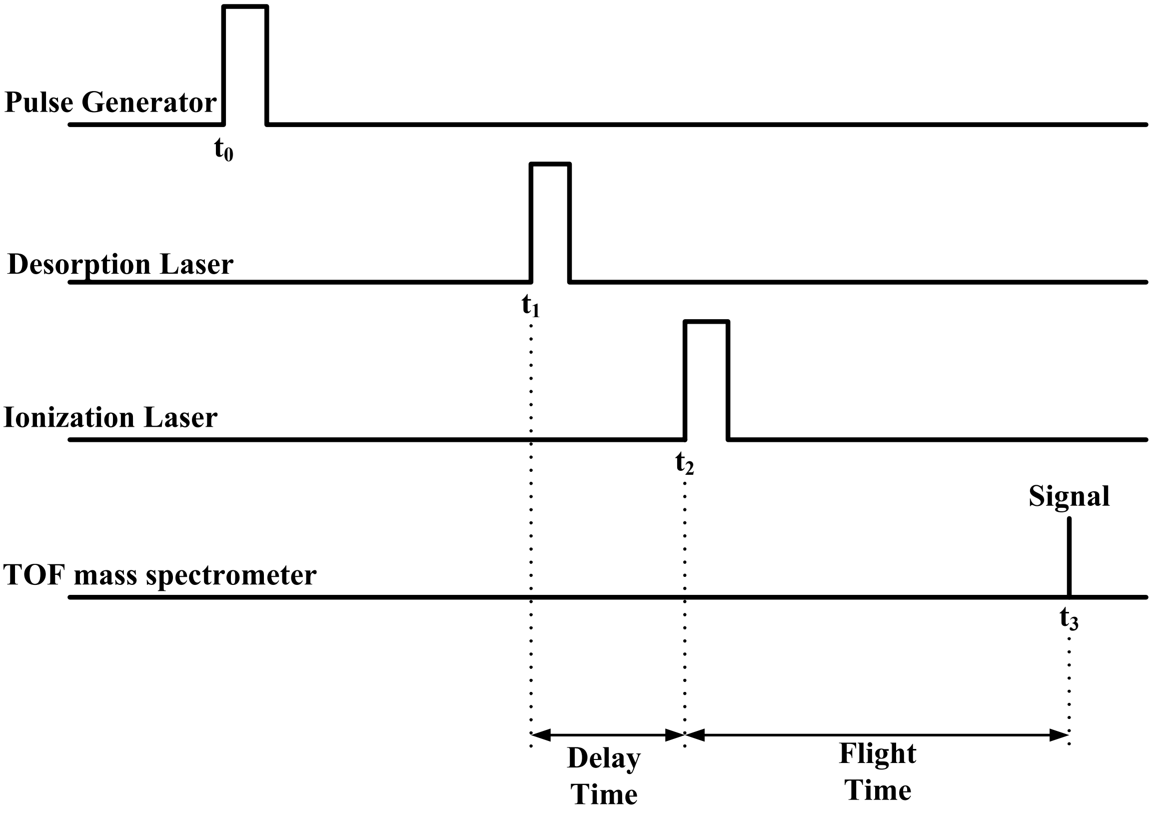

Figure 5-3. Pulse sequence of laser desorption single photon ionization mass spectrometry.

(TMSeI) (Organometallics Inc.), and (4) 1β-methylseleno-N-acetyl-D-galactosamine(N-Ac-SeGal) (synthesized in a modified version according to reference [23], details of the synthesis are described in chapter 2). Working standards were prepared daily.

5.2.3 Urine Sample Preparation

Urine sample preparation was modified from the method reported in ref [133]. Briefly, urine samples were collected from an adult man for seven consecutive days after a daily single intake of 200 µg of seleno-DL-methionine. The urine samples collected were stored at -76 ºC in pre-cleaned Teflon containers to minimize contamination or adsorption loss. Certain amounts (20 - 50 mL) of urine samples were then lyophilized using a freeze-dry system and then reconstituted to 1:10 with OPTIMA water. The reconstituted samples were centrifuged at 5000 rpm for 5 minutes and the supernatants were filtered through a 0.2 µm syringe filter. The pretreated urine samples were divided into two groups: Group A samples were directly deposited on graphite substrates for SPI analysis; Group B samples were further separated by HPLC-ICP MS.

5.2.4 HPLC-ICP MS Conditions

The details of HPLC-ICP MS operation conditions can be found in a previous paper.[133] Briefly, pre-concentrated urine samples (Group B) were first separated by HPLC and run through the ICP MS (PerkinElmer SCIEX ELAN 5000). Sample fractions were collected using a split valve with 1% of the effluent going to mass spectrometer and 99% to sample collection. Since ICP MS is an element-selective detector, fraction collection started when the selenium signals (^{74}Se, ^{77}Se, ^{78}Se, ^{82}Se) appeared.

5.2.5 HPLC-MS/MS Conditions

The HPLC-MS/MS system is comprised of an Applied Biosystems 4000 QTrap tandem mass spectrometer interfaced with two Shimadzu LC-10AT HPLC pumps and a PerkinElmer series 200 autosampler. HPLC separations were carried out using a 2.1 × 250 mm Waters XTerra C_{18} column packed with 5 μm particles at a flow rate of 200 μL min^{-1}. This was directly connected to the ABI 4000 QTrap where subsequent dispersal and desolvation of the eluent occurred via 6.0 L $min.^{-1}$ nitrogen bath gas flow at 250°C. The turbo ionspray needle was held at 5500 V and the declustering potential was held low (40 V) to prevent ions from fragmenting in the source. Mobile phase A consisted of H_2O and mobile phase B was CH_3OH both having 0.1% (v/v) heptafluorobutyric acid (HFBA). The elution protocol consisted of a 1 min. column pre-equilibration with 98:2 A/B (v/v), followed by 10 μL sample injection, a 5 min. sample load and wash with 98:2 A/B (v/v), a 20 min. linear gradient to 100% B, and a 3 min. hold at 100% B. Afterwards the column was re-equilibrated for 2 min. with 98:2 A/B before the next cycle was initiated.

Selenium containing species were detected on the ABI 4000 QTrap using multiple reaction monitoring (MRM) transitions. In these analyses the first mass analyzer is set to pass a specific precursor ion *m/z*, and the second mass analyzer is set to pass a structure specific product ion *m/z*. Therefore, only ions that meet both precursor and product ion *m/z* conditions simultaneously will be transmitted to the detector. Multiple precursor and product ion pairs may be monitored sequentially allowing numerous species to be detected. A total of 15 transitions were used to detect up to nine different species

Table 5-1. Summary of all precursor/product ion and associated selenium compounds

Selenium Species	Precursor ion *m/z*	Product ion *m/z*
Selenourea	125.1	108.0
	125.1	44.1
Trimethylseleninium	125.1	110.0
	125.1	95.0
Selenomethionine	198.1	181.9
	198.1	108.9
	198.1	56.1
Selenoethionine	212.1	166.1
	212.1	102.1
Unknown Decomposition Product	247.0	124.1
Selenocystamine	248.8	203.9
Selenocystine	337.0	248.0
	337.0	88.0
1β-methylseleno-N-acetyl-D-galactosamine	300.1	204.2
Selenoguanosine	348.1	216.0

(Table 5-1). Each was optimized with regard to both ionization and dissociation conditions and had a dwell time of 20 ms each.

5.2.6 SPI Sample Preparation

In the SPI experiments, 5 × 5 mm graphite substrates were cleansed by sonication in acetone, methanol, and nanopure water. Sample solutions were then directly deposited onto the graphite substrates. They were air-dried for 10 min in desiccators and immediately transferred into the antechamber for further vacuum drying. Finally, the samples were transferred into the main UHV chamber for SPI analysis.

5.3 RESULTS AND DISCUSSION

5.3.1 LD/SPI MS of Standards and Isotope Calibration

To evaluate the ability of LD/SPI MS for the analysis of organoselenium metabolites, selenomethionine (SeMet), selenoethionine (SeEt), trimethylselenonium iodide (TMSeI) and 1β-methylseleno-N-acetyl-D-galactosamine (N-Ac-SeGal) were first studied. Figure 5-4 and 5-6 show the LD/SPI MS spectra of four standard organoselenium compounds with the same concentration of 250 ng/mL. The mass spectrum in Figure 5-4 shows strong ^{80}Se molecular ions of SeMet and SeEt at *m/z* 197 and *m/z* 211. Major fragmentations of SeMet and SeEt ($[^{80}\mathrm{SeMet} - \mathrm{COOH}]^+$, *m/z* 152 and $[^{80}\mathrm{SeEt} - \mathrm{COOH}]^+$, *m/z* 166, respectively) as well as $[\mathrm{C_2H_5}^{80}\mathrm{Se}]^+$, *m/z* 109 were also observed. The selenium isotope patterns of all of these peaks match those expected from the natural abundances of the ^{74,76,77,78,80,82}Se isotope abundance ratios.[69] An example of the very good correlation is shown in Figure 5-5 for the SeMet and SeEt molecular ions.

The LD/SPI MS spectra of TMSeI and N-Ac-SeGal is shown in Figure 5-6. The two major peaks around *m/z* 125 and *m/z* 299 are TMSe$^+$ and N-Ac-SeGal$^{\cdot+}$ molecular ions, respectively. The third major peak at *m/z* 204 in Figure 3A corresponds to [N-Ac-SeGal − CH$_3$Se]$^+$, a major fragment of N-Ac-SeGal.[135] The selenium isotope patterns of TMSe$^+$ and N-Ac-SeGal$^{\cdot+}$ are compared with the expected Se natural abundances in Figure 5-7 and the correspondence is nearly perfect. As shown in Figure 5-6, the third major peak does not have a distinct isotope pattern as expected. The four standard organoselenium compounds were also tested individually (not shown in this paper) and the peaks of each standard compound have no differences relative to the mixture. This indicates that the desorption and ionization processes are not strongly affected by co-existing organoselenium molecules.

The dominant intact molecular ion signals for SeMet$^{\cdot+}$, SeEt$^{\cdot+}$, TMSe$^+$, and N-Ac-SeGal$^{\cdot+}$ clearly demonstrates that 118 nm (10.5 eV) photons could “softly” ionize organoselenium compounds. However, the highly characteristic fragmentation peaks of SeMet, SeEt, N-Ac-SeGal also provides useful information for molecular weight and structure determination. SeMet and SeEt are analog molecules of methionine and the excess energy of 2.5 eV relative to the first ionization potential of only 8.0eV[138], leads to facile loss of the COOH group. This is a typical fragmentation pathway of all amino acids under a wide range of photoionization conditions.[116, 139, 140] At the mean time, losing a SeCH$_3$ group from N-Ac-SeGal to form the *m/z* 204 peak is also a characteristic fragment ion of N-acetyl-D-galactosamine derivatives.[134, 135] It is interesting to note that the [TMSeI]$^{\cdot+}$ molecular ion is not observed in LD/SPI MS since it likely exists in

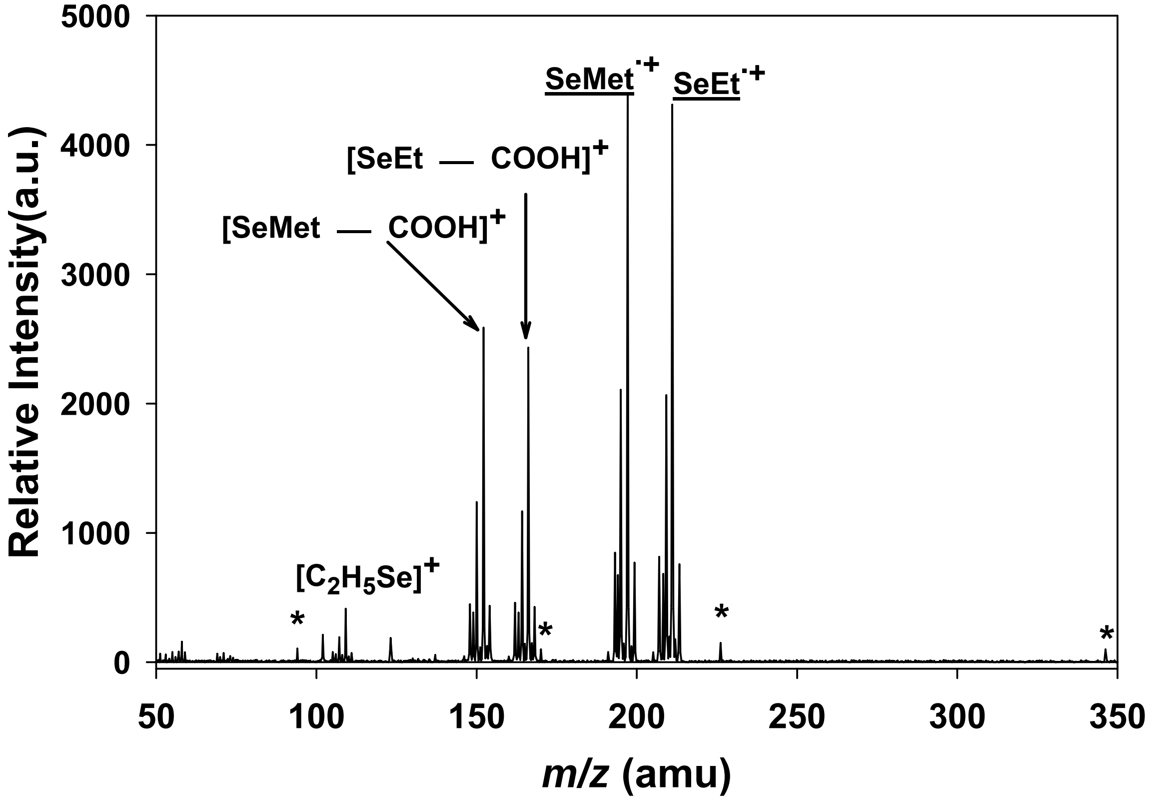

Figure 5-4. LD/SPI MS analysis of 250 ng/mL selenomethionine (SeMet) and selenoethionine (SeEt) (Background peaks from the graphite substrate were labeled with asterisks).

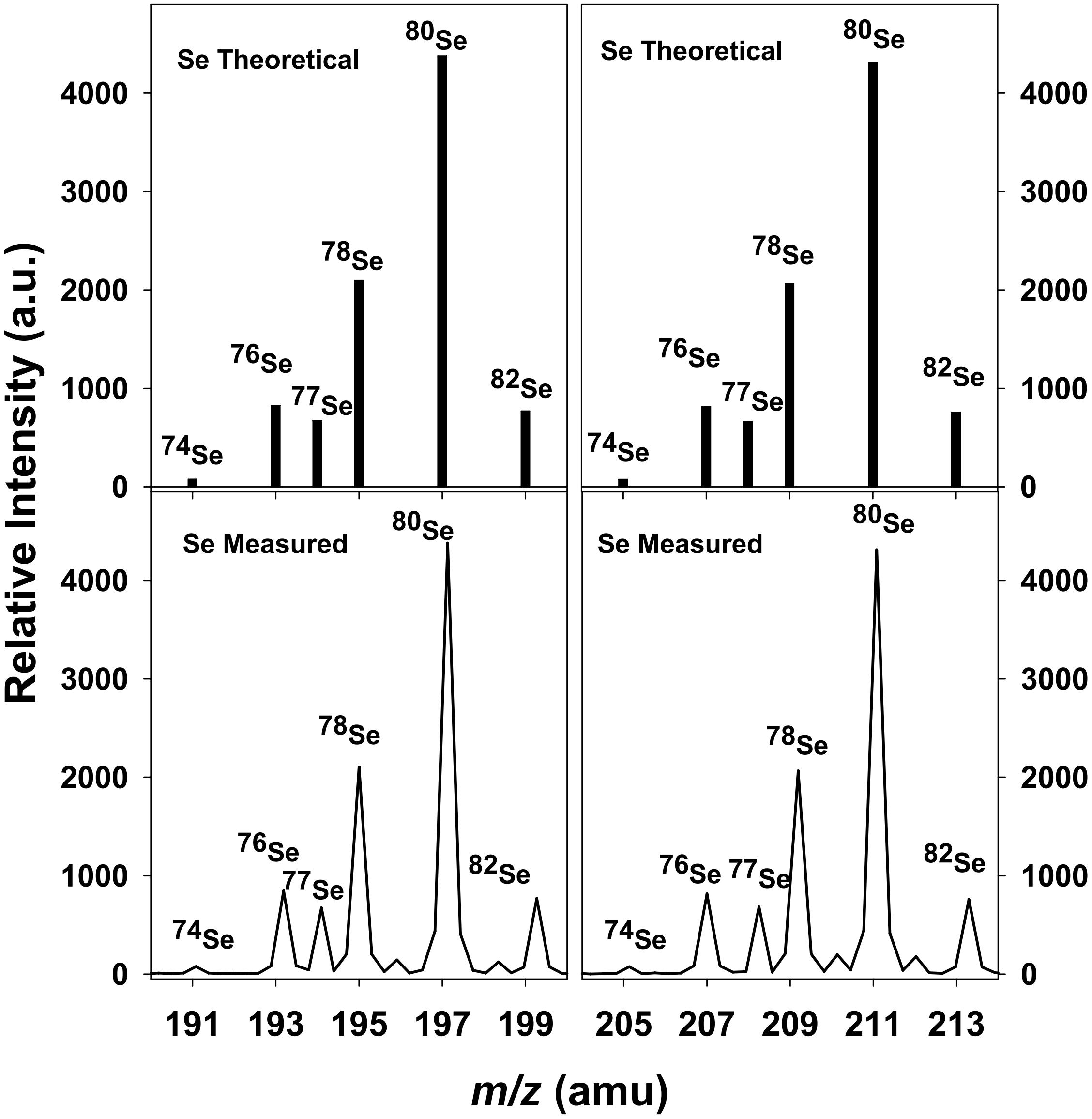

Figure 5-5. Selenium isotope pattern comparison between the natural abundances calculation and measured ion signals of SeMet$^{\cdot+}$ and SeEt$^{\cdot+}$.

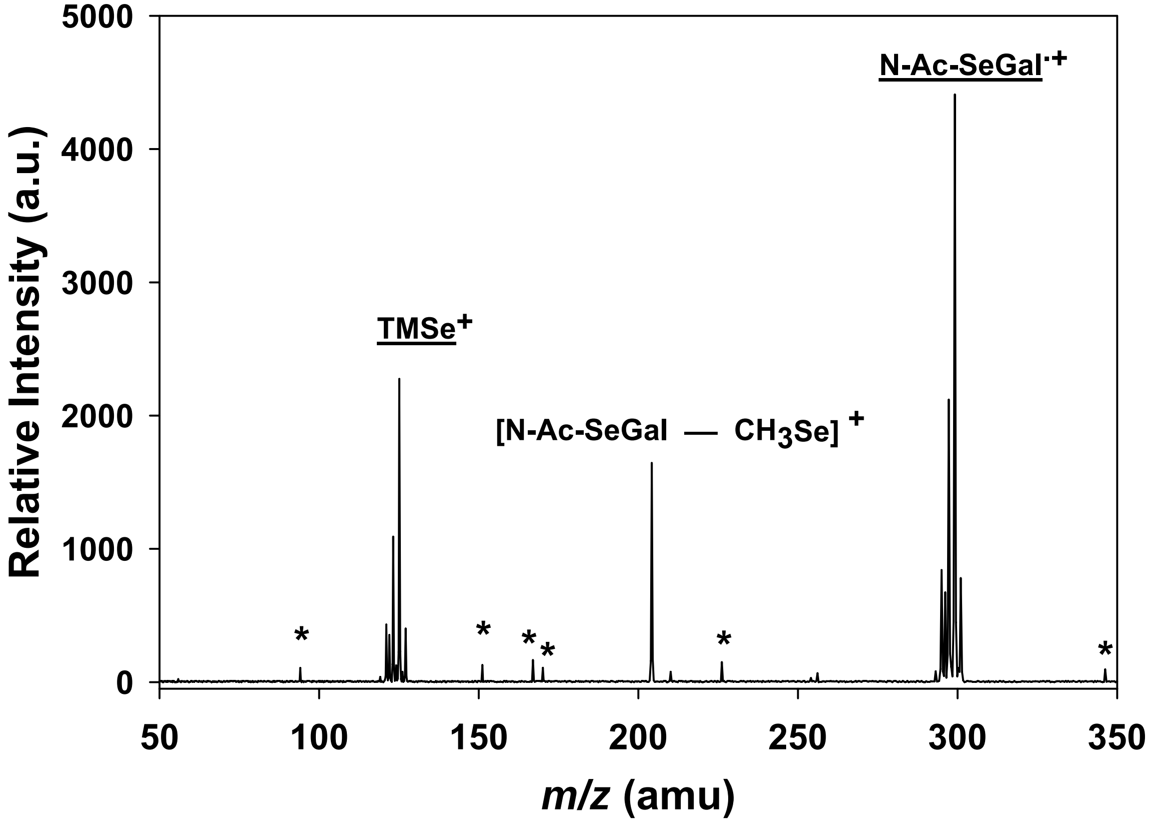

Figure 5-6. LD/SPI MS analysis of 250 ng/mL trimethylselenonium ion (TMSe) and 1β-methylseleno-N-acetyl-D-galactosamine (N-Ac-SeGal) (Background peaks from the graphite substrate were labeled with asterisks).

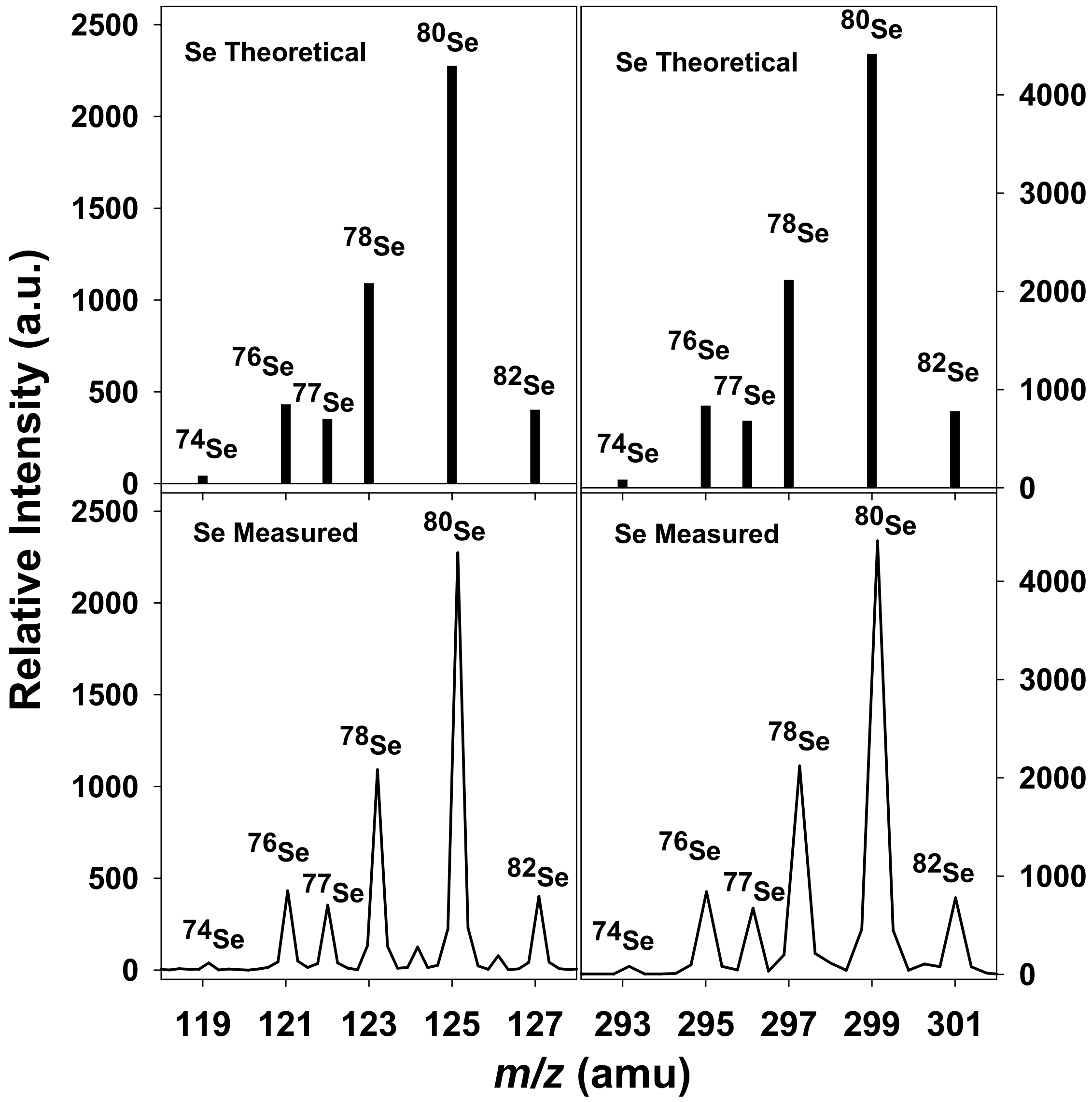

Figure 5-7. Selenium isotope pattern comparison between the natural abundances calculation and measured ion signals of $TMSe^+$ and N-Ac-$SeGal^{\cdot+}$.

solution as a very stable separated $TMSe^+$ and I^- ions.[141-143] TMSeI will therefore not be detected as an intact neutral molecule.

The neutral SeMet, SeEt, and N-Ac-SeGal analyte molecules were desorbed from the graphite surface and then ionized by VUV photons. Since the VUV photon ionization has relatively uniform ionization efficiency, the ion yields of SeMet, SeEt, and N-Ac-SeGal were very close. In contrast, much of the TMSe desorbs in ionic form and leaves the VUV ionization region during the delay time between the desorption and VUV pulse. However, it is very likely that some $TMSe^+$ is quickly re-neutralized during laser desorption, which is an electron rich environment.[144] The re-neutralized TMSe is then ionized by the VUV laser pulse. The $TMSe^+$ yield was about half of that of $SeMet^{\cdot+}$, $SeEt^{\cdot+}$, and $N\text{-}Ac\text{-}SeGal^{\cdot+}$. Assuming equal ionization efficiencies, this implies that about 50% of the $TMSe^+$ were neutralized during the laser desorption event.

The graphite substrate also produced some peaks in the LD/SPI MS. These peaks were labeled with asterisks in Figures 5-4 and 5-6. Their intensities were relatively weak compared to the analyte intensities. The graphite substrate was selected in this experiment because carbon could greatly enhance the signals in laser desorption and ionization.[21, 43, 82] The fragmentation of analyte molecules on graphite could also be controlled by the deposited total energy.[21] In our experiments, the desorption laser flux was optimized to a low level (~ 120 μJ/pulse) to produce relative strong analyte signals and reduce the fragmentation as well as background peaks generated form graphite substrate.

5.3.2 Time-of-Flight (velocity) Distributions of Neutral Products in LD/SPI MS

To better understand laser desorption of small biological molecules from graphite surfaces, the velocity distributions of the desorbing neutral products were measured by varying the delay time between the desorption and ionization laser pulses. Recall that ions produced directly as a result of the desorption laser are removed by an extraction field during the delay time between desorption and ionization laser pulses, but ions produced from neutral products by the VUV laser are accelerated down the flight tube and recorded. The flight distance and extraction field are fixed, thus the masses are determined by this flight time. As an example, the measured SeMet (*m/z* 197) velocity distribution is shown in Figure 5-8. We note that the temporal profile of this time-of-flight (TOF) distribution is very similar to those reported during LD/SPI MS measurements of aerosol samples.[21, 123] Since laser ionization is a flux density detecting scheme, the temporal profile can be explained in terms of the spatially averaged solid angle and the non-selectivity of both the desorption and ionization events. Specifically, since the VUV laser is weakly focused, detection of normal and off-normal trajectories are equally probable. More importantly, since the VUV photoionization event is not chemically selective, the ionization efficiency for most products with IPs below 10.5 eV is similar. *Thus, the TOF distribution is the integrated intensity of nearly all the neutral desorption products which can give rise to the product of interest.* This includes the primary monomeric species as well as more complicated higher mass clusters. An inspection of Figure 5-8 shows that the neutral yields have a fast component peaked at 3 μs, a maximum at 9 μs, and a large signal which extends beyond 40 μs. The TOF distribution can be fit assuming it is a superposition of monomeric and cluster distributions which are both characterized by fast and thermalized temperature

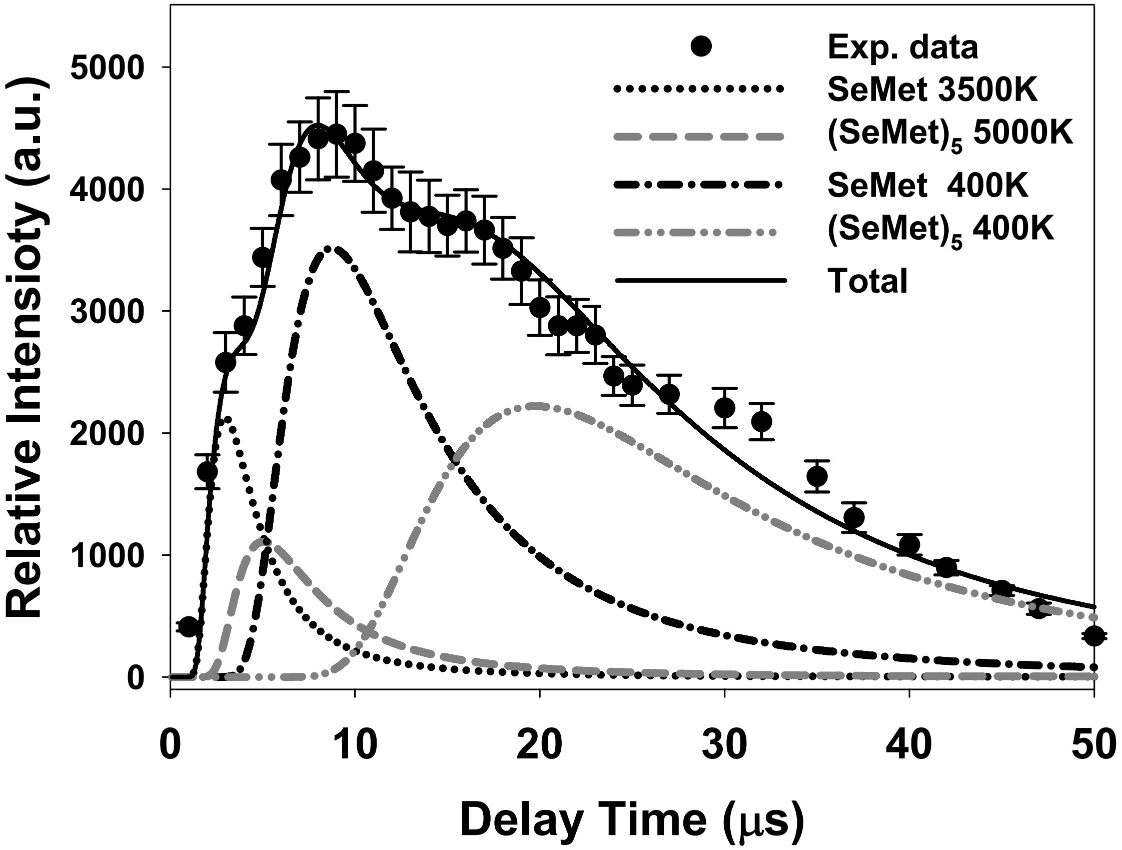

Figure 5-8. Signal intensity of *m/z* 197 ($^{80}SeMet^{\cdot+}$) vs. delay time between desorption and ionization pulses. The solid line is the sum of the four Maxwell-Boltzmann velocity distributions.

distributions. As shown in Figure 5-8, four Maxwell-Boltzmann distributions can be summed to reproduce the data very well base on equation 5-1.[145] In equation 5-1, C is

$$I(t) = Ct^{-3} \exp\left(-\frac{m}{2kT}\frac{d^2}{t^2} \right) \qquad \text{(Equation 5-1)}$$

proportionality constants, m is the mass of the neutral desorbates, k is Boltzmann's constant, d is the flight distance from the sample surface to the VUV laser beam, t is the time delay between the pulses of desorption laser and ionization (VUV) laser, T is the effective temperature and t^{-3} is the pre-exponential term indicating a two-dimensional detection arrangement.

These distributions in Figure 5-8 represent the fast (black dotted line, 3500 ± 100K) and thermalized (dash-dot line, 400 ± 20 K) components for the SeMet monomeric unit and the fast (gray dash line, 5000 ± 200 K) and thermalized (dash-dot-dot line, 400 ± 20 K) components for SeMet higher mass species. The high mass species is a weighted average cluster size of 5 and is consistent with magic clusters reported in ESI experiments of amino acids such as methionine.[146] This cluster undergoes a fragmentation pathway giving rise to the monomer which can be ionized during the 5 ns VUV laser pulse. Assuming a parent monomer (*m/z* 197), the very fast distribution corresponds to a molecular velocity of 664 m/s and a most probable kinetic energy of 150 meV. The fast distribution for the higher mass species (*m/z* 985) corresponds to molecular velocity of 354 m/s and a most probable kinetic energy of 218 meV.

The appearance of these fast peaks clearly indicates that the initial desorption process is not entirely thermal. The non-thermal step could be explosive expansion, in which most analyte molecules were evaporated from the overheated graphite substrate.

However, the heating and explosive expansion must come from rapid electron-phonon coupling within the molecular solid and more likely at the graphite-multilayer interface. Graphite can be described as a two-dimensional electron gas which is non-wetting and optically dense. This material absorbs the photon energy efficiently and responds via rapid electron-phonon interactions within the graphite. In the case of UV excitation, copious electron emission into the overlayer also occurs which sets up a space charge separated plasma at the interface. In vacuum, this can lead to dynamical acceleration of ions.[147] In the multilayer, the space charge is screened but hot electrons and holes can propagate through the media, especially if it contains water. Thus, for aqueous samples, the electrons and holes can actually pile up at the surface/interface and when they recombine, several volts of energy must be released locally. This is similar to exciton decay at an interface which is known to lead to nonthermal desorption events. Clusters are formed when the sample is amorphous or by three body interactions above the surface. There is also evidence which indicates that clusters may form in solution and remain intact in the adsorbed state. The charges on these clusters are likely balanced due to the zwitterion character. However, hole production in the vicinity of a local positive charge could lead to Coulomb expulsion as observed for the formation of protonated water clusters.[136, 148]

5.3.3 Detection Sensitivity

Because the VUV photon energy (10.5 eV) is fixed, the degree of fragmentation is relatively invariant for most desorbates.[123] Therefore, quantitative measurements can be achieved by LD/SPI MS. In these experiments, the optimized laser desorption and ionization conditions were controlled and kept constant between experiments. The amount of each analyte deposited per spot on the substrate was calculated using the molecular densities (total amount of analyte divided by sample plate area) multiplied by the spot size of the desorption laser. The relative peak areas were obtained by integrating the ^{80}Se containing peak of each molecular ion. Figure 5-9 (A), (B), and (C) show the relationships between the detected intensities and amounts of TMSe, SeMet, and N-Ac-SeGal deposited on each sample spot, respectively. The detection of all three organoselenium standards is linear in the range from 5 pg to 100 pg/spot (Table 5-2) and this data serves as the calibration for the quantitative analysis of human urine discussed in the following section. Note similar data was obtained for SeEt, however, it is not included in Figure 5-9 since SeEt is not a possible metabolite in human urine. The detection limits (S/N = 3) determined from Figure 5-9 are 5 pg/spot (25 ng/mL) for TMSe and 3 pg/spot (15 ng/mL) for SeMet and N-Ac-SeGal, respectively. These correlate to detection sensitivities of about 1~10 femtomoles and is comparable to the detection limits reported by other LD-SPI experiments.[21,123]

5.3.4 Analysis of Urine Samples

Since the observed detection limit is in the range of several picograms per sample spot (low ppb level), it should be applicable to the analysis of low concentrations of selenium metabolites in urine samples.[149] In order to verify the presence of these metabolites in our samples, conventional HPLC-MS/MS techniques were used to analyze the Group B samples (fractions of HPLC-ICP MS) described earlier. Electrospray ionization MS (ESI MS) was first tried but this approach failed to provide any useful

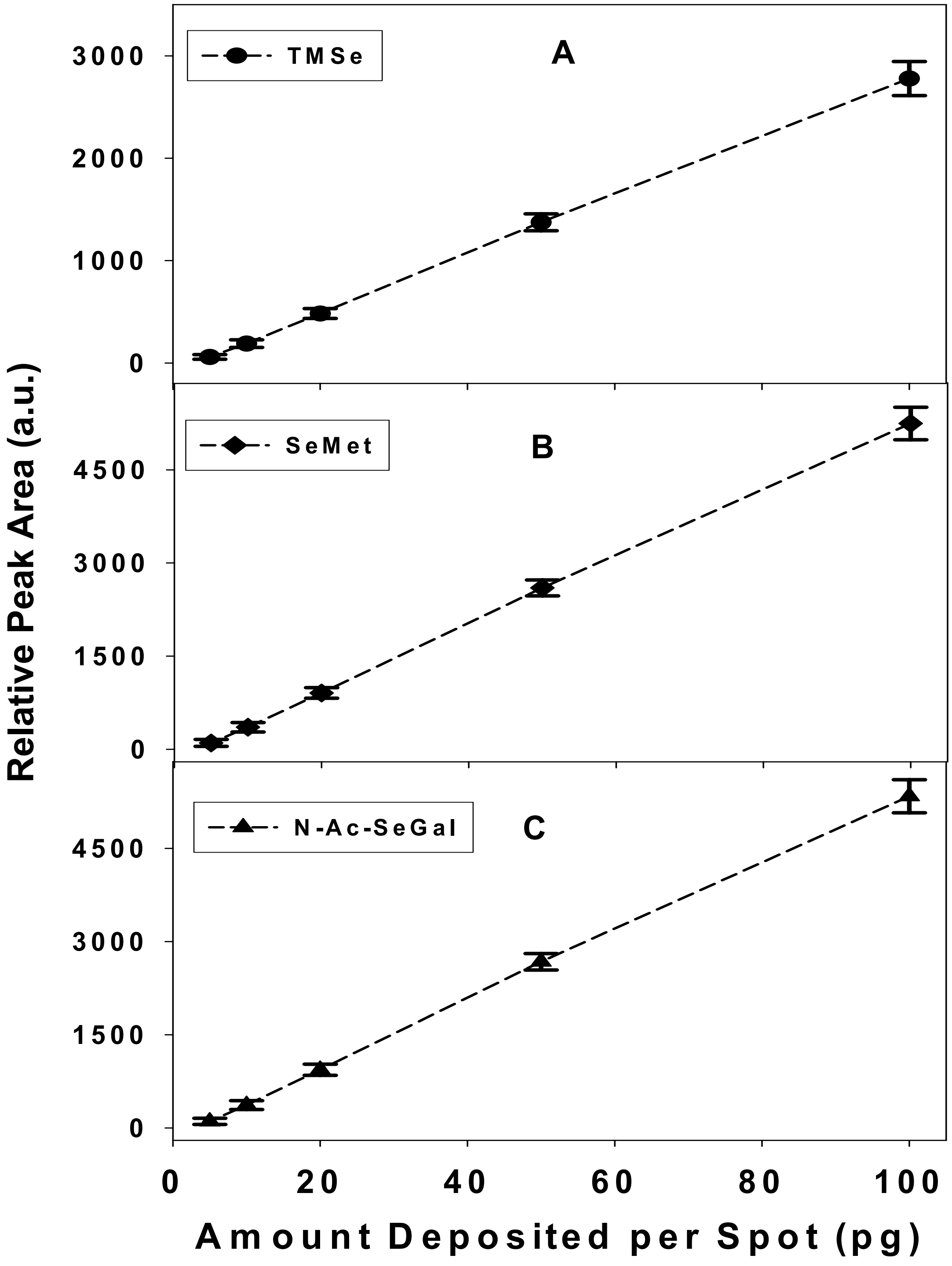

Figure 5-9. Signal intensity vs. amount of (A) TMSe, (B) SeMet, and (C) N-Ac-SeGal deposited on sample spot. The dotted lines in (A), (B), and (C) are linear fitted line. The R-squared values for each fit were listed in Table 5-2.

Table 5-2. Comparison of correlation coefficients and limits of detection

Selenium Standards	R^2	Limit of Detection
TMSe	0.998	30 ng/mL
SeMet	0.998	15 ng/mL
N-Ac-SeGal	0.996	15 ng/mL

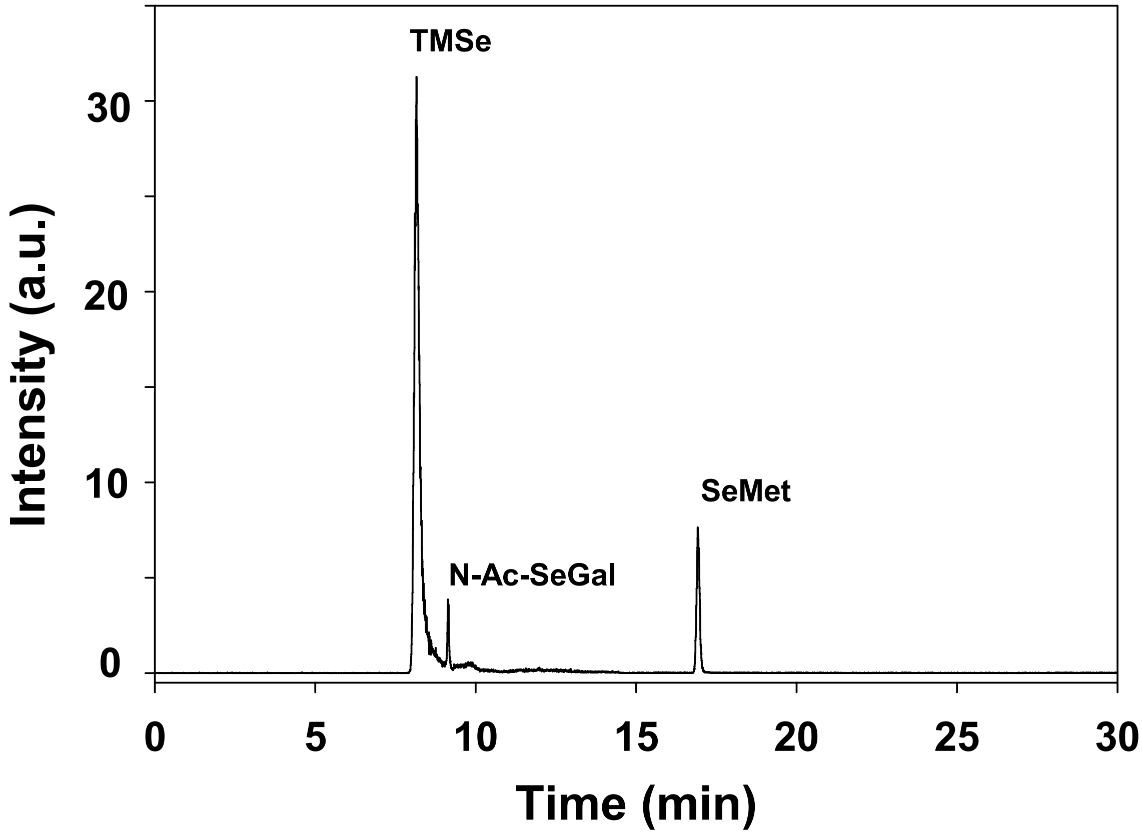

Figure 5-10. HPLC-MS/MS result of human urine fraction obtained by HPLC-ICP MS (retention time = 500 s).

information. ESI MS/MS (multiple reaction monitoring, MRM) was then used for the detection of organoselenium compounds. The results of these experiments are shown in Figure 5-10 and the data demonstrates the presence of three main Se containing metabolites, TMSe, SeMet and N-Ac-SeGal. A series of calibration solutions were then analyzed by HPLC-ESI MS/MS to determine the detection efficiency and sensitivity. The weakest signal, N-Ac-SeGal, was present at a concentration 5.63 μg/L. Due to organoselenium compounds as standard molecules, the HPLC-MS/MS method could only analyze the known TMSe, SeMet and N-Ac-SeGal metabolites. Though HPLC treatment followed by ESI/MS/MS was tedious, these established techniques did allow us to unambiguously identify the presence and concentration of TMSe, SeMet and N-Ac-SeGal.

A fraction of the Group B sample was also analyzed using LD/SPI MS. The spectrum shown in Figure 5-11 was obtained within 10 minutes and is an average of 10 spectra obtained with 1000 laser pulses on different sample spots. Several peaks with the characteristic selenium isotope pattern are observed and a high resolution scan should allow exact mass determination. The selenium isotope pattern is shown in Figure 5-12 for the *m/z* 257 and 299 ions. The ^{80}Se peak at *m/z* 257 is very likely to be methylseleno-galactosamine (SeGal), which has been recently reported as a metabolites in human urine[135, 150]. The fragmentation feature at *m/z* 162 $[M - SeCH_3]^+$ further confirmed the existence of this metabolite. The peak at *m/z* 299 corresponds to N-Ac-SeGal and the peaks at *m/z* 125 and 197 are clearly due to TMSe$^+$ and SeMet$^{\cdot+}$, respectively. Note there are also several higher mass Se containing metabolites which could not be identified but with the possibilities of being derivatives of SeGal and N-Ac-SeGal. Experiments were

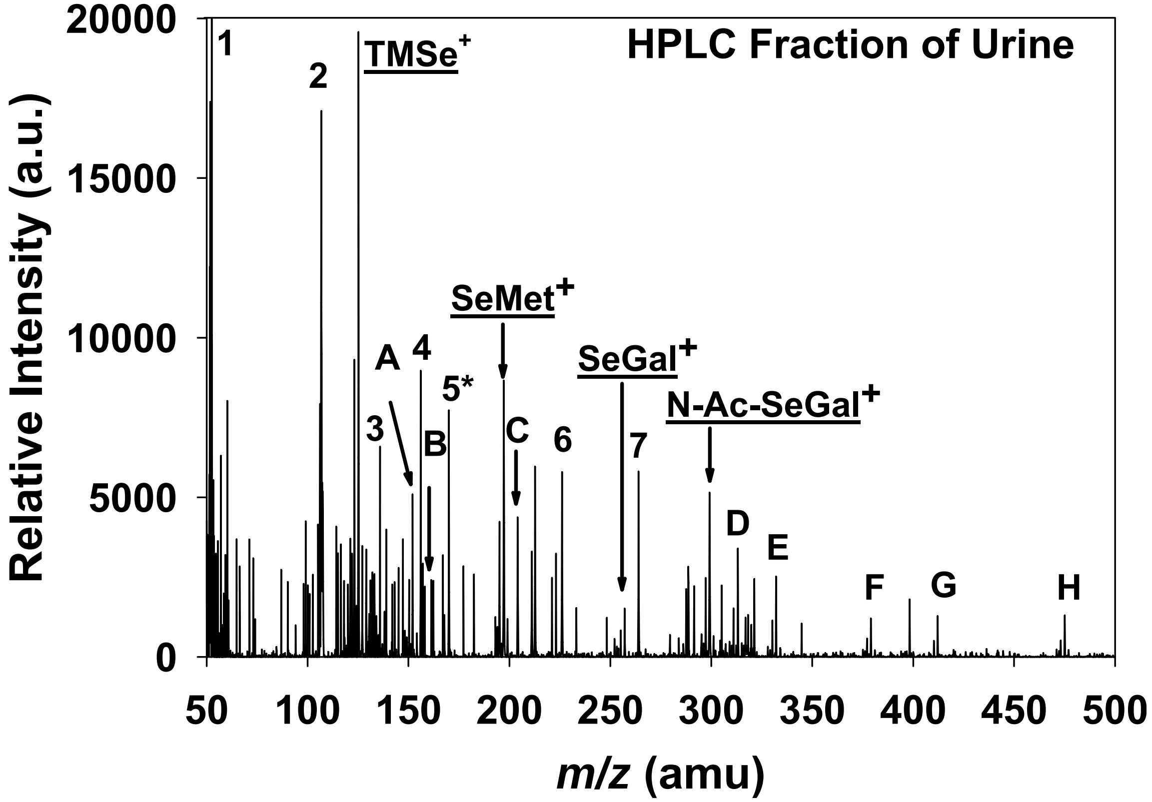

Figure 5-11. LD/SPI mass spectrum of the Group B HPLC-ICP MS fraction (retention time = 500 s) of human urine samples. Organic components not associated with Se metabolites are marked as masses 1-6, whereas the Se containing metabolites and fragments are labeled and listed as peaks A-H. Background peaks from graphite substrate were labeled with asterisk.

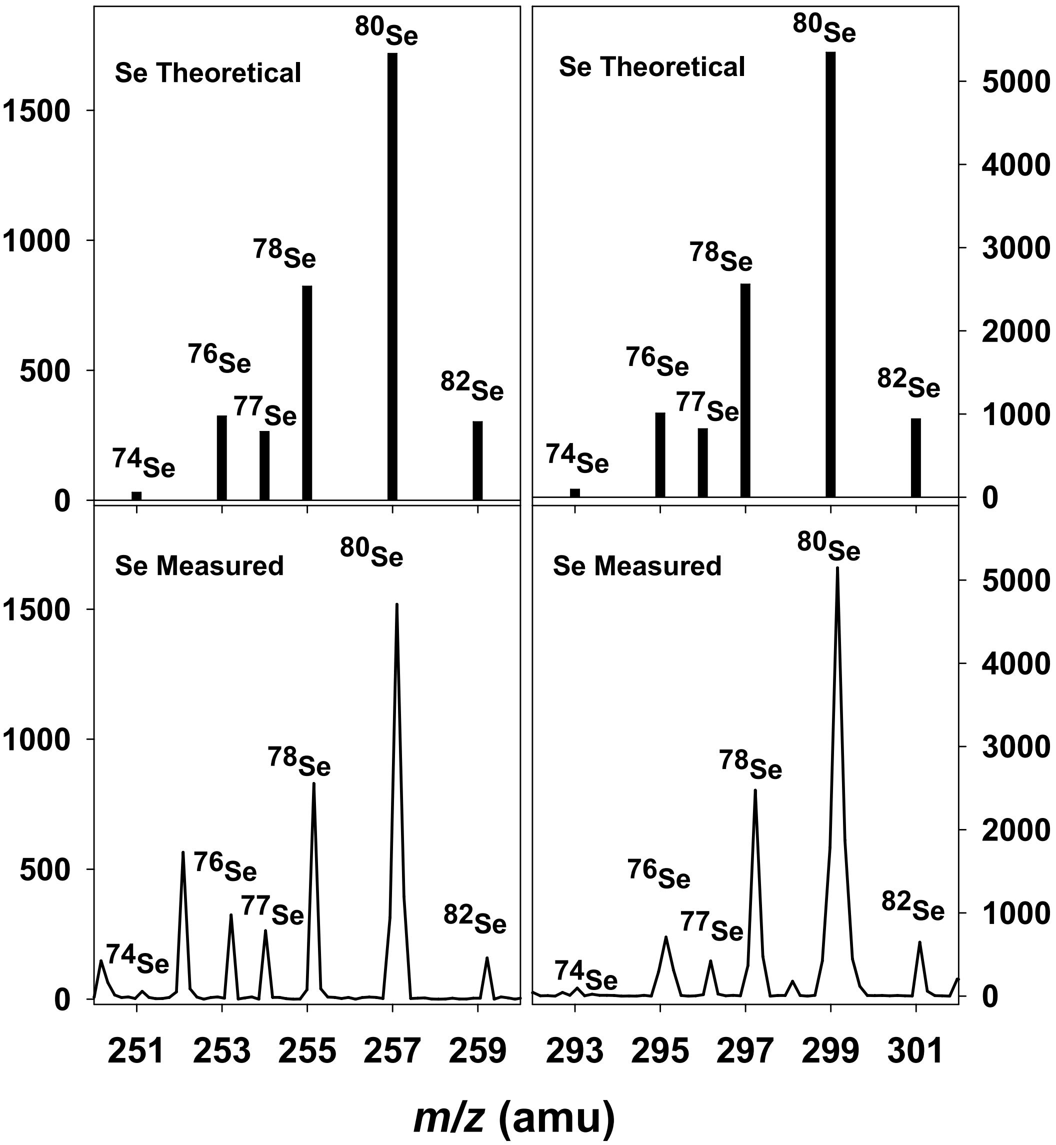

Figure 5-12. Selenium isotope pattern comparation between theoretical calculations and measured ion signals of Se-Gal and N-Ac-SeGal.

Table. 5-3 Peak assignments of LD/SPI MS data from the Group A HPLC fraction of human urine samples shown in Figure 5-11.

Peak label	Measured mass	Assignment	Theoretical Mass
1	60.3	Urea	60.0
2	106.5	Benzaldehyde	106.0
3	135.8	Propylphenol	136.1
A	152.0	SeMet – COOH	152.0
4	156.0	Orotic acid	156.0
B	162.1	SeGal – $SeCH_3$	162.1
C	204.1	N-Ac-SeGal – $SeCH_3$	204.1
5	226.0	3-nitrotyrosine	226.1
6	264.0	2-amino musk ketone	264.1
D	313.2	organoselenium compound	n/a
E	332.1	organoselenium compound	n/a
F	379.1	organoselenium compound	n/a
G	412.1	organoselenium compound	n/a
H	475.1	organoselenium compound	n/a

also performed by injecting standards (100 ng/ml) into the urine samples and the detected recovery for TMSe, SeMet, and N-Ac-SeGal were 86%, 94%, and 92%, respectively.

In addition to the presence of Se containing metabolites, other species such as urea, benzaldehyde,[151] propylphenol,[152] orotic acid,[153] 3-nitrotyrosine,[154] and 2-amino musk ketone[155] were all possibly present in the Group B sample. The organic components not associated with Se metabolites are marked as masses 1-6 whereas the Se containing metabolites and fragments are labeled and listed as peaks A-H. The assignments are summarized in Table 5-3.

Figure 5-11 and 5-12 clearly demonstrate the ability of LD/SPI MS to detect the absolute concentrations of isotopically resolved Se metabolites as well as a series of organic components. The concentrations of the three primary selenium metabolites (TMSe, SeMet, and N-Ac-SeGal) were determined to be 8.1, 4.5, and 4.1 μg/L, respectively. This is in very good agreement with the ESI MS/MS measurements. Though using LD/SPI MS allowed accurate determination of metabolites on samples treated or pre-concentrated using HPLC, the extreme sensitivity of LD/SPI MS should allow the direct examination of urine samples without any preparation and treatment. Indeed, this result (Group A sample) is shown in Figure 5-13 and is very rich with a clear signature of the expected Se containing metabolites. In addition, many other molecules such as tartronic acid (*m/z* 120), glutaric acid (*m/z* 132), orotic acid (*m/z* 156), uric acid (*m/z* 168), suberic acid (*m/z* 174), and hydorxyhippuric acid (*m/z* 195) are present and easily detected. Most of these are typical urinary acids.[153] All of the assignments for this data are given in Table 5-4.

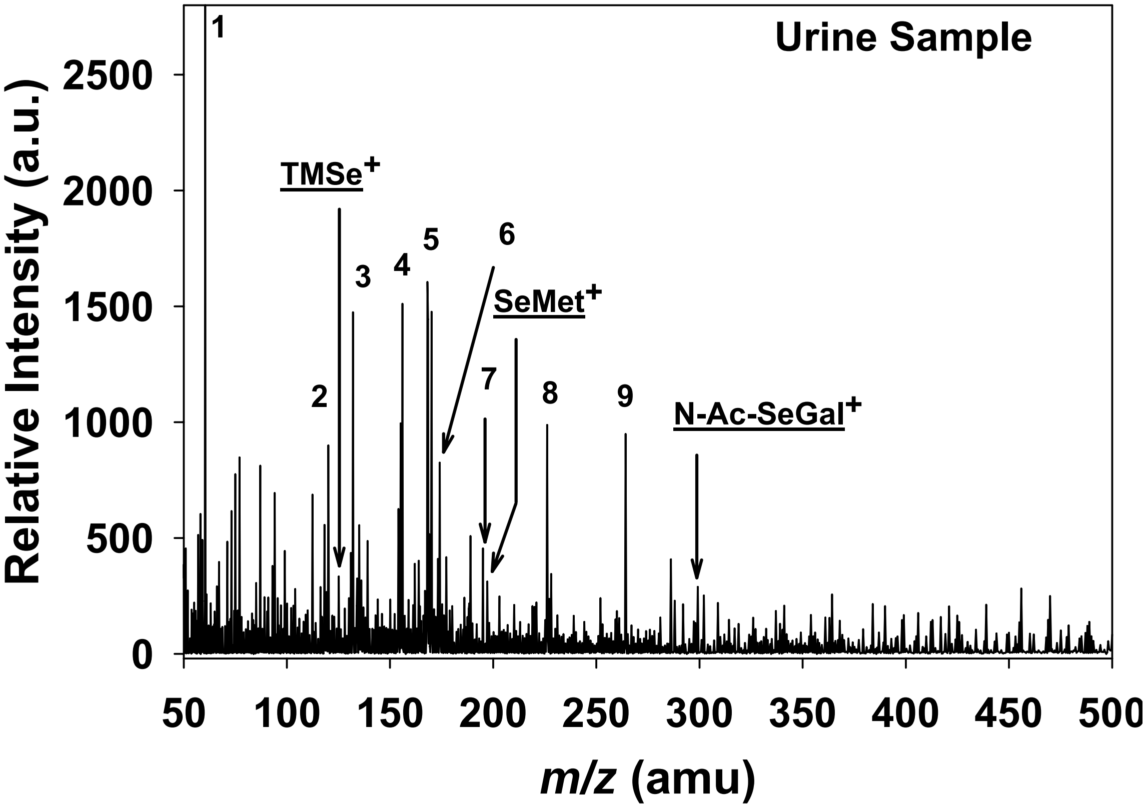

Figure 5-13. LD/SPI MS analysis of human urine with daily intake of 200μg selenomethionine. Organic compounds not associated with Se metabolites are marked as masses 1-9.

Table 5-4. Peak assignments of LD/SPI MS data from Group B human urine samples shown in Figure 5-13.

Peak label	Measured mass	Assignment	Theoretical Mass
1	60.3	Urea	60.0
2	120.0	Tartronic acid	120.0
3	132.0	Glutaric acid	132.0
4	156.0	Orotic acid	156.0
5	168.1	Uric acid	168.0
6	174.0	Octanedioic acid	174.1
7	195.0	Hydroxyhippuric acid	195.1
8	226.0	3-nitrotyrosine	226.1
9	264.0	2-amino musk ketone	264.1

The relative ratios of the primary Se containing metabolites and the distributions and identities of the various organic components differ from the data obtained using HPLC pre-treatment. Specifically, the TMSe signal is rather small and several organic acid signals are strong in the direct analysis spectra. As discussed above, the TMSe is likely in the ionized form in solution and may be concentrated during the elution and HPLC separation. In addition, some of the organic acids are not captured and eluted in the HPLC treatment. Thus, assuming equal ionization efficiency with the VUV photons, the spectra from the direct analysis is more representative of the actual concentrations and composition.

Since there are conflicting reports in the literature over the last several decades, the identity of the important Se containing metabolites remains unclear. The low concentration of Se metabolites, the thermally labile nature of possible Se species, and the complexity of analyte / matrix interactions present serious experimental challenges. The LD/SPI MS overcomes many of these challenges and provides a unique and sensitive method of reliably detecting metabolites such as trimethylselenium, selenomethionine, methylseleno-galactosamine, and 1β-methylseleno-N-acetyl-D-galactosamine with femtomolar sensitivities. Our LD/SPI MS results from direct and HPLC fractional analysis of urine samples suggest that TMSe, SeMet, SeGal, and N-Ac-SeGal are all possible selenium metabolites in human urine with a daily intake of 200 μg of selenomethionine. The control urine samples showed only trace amounts of N-Ac-SeGal. Therefore, it seems that N-Ac-SeGal is the major natural metabolite.

5.4 CONCLUSION

A method for analyzing organoselenium and organic acid metabolites using laser desorption from graphite surfaces coupled to vacuum ultraviolet (VUV) single photon ionization mass spectrometry (LD/SPI MS) is described. The femtomolar sensitivity and linear dynamic range allows quantitative detection of selenomethionine, trimethylselenonium ion, and 1β-methylseleno-N-acetyl-D-galactosamine in complex biological samples such as human urine. In addition, common urinary metabolites such as tartronic, glutaric, orotic, uric, suberic and hydroxyhippuric acids, are readily detected. Screening and quantitative detection of these organoselenium and organic acid metabolites is achieved within minutes. LD/SPI MS is a matrix free and rapid analysis technique which allows direct analysis of biological samples (such as human urine) without complicated sample preparation. Therefore, LD/SPI MS is a simple, powerful, and promising technique for fast and sensitive analysis of a wide variety of biological molecules. Overall, our study demonstrates the viability of matrix free LD/SPI MS for molecular characterization and quantitive analysis of biological metabolites in the *m/z* 10 - 600 range that are present in complex biological fluids. It may be utilized for many applications such as biomarker identification, metabolite profiling, pharmacokinetic assessments, and clinical monitoring.

CHAPTER 6

INVESTIGATION OF LOW-ENERGY ELECTRON-INDUCED DNA DAMAGE USING ELECTRON STIMULATED DESORPTION SINGLE PHOTON IONIZATION MASS SPECTROMETRY

6.1 OVERVIEW

DNA is one of the most important biological molecules for the survival of living organisms. The DNA molecule is composed of two anti-parallel strands of repeated sugar-phosphate unit hydrogen bound by the four bases, which are covalently linked to the sugar moiety of the backbone (Figure 6-1). DNA contains the genetic instructions specifying the biological development of all cellular forms of life (and most viruses). It is involved in cellular reproduction by self-replication and RNA transcription, which produces proteins by translation.

A complete description of the effects of ionizing radiation on DNA in living cells is fundamental to the radiobiology， public health, and clinical applications such as radiation protection, chemotherapy, and radiosensitizer development. DNA damage caused by radiation has been extensively investigated over the past several decades.[156-163] It is well known that high-energy ionization radiation, such as α-, β-, x-, γ-rays, or heavy ions can cause sugar-phosphate cleavage (strand breaks) in DNA, which might be critical DNA lesions responsible for toxic, mutagenic, and cell malfunction or death. Depending on the site of chemical bond dissociation on double helix backbones, the DNA damage could be either single stand break (SSB) or double strand break (DSB) (Figure 6-2).

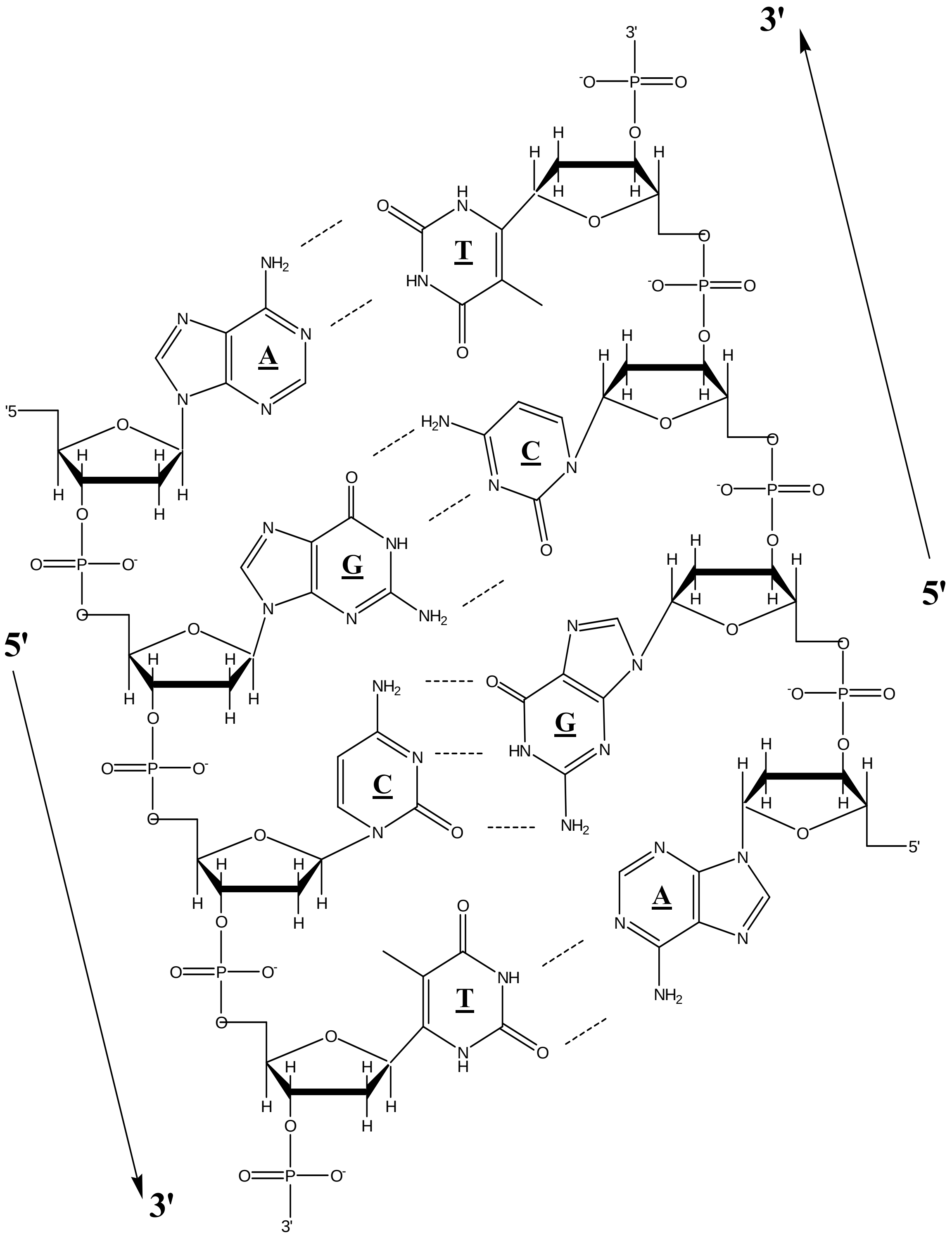

Figure 6-1. Schematic of DNA structure with hydrogen bonds between base pairs. (A: adenine; G: guanine; C: Cytosine; T: Thymine)

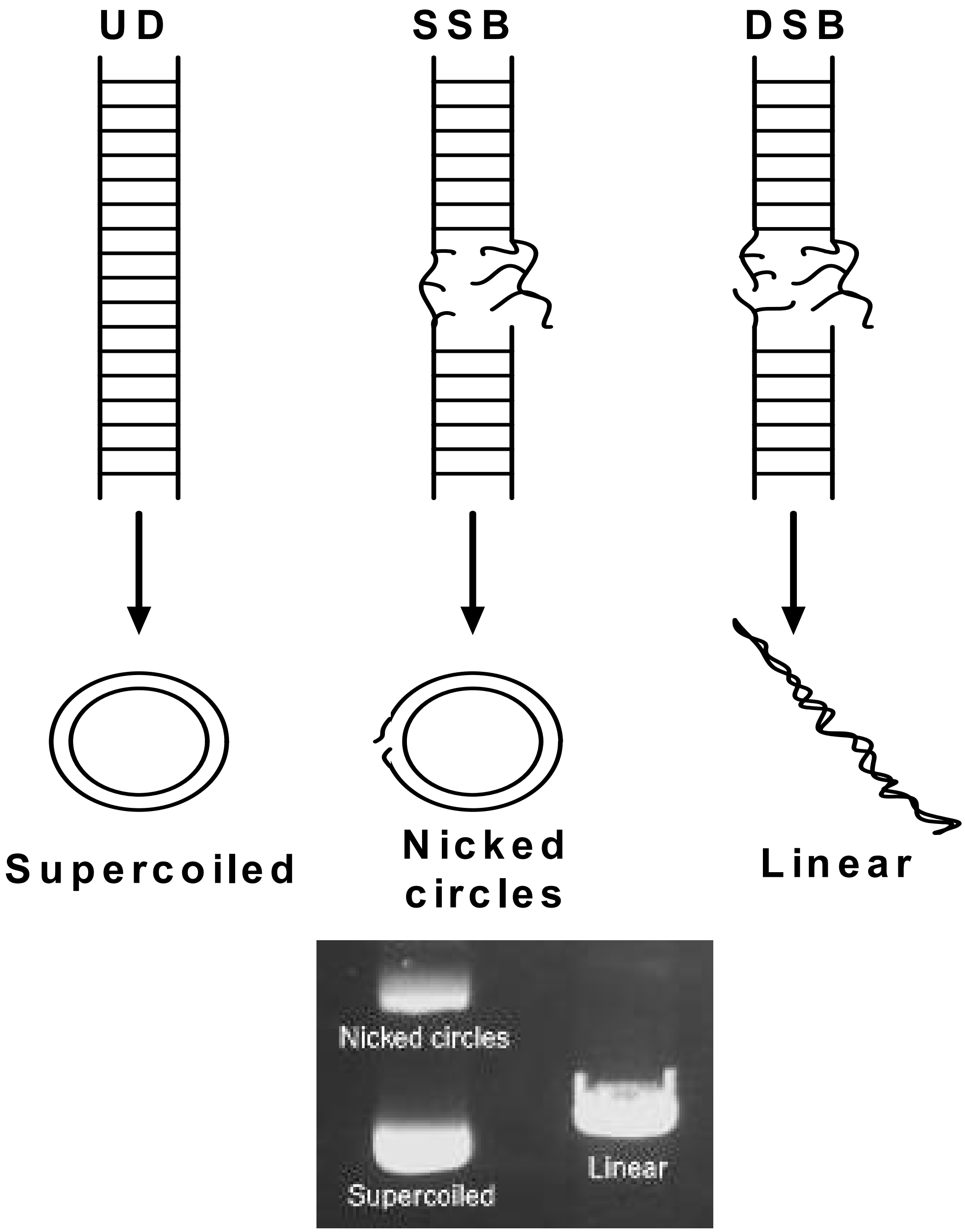

Figure 6-2. A schematic comparing intact DNA (UD), single strand break (SSB) and double strand break (DSB). A DSB is formed when two or more strand breaks are formed in opposite strands of DNA within about 10 to 20 base pairs of each other.[164] In agarose gel electrophoresis analysis, circular forms of DNA migrate in agarose distinctly differently from linear DNA of the same mass. Typically uncut plasmid (supercoiled) DNA migrates more rapidly than the linearized (DSB) DNA and nicked circular (SSB) DNA. The image at the bottom shows an ethidium-stained gel with supercoiled and nicked circular DNA in the left lane and the linearized DNA at a single site in the right lane.

Radiation induced DNA damage is usually divided into two groups: i) "direct" damage resulting form direct ionization of DNA and/or the closely bound water molecule, and ii) "indirect" damage rising from radicals generated by energy deposition in water molecules or other biological molecules surrounding the DNA.[165] It is estimated that the direct/indirect DNA damage ratio is about 1:2 in all the cellular damages.[166] Most of the energy deposited in living cells by ionizing radiation produces into secondary species such as ballistic electrons (1 ~ 20 eV), neutrals, or ionic radicals.[167] Electrons are the most abundant secondary species with an estimated yield of about 4×10^4 electrons per MeV [168] and most have initial kinetic energies below 20 eV.[169] Pioneering work by Sanche and co-workers has demonstrated that low-energy electrons could localize on various DNA components (base, deoxyribose, phosphate, or hydration water) to from transient negative ions (TNI). The decay of the local transient anions into dissociating pathways, such as dissociative electron attachment (DEA) or autoionization, directly leads to the DNA strand breakage.[170] For example,[171] the strand break has been related to the dissociation of covalent bound in DNA components by the following reactions:

$$\mathbf{e + RH \rightarrow (RH)^{*-} \rightarrow (RH)^{*} + e \rightarrow R\cdot + H\cdot + e}$$

and/or

$$\mathbf{e + RH \rightarrow (RH)^{*-} \rightarrow R\cdot + H^{-} \text{ or } R^{-} + H\cdot}$$

It has been reported that strand breaks in supercoiled DNA were induced by free ballistic electrons(3 ~ 20 eV).[170] The electron energy dependence of SSB and DSB presented strong resonance features in the energy range of 5 ~ 15 eV with a maximum around 8 ~ 10 eV. These results provided a fundamental challenge to the traditional view that genotoxic damage by secondary electrons can only occur at energies above the onset of ionization, or upon solvation when they become slowly reacting chemical species.

Recently, DEA of related molecules (water, bases, deoxyribose analog and phosphate) in the condense phase have been intensively investigated by measuring electron energy-dependent desorption yields of negative ions, (H^- , OH^-, or R^-).[172-175] The yields of desorbing anions below 15 eV supported the hypothesis that electron resonance can contribute to DNA damage.[171, 176]

One factor that could contribute significantly to the investigation of DNA damage is the effects of water on the formation and reaction of radiation-induced species. It has been reported that water molecules in DNA hydration shells have unique properties.[177, 178] They are less mobile than free water, more mobile than ice water molecules, and impermeable to cations. The unique properties of hydration water in DNA could play a major role in the interaction between slow electrons and DNA. In other words, DNA damage resulting from low-energy electron irradiation could be greatly affected by intrinsic water molecules close to DNA. In the studies of low-energy electron induced DNA damage, plasmid DNA molecules were usually transferred into ultrahigh vacuum (UHV, 10^{-8}~10^{-9} torr) for electron bombardment and mass spectrometric analysis. Under these conditions, most of the free water molecules around DNA have been removed by evaporation. However, water molecules tightly bounded to or trapped in supercoiled plasmid DNA were likely to remain. *To the best of our knowledge, no studies have been done to assess the role of water content and water-plasmid DNA interactions under UHV condition. This is critical to understand the mechanisms of low-energy electron induced strand breaks.*

Another important issue in the study of irradiation induced DNA damage is the detection of neutral products desorbing from DNA during the electron bombardment. By observing those intermediate or final neutral products, the detailed physical and chemical process leading to DNA damage could be better elucidated. Most of previous works on DEA of DNA monitored the resonance features of negative ions between 5 ~ 10 eV.[179] However, the DEA active site was not clear because the observed small negative ions could result from many different components of the DNA molecules. The neutral products could provide additional information regarding DEA, and thus a complete picture of electron attachment and TNI formation could be revealed when both the negative and neutral products were detected. Electron ionization quadrupole mass spectrometry (EI QMS) has been used to analyze the neutral species that desorbed from biomolecular films irradiated with low-energy electrons.[179] However, this method does not always generate molecular ions because the EI uses 70 eV electrons to ionize molecules. Most organic molecules fragment when ionized by high energy electrons in the EI process. Therefore, there is less structural information about the neutral product in the EI QMS analysis. Single photon ionization mass spectrometry(SPI MS) is a novel technique developed recently with special advantages regarding the detection of neutral molecules.[15, 45, 113-120] In this technique, pulsed or continuous vacuum ultraviolet (VUV) radiation with a photon energy higher than 10 eV are used to ionize the neutral molecules.[108] One of the most commonly used SPI wavelength is 118 nm (10.5 eV) produced via third harmonic generation (THG) of a 355 nm laser in xenon gas. Since the ionization potentials (IP) of most organic species range from 7 to10 eV,[88] which is below the energy of VUV photons, SPI deposits less excess energy and favors the formation of molecular ions. SPI is also a relatively non-selective method with nearly uniform detection selectivity for all species and a powerful tool for the observation of neutral products produced during the interaction of low-energy electrons with DNA molecules.

In this chapter, the water content of P14 DNA in UHV vacuum was investigated by temperature programmed desorption (TPD). DNA damage was also investigated by monitoring the neutral yields as a function of incident electron energy. In addition, SSB and DSB were examined by post irradiation gel-electrophoresis and the results were correlated with the water content and neutral product yields.

6.2 EXPERIMENTAL

6.2.1 Chemicals and Reagents

All solvents were HPLC grade (Fisher Scientific, Atlanta, GA, USA). Other chemicals used were: (i) tantalum foil, 99.95% purity(Alfa Aesar, Ward Hill, MA,USA); (ii) agarose, Ethylenediaminetetraacetic acid, boric acid, and ethidium bromide (Fisher Scientific, Pittsburg, PA, USA); (iii) Tris(hydroxymethyl)aminomethane (Promega Corporation, Madison, WI, USA)

6.2.2 Sample Preparation

P14 double stranded circular DNA was derived from pBluescript SK II (-). It contains 6360 base pairs. The molecular weight is about 4.2×10^6 Dalton. The DNA was extracted from Stratagene, purified and resuspended in 1×TBE solution. The DNA solution was then deposited on 5 mm × 5 mm Tantalum substrate, which was previously cleaned by acetone, methanol, and nanopure water with 10-minute sonication. Because some biomolecules could chemically decompose upon adsorption onto metal surfaces,[179,55,56] certain amounts of DNA molecules were included the solution to form relative thick (>5 monolayers) films. The thick DNA layers (> 100 nm) also prevent the effects of back scattered electrons from the metal substrate. The penetration depth/mean free path of 5 ~ 100 eV electrons is in the range of 15 ~ 35 nm in liquid water or amorphous ice.[180] It ensured the measured signals were produced from electron interaction with the DNA molecules. The DNA sample was first held in a desiccator for 10 minutes and then moved into the loading chamber to be vacuum-dried. After about 24 hour evacuation, the solid DNA film was transferred into the analysis chamber (UHV, 10^{-9} torr) for temperature programmed desorption (TPD) measurements or low-energy electron irradiation experiments. The vacuum-dried sample was also characterized by scanning electron microscopy (Hitachi S-800 SEM, Tarrytown, NY, USA).

6.2.3 Temperature Programmed Desorption

TPD measurements were made in the analysis chamber, equipped with a homemade temperature control system and a quadrupole mass spectrometer (Extrel C50, ABB Analytical Instruments, Inc., Pittsburg, PA, USA). A LabVIEW program (TPD-QMS 6) was designed to facilitate the experiment. The DNA sample was heated by applying a voltage increment to the button heater (HeatWave Labs, Inc., Watsonville, CA, USA) controlled by TPD-QMS 6. The temperature increase has a linear ramp ($T=T_0+\beta T$) with β as 0.5 K/s. The signal of H_2O at $m/z = 18$ was recorded using a quadrupole mass spectrometer mounted directly in front of the sample surface.

6.2.4 Electron Irradiation

DNA solid films were irradiated at room temperature with pulsed electron beam at various incident electron energies and fluxes. The pulsed electron beam was generated by a focusing low-energy electron gun (Kimball Physics, Wilton, NH, USA). The full-width at half maximum (FWHM) of the electron energy distribution was < 0.5 eV. The focused beam size was about 1 mm, depending on the electron energies. Irradiation of the sample (grounded or with an externally applied potential) was performed by the pulsed electron beam operated at 20 Hz with a 100 μs pulse width. Variation of the electron flux was performed exclusively by changing the gun emission current. The electron flux was measured by picoammeter (Keithley Instruments Inc, Cleveland, OH, USA) in the range of 10^{14} electrons s^{-1} cm^{-2}. The pulsed electron beam was focused on the target and controlled by x-y deflection to scan the entire substrate surface. When the electron interacts with the substrate, the image of the substrate could be obtained by monitoring the voltage or current on the substrate. By pulsed electron beam scanning, the charging effects were greatly reduced with even electron dissipation unto the DNA molecules. The total number of electrons exposed to the DNA molecules was on the order of 10^{14} with a 100 second scanning interval.

6.2.5 VUV Ionization and Neutral Detection

The neutral species produced and desorbed by the low-energy electron irradiation of DNA molecules were ionized by VUV photons and detected by a quadrupole mass spectrometer, as shown in Figure 6-3. The VUV photon (118 nm, 10.5eV) was generated by frequency tripling 355 nm photons from a Nd:YAG laser (Precision II, Continuum,

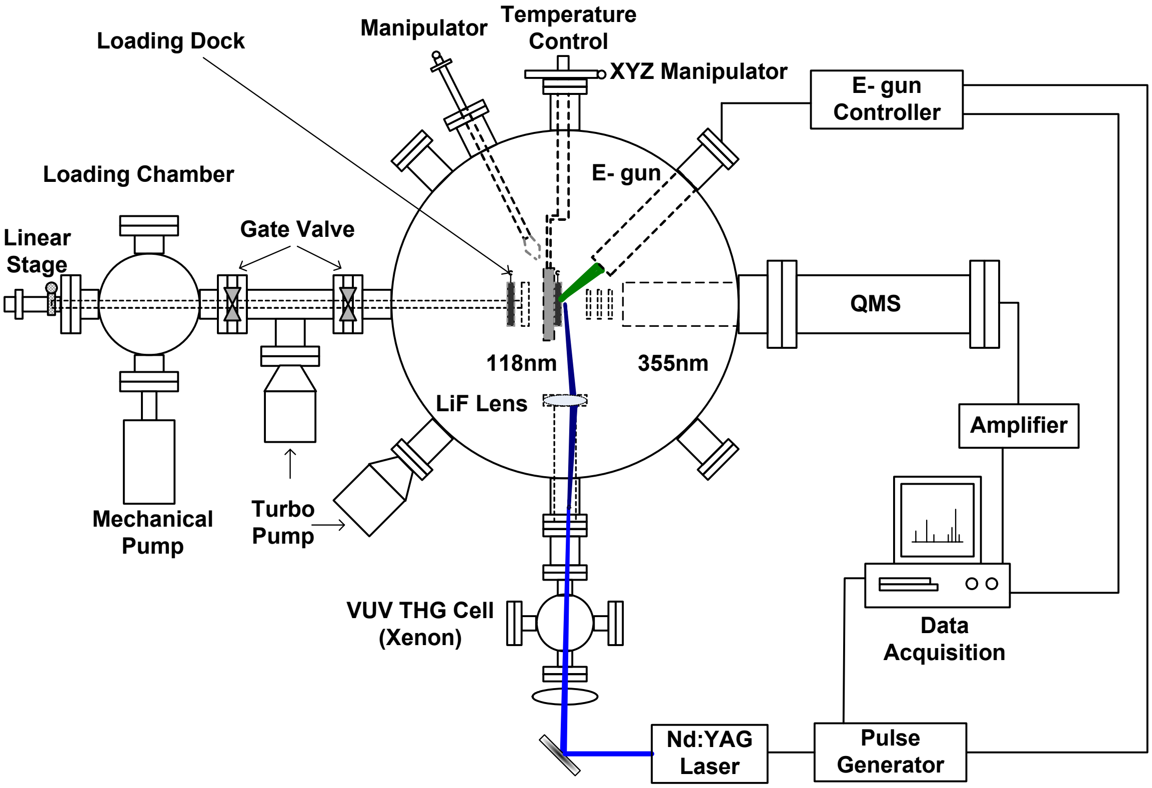

Figure 6-3. Schematic of single photon ionization mass spectrometry developed to study low-energy electron beam induced damage of DNA.

Santa Clara, CA, USA) in the THG cell filled with high purity xenon gas (Matheson Tri-gas, Parsippany, PA, USA). The 118 nm photon intensity was optimized by increasing the power of 355 nm laser and adjusting the pressure of the xenon. In this work, the 20 Hz 355 nm laser (~ 25 mJ) was focused in the tripling cell by a quartz lens (200mm), and the xenon pressure was adjusted to ~ 8 torr by observing the highest ionization signals from neutral molecules (Figure 6-4). The VUV pulse energy was not measured but is expected to be approximately 0.1 μJ based on an approximate conversion efficiency of 10^{-5} reported in literature.[21,22] To avoid multi- photon ionization due to the 355 nm laser, the 118 nm photons were separated from the 355 nm beam by taking advantage of the chromatic aberration of a LiF lens (f = 75 mm) which also serves as a window. The distance between the sample surface and the 118 nm beam is about 1.5 mm. The electron beam incident angle was 45° with respect to the DNA surface. Neutral molecules that desorbed as a result of electron impact on DNA and ionized by 118 nm photons were detected by a modified quadrupole mass spectrometer (Extrel C50; ABB Analytical Instruments, Inc., Pittsburg, PA, USA) mounted perpendicular to the sample surface. An extraction plate was added to the region of ion optics to improve the signal by applying pulsed negative voltage after the pulsed electron beam irradiation. The e-gun, laser, and extraction plate pulse sequence is shown in Figure 6-5. The filament of electron ionizer in the quadrupole mass spectrometer was disconnected from the power supply to avoid further ionization and fragmentation.

6.2.6 Post-irradiation Gel Electrophoresis

After electron irradiation, the DNA samples were removed from the chamber and re-dissolved into water. The amount of DNA was quantitated by measuring absorbance

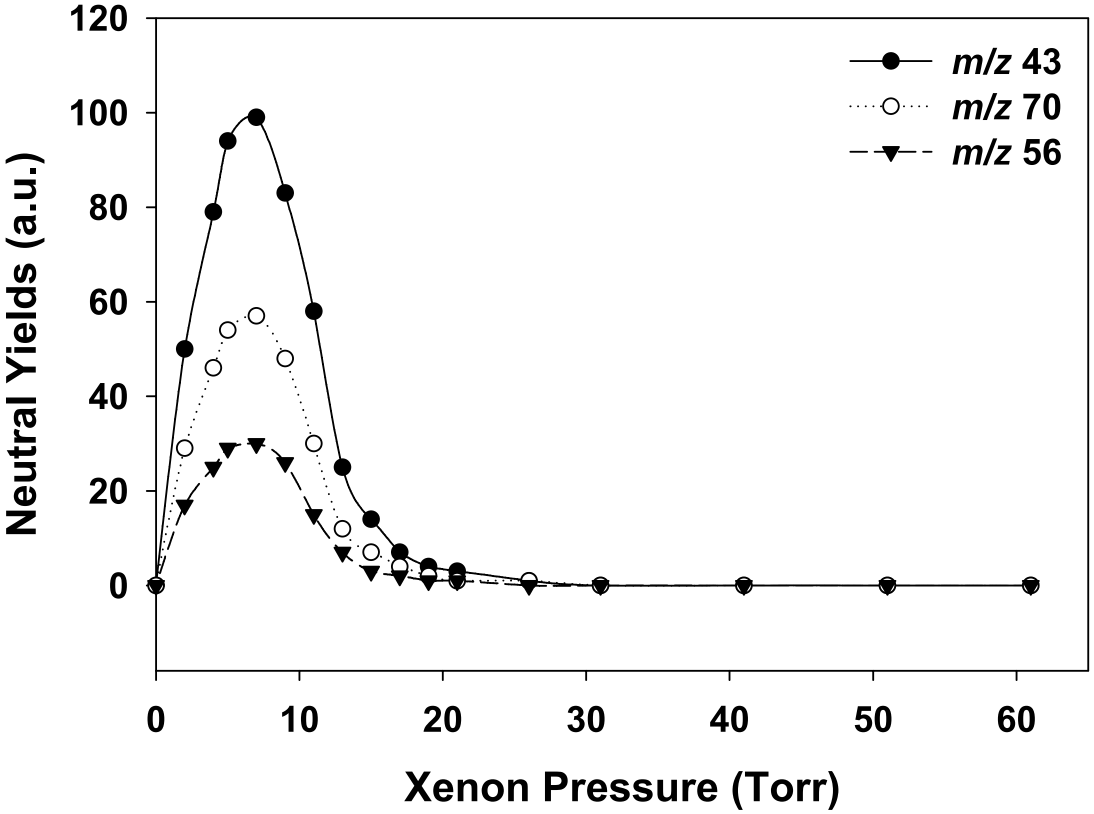

Figure 6-4. The dependence of VUV ionization on xenon pressure at an incident electron energy of 20 eV. The data represent different fragments produced during 20 eV electron beam bombardment on DNA. The maximum VUV conversion efficiency is obtained at ~8 torr. (▼) *m/z* 43; (○) *m/z* 70; (●) *m/z* 56

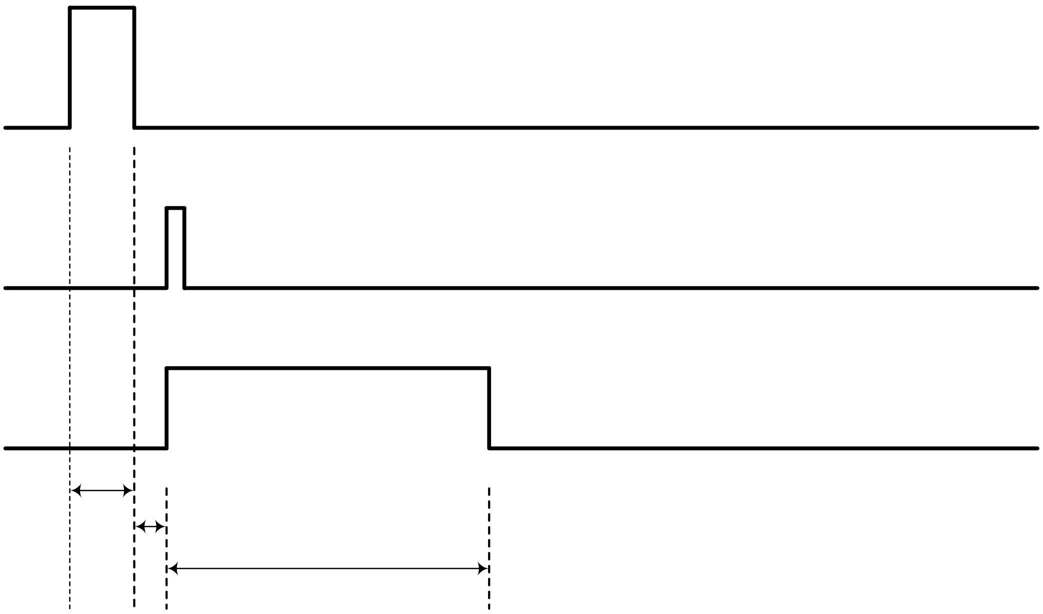

Figure 6-5. The pulse sequence of a typical ESD/SPI MS experiment. (t1) pulse width of the electron beam (100μs); (t2) delay between the electron beam and the laser beam (10 μs); (t3) pulse width of the extraction potential (200 ~ 400 μs).

E-gun

at 260 nm before and after the irradiation. Usually, more than 95% of the deposited mass of DNA could be recovered. The post-irradiated DNA samples were then analyzed by agarose gel electrophoresis (C.B.S. Scientific Inc., Del Mar, CA, USA). As shown in Figure 6-1, the supercoiled, SSB and DSB DNA could be separated by their different migrating abilities in agarose. Three controlled DNA samples were usually analyzed together with post-irradiation samples: (i) original plasmid DNA solution (ii) a DNA sample that was dried, transferred in vacuum and recovered in water without irradiation, and (iii) DSB DNA made by restriction enzyme Sca I. Quantitative analysis of SSBs and DSBs was carried out by reading and integrating the light intensities of corresponding ethidium-stained DNA bands. This is discussed in detail in section 6.3.3.

6.3 RESULTS AND DISCUSSION

6.3.1 SEM Characterization of DNA Molecules in Vacuum

P14 DNA films (10^{12} molecules/cm^{-2}) in vacuum were characterized by scanning electron microscopy (SEM). In Figure 6-6, the SEM images of DNA are shown. The DNA molecules form aggregated structures of variable size. Two different regions can be identified in Figure 6-6A: (i) in the bottom region, plate structures with irregular shapes were observed. The plate structures were further studied by a 100,000 × magnification shown in Figure6-6B. The plates were formed by DNA molecules in the size of 200 ~ 400 nm. (ii) in the top region, branch-like structures in a parallel pattern were observed. By a 150,000 × magnification shown in Figure6-6(c), the aggregations were found to be composed of DNA molecules with 100 nm diameter.

The SEM results clearly showed that DNA molecules were not evenly distributed on the solid surface. In the ESD studies discussed in this chapter, the whole sample area was scanned by a pulsed electron beam.

As shown in Figure 6-6B and 6-6C, DNA molecules may exist as spheres of 100 ~ 400nm diameter under UHV condition. This compact structure could contain many counter ions and water molecules inside the double helix and/or supercoil. Furthermore, the big clusters formed by DNA in different shapes could trap molecules such as water. To fully understand the water content in DNA multilayers, the TPD of water was studied, and the results are shown in the following section.

6.3.2 TPD of DNA Molecules Deposited on Tantalum Surfaces

The desorption behavior of water in plasmid DNA films were investigated by TPD-MS. Figure 6-7 shows the intact H_2O molecules desorbing from a 1 × TBE buffer film and P14 DNA multilayers (10^{11} molecules·cm^{-2}, > 5 monolayers) with storage time of 24 and 48 hour under UHV (10^{-9} torr) condition. The water signal from 1×TBE buffer had smaller intensity compare to the DNA films. The amount of water related to the buffer molecules was less than 15% of that in the DNA molecules. Calibrated by the water yield in TPD of boric acid through thermal decomposition of H_3BO_3 ($H_3BO_3 \rightarrow HBO_2 + H_2O$), the peak area in this measurement can be related to the numbers of water molecules. It is estimated that there were at least 30 water molecules per base pair in the P14 DNA multilayers even under UHV condition for 48 hours. Since most of the low-energy electron (LEE) induced DNA damage experiments were carried out within 24

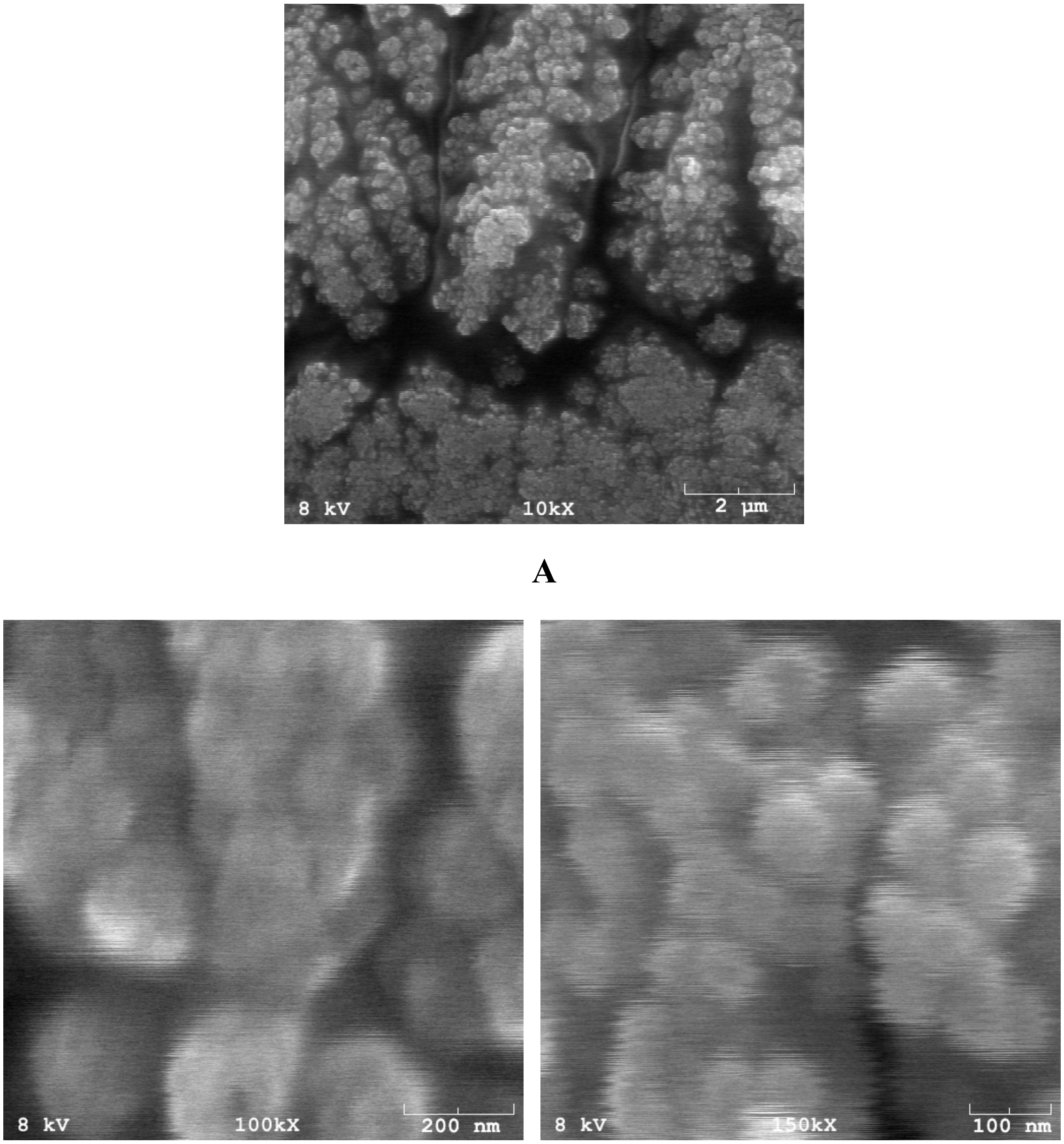

A

B

C

Figure 6-6. SEM image of solid P14 plasmid DNA (A) a 10,000 × magnification; (B) a 100,000 × magnification of bottom region in (A); (C) a 150,000 × magnification of top region in (A) hours after the sample was transferred into vacuum chamber, the effects of water molecules around DNA components have to be considered.

The desorption temperature of water in buffer molecules was greatly lowered relative to the bulk peaks of water TPD from DNA. It clearly indicates that water molecules have relatively stronger interactions to the P14 DNA in its grooves or coils. The desorption energies of water in DNA were calculated using the Polanyi-Wigner equation[87, 88] (equation 6-1) by assuming a first order of desorption, a linear increase of the sample temperature ($\beta = 0.5$ K/s), and a pre-factor ν of 10^{13} s^{-1}. In equation 6-1, the

$$-\frac{d\theta_M}{dT} = \frac{\upsilon \cdot \theta_M^n}{\beta} \cdot \exp\left(\frac{-E_{des}}{R \cdot T}\right) \qquad \text{(Equation 6-1)}$$

θ_M is the instantaneous coverage, n is the kinetic order (desorption order), E_{des} is desorption energy, β is the heating rate, R is the gas constant, and T is the temperature.

The fitted curves produced by the equation 6-1 are shown in Figure 6-8. In Figure 6-8A, three major desorption temperatures (335 K, 365 K, and 405 K) in the water TPD of the 24-hour-storage DNA were fit. The corresponding desorption energies are 91.14 kJ/mol, 98.7 kJ/mol, and 111.3 kJ/mol respectively. In Figure 6-8B, four major desorption temperatures (380 K, 417 K, 470 K, and 525 K) in water TPD of 48-hour-storage DNA were fit. Their desorption energies are 92.4 kJ/mol, 113.4 kJ/mol, 130.2 kJ/mol, and 147 kJ/mol. The desorption energies calculated above are much higher than energies of a hydrogen bond in ice (~31 kJ/mol) and in liquid water (~ 28 kJ/mol).[181] The water molecules around DNA in the vacuum have a stronger interaction to DNA molecules or are better trapped by the DNA in the form of supercoils than the hydration shells of DNA in solutions.

It is also noticed that the water TPD peaks shifted to higher temperature (higher desorption energy) with longer storage time in vacuum. This may indicate that the

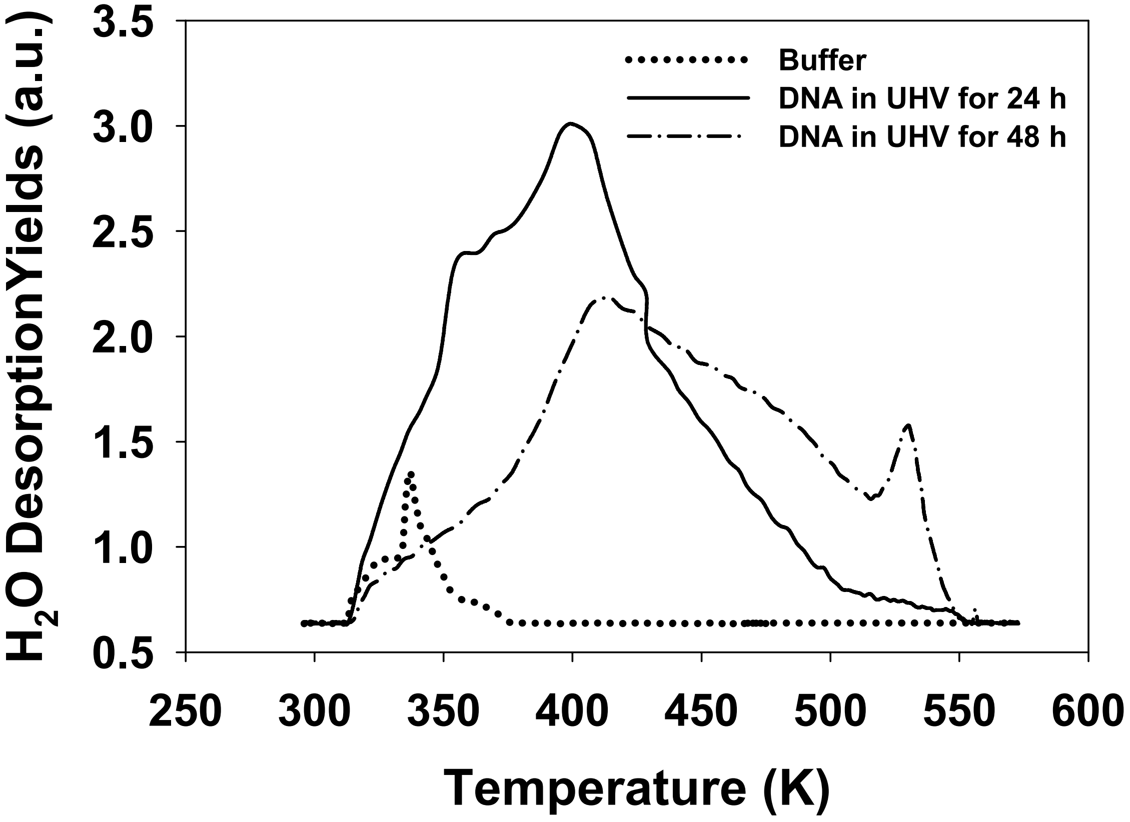

Figure 6-7. TPD of H_2O in P14 DNA. Dotted line: Buffer solution (control); Solid line: DNA sample stored in UHV (10^{-9} torr) for 24 h; Dash-dot line: DNA sample stored in UHV (10^{-9} torr) for 48 h.

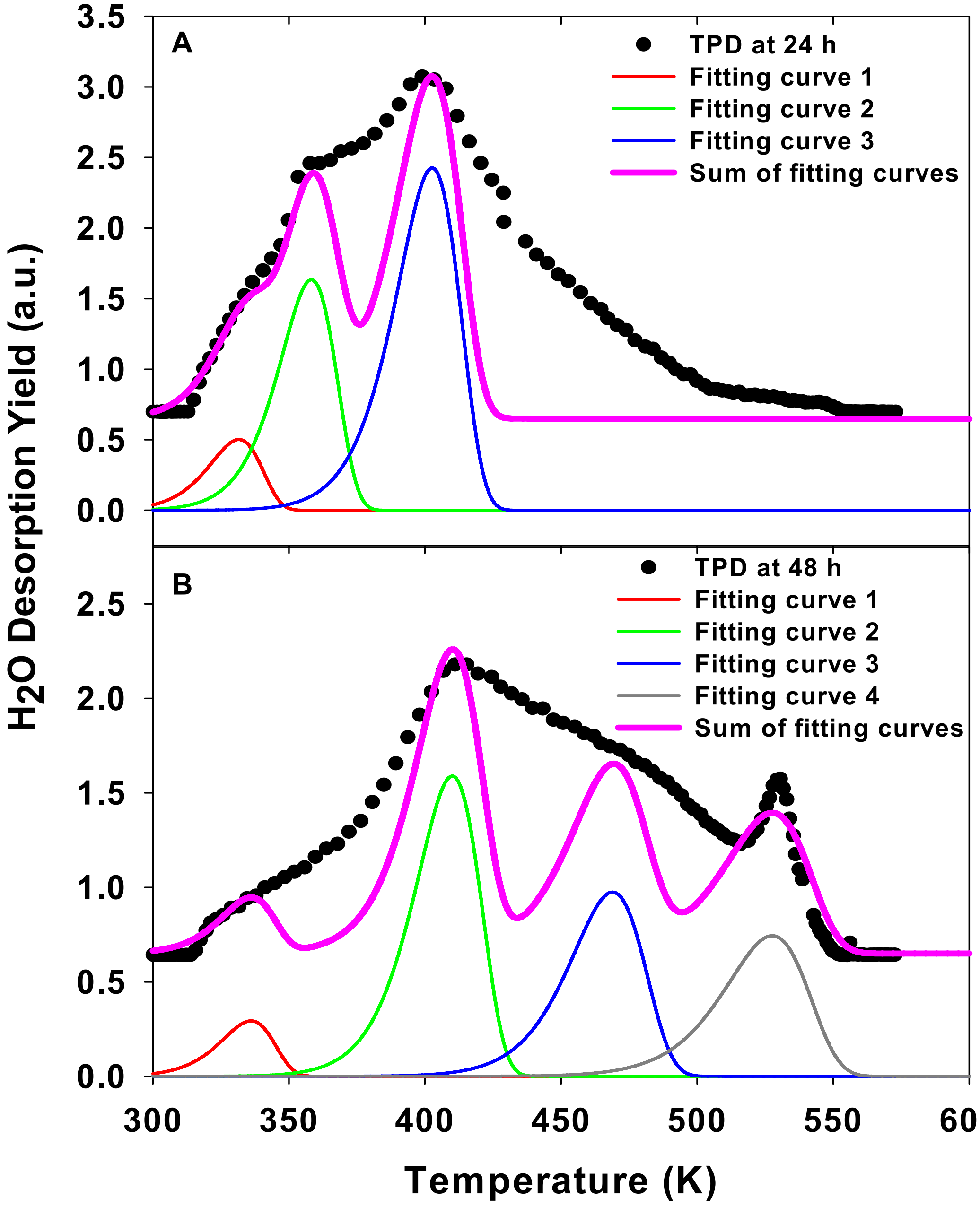

Figure 6-8. Analysis of H_2O TPD from P14 DNA. (A) DNA sample stored in UHV (10^{-9} torr) for 24 hours; (B) DNA sample stored in UHV (10^{-9} torr) for 48 hours; Circle: experiment data; Solid line: TPD fitting curves with different activation energy; Bold line: sum of TPD fitting lines.

conformation of DNA changed after being stored in the vacuum for a long period of time. The decrease of integrated water TPD peak area indicates that 20% of the water molecules per base pair were lost from 24-hour UHV storage to 48-hour UHV storage.

6.3.3 ESD/SPI Study of Neutrals in LEE DNA Damages

The neutral species generated from DNA during the low-energy electron interaction with DNA molecules were investigated by ESD/SPI MS. Figure 6-9 shows the mass spectrum of neutral molecules ionized by 118 nm photon at various incident electron energies. To distinguish the ions and neutrals produced by LEE bombardment on DNA, the intensities of 355 nm laser were adjusted in ESD/SPI measurements at each incident electron energy. Since the VUV photon intensity varied by the changes of 355nm photon flux, the signals of neutral molecules ionized by VUV were also related to the laser intensity. Therefore, signals generated from neutral species during electron irradiation can be easily identified from background ions by their intensity dependence on laser.

In Figure 6-9, more than seven peaks in the mass range of 20 ~ 75 amu were detected when DNA was irradiated by the electron beam (0 to 25 eV). Most of the neutral species could be assigned as fragments of the deoxyribose and bases (Table 6-1). These studies directly link the dissociation of deoxyribose and base groups to the SSB and DSB induced by low-energy electrons. The yield changes of *m/z* 56, 68, 69 and 70 at different irradiation energies also indicates that related molecules might be activation sites for DEA or important intermediate molecules for DNA damage.

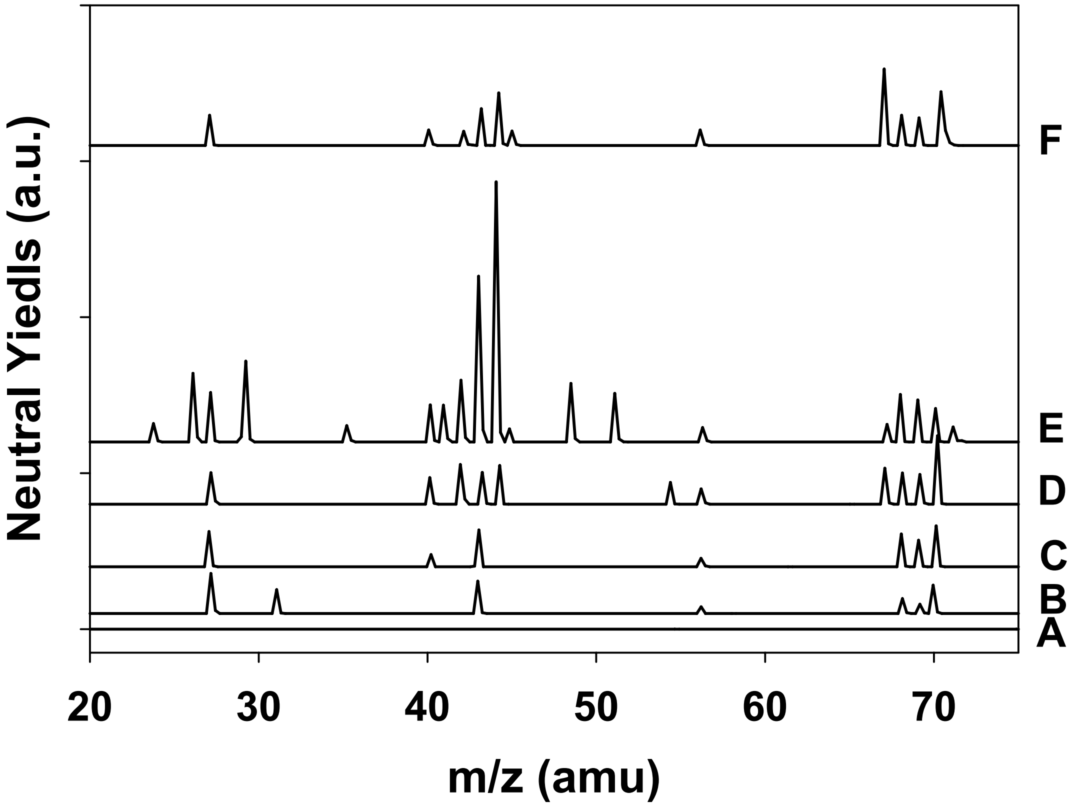

Figure 6-9. Mass spectrum of neutral species produced and desorbed from P14 DNA as a result of low-energy electron bombardment and subsequent ionizatioin by VUV photons at 5 eV increments of incident electron energy. (A) 0 eV; (B) 5 eV; (C) 10 eV (D) 15 eV; (E) 20 eV; (F) 25 eV.

Table 6-1. Neutral species detected by ESD-SPI-MS in LEE induced DNA damage

m/z	Molecular Formula	Possible Source
27	C_2H_3 or HCN	Four bases
43	HCNO or NH_2CNH	T,C or A,G
56	C_3H_4O	T
67	$C_3H_3N_2$	A
68	C_4H_4O	deoxyribose
69	C_4H_5O	deoxyribose
70	CH_2N_2O or $C_2H_4N_3$	T , C or A,G

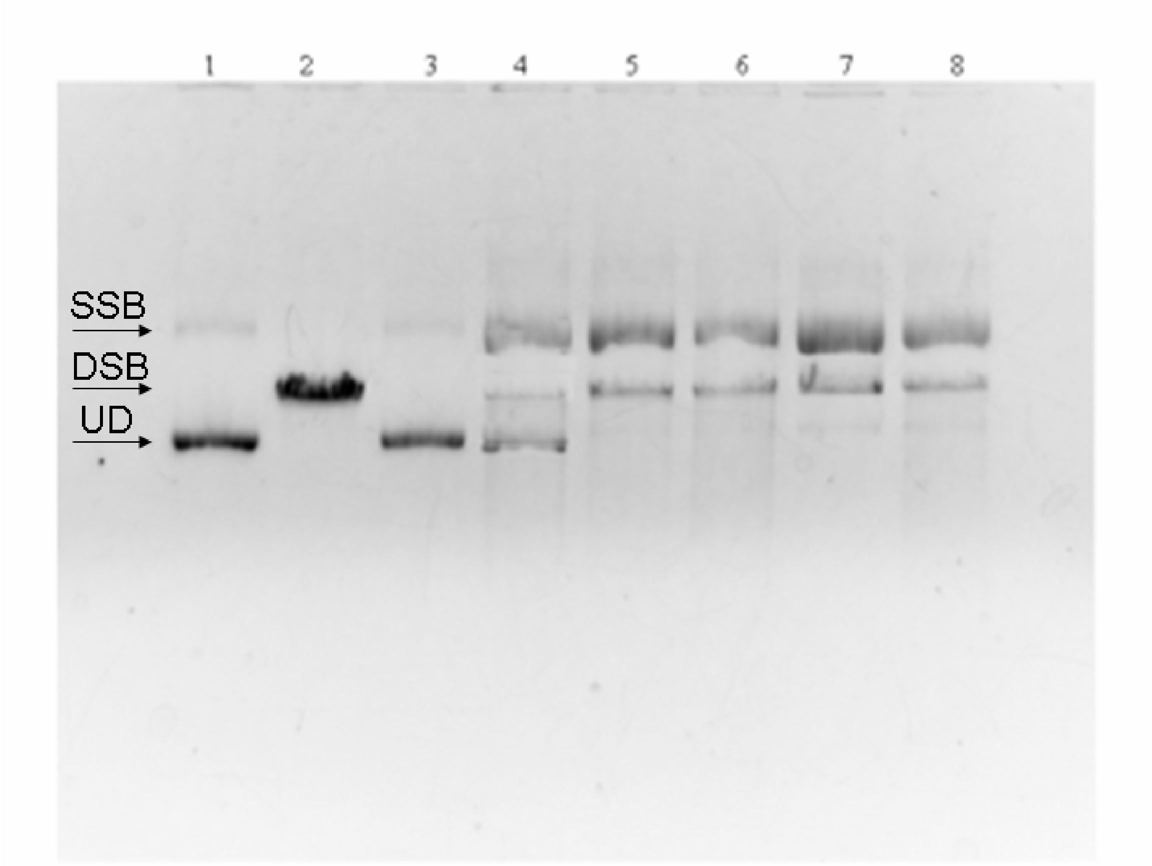

Figure 6-10. Post-irradiation DNA analysis using agarose gel electrophoresis.

Single strand break (SSB); Double strand break (DSB); Undamaged DNA (UD).

Lane 1- p14 solution control (230 ng)
Lane 2- p14-Sca I (DSB + control) (200 ng)
Lane 3- p14 vacuum control (200 ng)
Lane 4- 5 eV (217 ng)
Lane 5- 10 eV (220 ng)
Lane 6- 15 eV (218 ng)
Lane 7- 20 eV (220 ng)
Lane 8- 25 eV (219 ng)

After electron irradiation, DNA samples were analyzed by agarose gel electrophoresis (Figure 6-10). In the energy range of 10 to 25 eV, a smear pattern of multi double strand break appeared and the bands of supercoiled DNA were almost invisible. This result indicates that DNA molecules were severely damaged at the dose of 10^{14} electrons/cm^2.

The quantitative results of DSB and SSB are shown in figure 6-11A. The SSBs are more than 10 times larger than the DSBs. This implies that most of the LEE induced damage is in the form of SSBs. Both SSBs and DSBs show resonant features below 25 eV and another resonant peak at 20 eV. Therefore, there are at least two damage processes involved in the low-energy electron induced damage of DNA.

Since the some of the neutral species desorbed from DNA were DNA fragments, the yields of *m/z* 56, 68, 69 and 70 versus electron energy were compared to the corresponding gel results of SSB and DSB as a function of the incident electron energy. In Figure 6-11B, the yield of *m/z* 68 and 69 showed similar trends in the SSB and DSB probability, which directly corresponds to the DNA damage. In Figure 6-11C, the intensities of neutral peaks at m/z 56 and 70 were found to be opposite to the production of SSB and DSB. These neutrals were generated from DNA bases, and these fragments might also be involved in reactions between other DNA damage related intermediate molecules.

6.3.4 Mechanism of LEE Induced DNA Damages

Recently, several mechanisms of LEE induced DNA have been proposed by observing DNA fragments by HPLC (i) or negative ions using mass spectrometry (ii, iii):

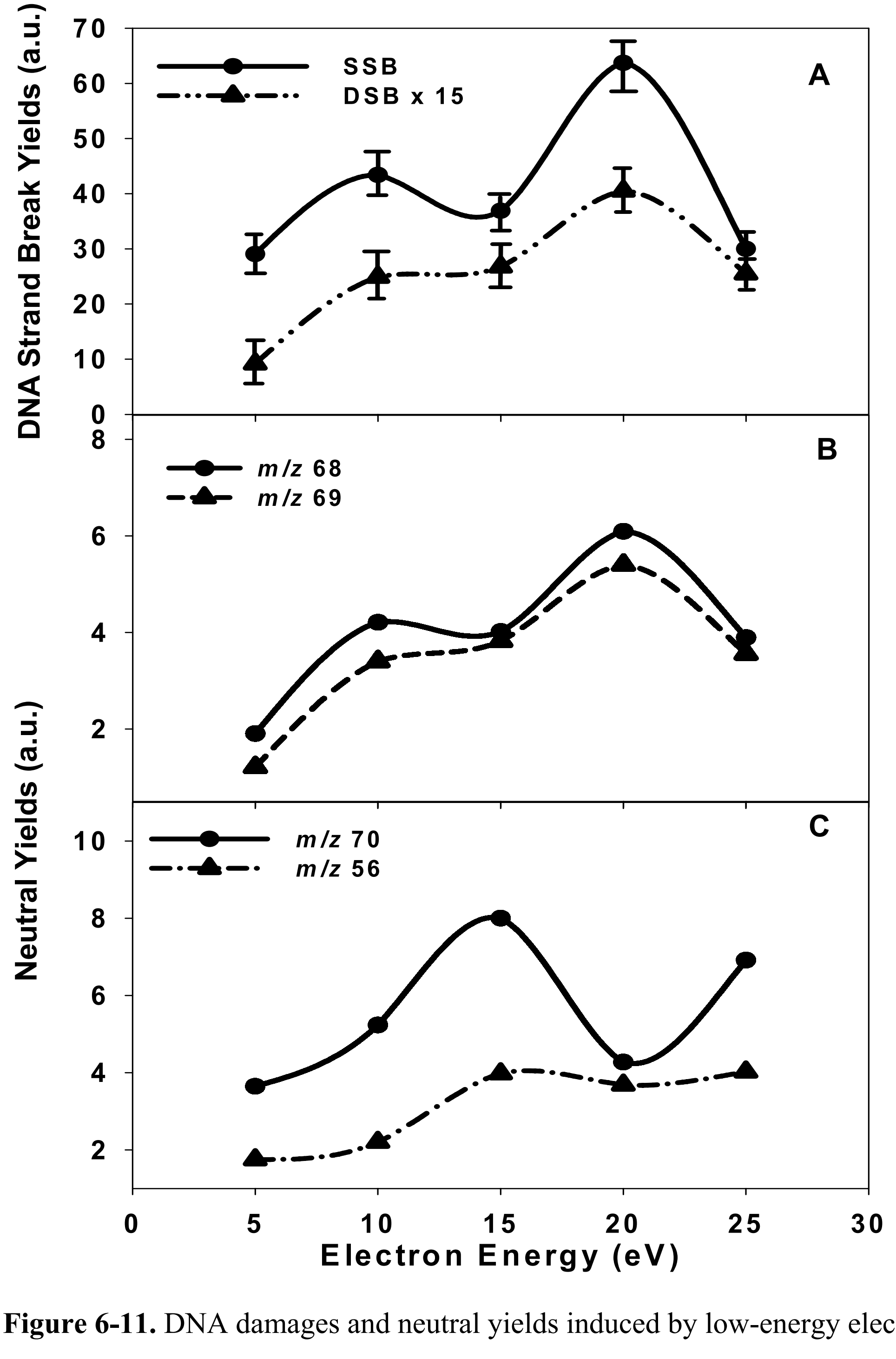

Figure 6-11. DNA damages and neutral yields induced by low-energy electrons.

(A) DNA strand breaks determined by gel electrophoresis;

(B) Neutral yields of *m/z* 68(solid line) and *m/z* 69 (dash-dotted line);

(C) Neutral yields of *m/z* 70 (solid line) and *m/z* 56 (dash-dotted line).

(i) low-energy electron could attach to nucleobase moieties, followed by charge transfer to sugar-phosphate backbone, and induce phosphodiester bond dissociation.[175] (ii) low-energy electrons could impact the DNA and produce OH^- via DEA of the phosphate in the backbone to induce strand breaks,[182] and (iii) DEA with resonance structure at 18ev can lead to C-O bond cleavage by transient electron attachment to a σ^* anion state of the deoxyribose group, followed by dissociating into H^- and corresponding radicals.[183]

By analyzing the ESD/SPI MS results, it was found that all three of these pathways are likely to exist. A generalized DNA damage mechanism is proposed and shown in Figure 6-12. Two different processes should be involved in the strand breaks at 10 and 20 eV resonance features:

(a) At 10 eV, the DEA process basically follows mechanism (i). The bases first capture electrons and transfer them to phosphor group. Sugar radical connected to 5' end (**X**) was produced by 3' cleavage. The sugar radical then formed a sugar-base intermediate neutral molecule (**Y**) through the 5' cleavage. Neutral molecule **y** could then undergo DEA or dissociation to desorb as neutral products (*m/z* 68 and 69) that could be detected by SPI MS. Another fate of molecule (**Y**) is reacting with radicals or excited molecules (m/z 56, 70, or R in figure 6-12) that were created from the bases by DEA which quench them and produce neutral molecules (*m/z* 68 and 69) at 10 eV.

(b) At 20 eV, the intermediate species could be formed by two pathways: (1) reactive scattering O^- was generated through the $2a_1$ core-excited resonance[184] and/or reactive scattering OH was created by the 2 hole-1 electron ($3a_1^{-1}1a_1^{-1}4a_1^{1}$) process[185] from water molecules surrounding DNA. The active intermediate species further react with phosphate sugar moieties[165] to induce the strand break, which is similar to

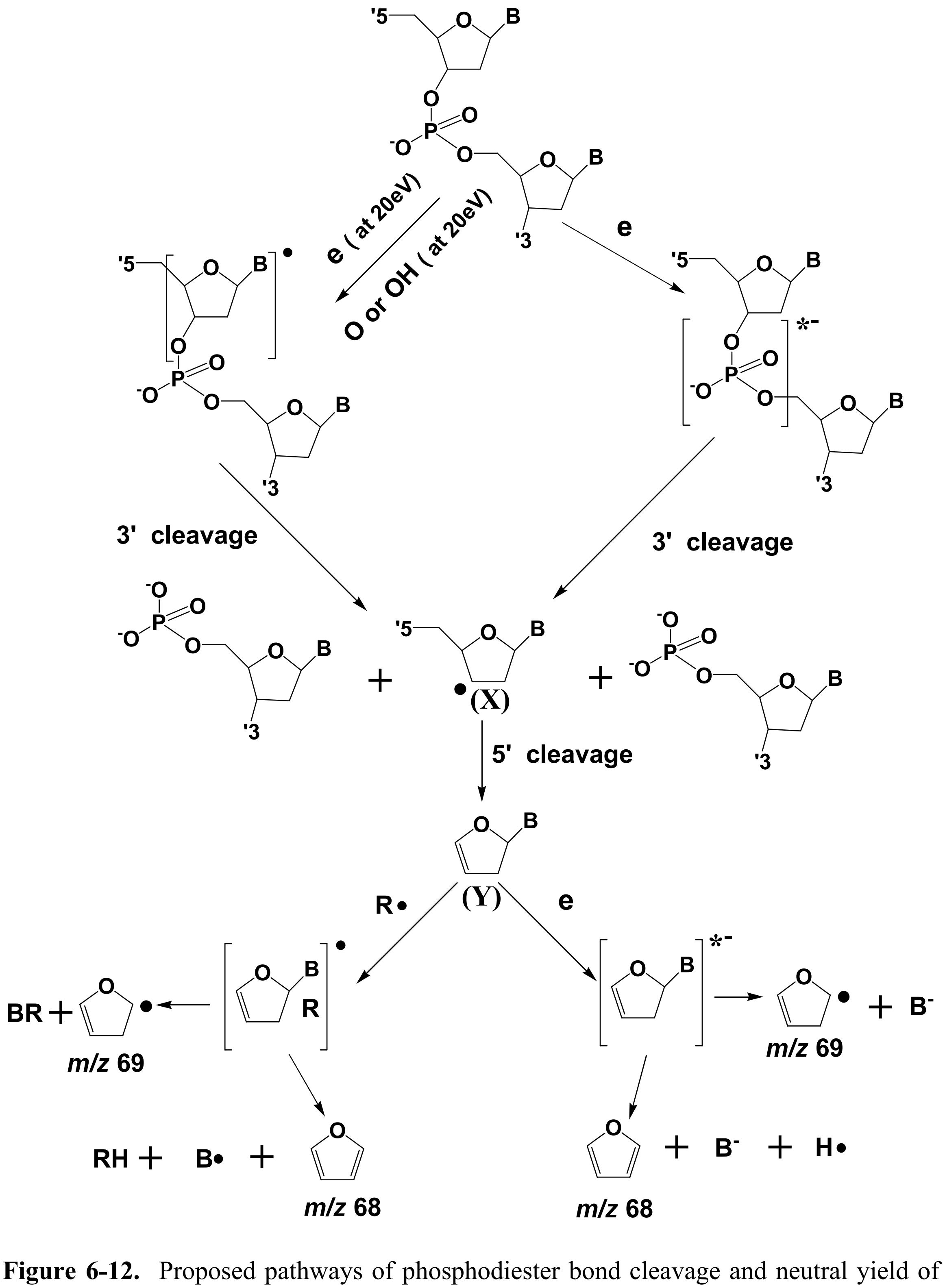

Figure 6-12. Proposed pathways of phosphodiester bond cleavage and neutral yield of *m/z* 68 and 69. B (structures) = DNA bases: A, T, C, and G; R: radicals

mechanism (ii) mentioned above;[182] (2) similar to mechanism (iii),[183] the TNIs are formed by attachment to a σ* anion state of the deoxyribose group with a DEA peak at 18eV. This TNI then dissociates into the sugar radical (**X**) which could eventually generate neutral species *m/z* 68 and 69 by reacting with other active intermediates. Another possible reason for DNA damage at 20 eV is multiple scattering electron energy loss (EEL) followed by resonance formation at lower energies (such as 10 eV).[15] However, this process should generate a much stronger resonance damage peak at low energy, which opposes to the results in Figure 6-11. Therefore, multiple scattering electron energy loss should not be a dominant pathway for stand breaks in this study.

Based on the proposed DNA damage mechanism, it is concluded that the low-energy electron induced DNA damage is a complicated process which involves different DNA components and surrounding water. When electron energy is low, DEA on the phosphate group is the major source of strand breakage. Although the electron capturing of nucleobases does not directly induce the DNA damage, it facilitates the formation of TNI by electron transfer to the phosphate-deoxyribose moiety. At higher energy, electrons interact with the deoxyribose group and surrounding water more effectively to produce strand breaks. The detection of the sugar related molecules (m/z=68) proves that the sugar radical are main precursors in DNA damage induced by electron irradiation.

6.4 CONCLUSION

In this work, the DNA molecules adsorbed on solid surfaces in UHV were studied by SEM. The size and cluster structure of plasmid DNA were determined. It provided a useful guide for ESD/SPI MS and supported the results of water TPD from plasmid DNA. The water TPD from P14 DNA was obtained for the first time, and the water content (~ 30 molecules per base) as well as desorption energies (in the range of 90 ~ 150 kJ/mol) were reported. The results were highly beneficial in the characterization of DNA conformation and interactions between water and DNA under UHV conditions and the understanding of the details of LEE induced DNA damage by estimating the composition of the chemical environment of DNA.

The ESD/SPI MS followed by gel electrophoresis was developed for irradiation induced genotoxic damage. This novel method successfully detected neutral species generated from DNA molecules during irradiation and are correlated with the SSBs and DSBs as a function of incident electron energy. This technique provides a new way to understand the active sites in low-energy electron induced DNA damage by identifying large neutral molecules which could be easily linked to functional groups in DNA. .

A mechanism of DNA strand breakage under the irradiation of LEE was also proposed based on the results of water TPD and ESD/SPI MS. It indicated that DEA of base pairs would not directly result in DNA damage. More than one DEA process and core level ionization of O were involved in the mechanisms for the two resonance features appearing in DNA damage and neutral marker molecule yields (*m/z* 68 and 69) at 10 eV and 20 eV. Water molecules around plasmid DNA play an important role in generating resonance DNA damages induced by LEE. The results in this study provide further insights concerning the mechanisms of LEE-induced damage to DNA.

CHAPTER 7

CONCLUSIONS

7.1 CONCLUSIONS

Surface-assisted laser desorption/ionization mass spectrometry (SALDI MS), laser desorption single photon ionization mass spectrometry (LD/SPI MS), and electron stimulated desorption single photon ionization mass spectrometry (ESD/SPI MS) methods for analysis of small organic/biological molecules were successfully developed and performed on a specially designed UHV analytical system. These techniques provide simple, fast, and sensitive detection of amino acids, small peptides, selenium metabolites and DNA damage intermediates in complex samples. The mass analysis capability of biological mass spectrometry has been greatly extended by the three new stimulated desorption/photoionization (SD/PI) techniques. Based on the investigation of the desorption and ionization mechanisms on selected surfaces, an SD/PI platform has been established to facilitate the analysis of various small molecules in different biological, environmental, pharmaceutical, and clinical systems.

Surface-assisted laser desorption/ionization mass spectrometry (SALDI MS) is a novel technique for direct analysis of organic and biological molecules. In this matrix-free method, specific surfaces are selected to trap analytes and to assist/enhance the laser desorption/ionization process. Thermally unstable molecules such as amino acids, dipeptides, and organoselenium compounds were successfully detected by SALDI MS on carbon and silicon surfaces. The readily interpretable mass spectra of analyte molecules with the high sensitivity and good spot-to-spot reproducibility proves that SALDI MS is a powerful method for many potential applications, such as free amino acid analysis in physiological fluids, peptide identification in protein digest component mapping, and metabolite detection in biological samples.

Surface effects, solvent effects, temperature effects and pH effects were studied. It has been found that surface morphology plays an important role in the performance of SALDI-MS. The existence of water molecules on the SALDI substrates also proved to be critical in the SALDI process. Surface terminated hydroxyl groups were correlated with the yield of SALDI signals. A possible mechanism of SALDI was proposed based on the observed results.

In general, stimulated desorption results in neutral yields that are much larger than ion yields. Thus, we have exploited and further developed laser desorption/single photon ionization mass spectrometry (LD/SPI MS) as a means of examining biomolecules. LD/SPI-MS uses one laser to desorb intact neutral molecules from the sample surface and another vacuum ultraviolet (VUV) laser to ionize the desorbed neutral molecules. The experimental results clearly illustrate that LD/SPI MS is a sensitive and fast analysis method with uniform selectivity and high sensitivity. It also demonstrates the viability of matrix free LD/SPI MS for molecular characterization and quantitive analysis of biological metabolites in the *m/z* 10 ~ 600 range that are present in complex biological fluids.

Selenium (Se) is an essential ultra-trace element in the human body. Se metabolites, especially organoselenium compounds, have been linked to toxicity, antioxidant enzymes, endocrine processes, and proper functioning of the immune system. In efforts to obtain more useful information of Se-containing metabolites in human urine, mass determination of unknown organoselenium compounds in biological matrices using SALDI-MS was investigated. In another approach, several selenium metabolites in human urine were successfully detected by LD/SPI MS. A HPLC-MS/MS method was further developed for quantitative studies of selenium metabolites in human urine and showed consistent results with LD/SPI MS.

Low-energy electrons (LEE, 3-20 eV) have been shown to induce single and double strand breaks (SSB and DSB) in plasmid DNA. LEE-induced DNA strand breaks were related to the formation and decay of transient negative ion (TNI) states localized on various components of the DNA (i.e. bases, phosphates, deoxyribose, hydration water, etc). To understand the genotoxic effects and cell damage due to secondary species of high-energy radiation, we investigate the role of TNIs and the specificity in LEE-DNA damage by examining the neutral product yields using ESD/SPI MS. The neutral yields as a function of incident electron energy are then correlated with the SSBs and DSBs measured using post-irradiation gel electrophoresis. The results provide further insight concerning the mechanisms of LEE-induced damage to DNA.

Overall, this research provided an in-depth understanding of new mass spectrometric techniques in the analysis of biomolecules. It demonstrated that SD/PI MS is a uniquely advantageous tool for direct analysis of small molecules in complex biochemical systems. This work also leads to a better understanding of electron induced damage on large biological molecules. Furthermore, LD/SPI MS shows great potential for future work in the analysis of metabolites, drug discovery, and biomarker imaging.

7.2 CONTINUATION OF RESEARCH

Since an imaging TOF mass spectrometer has been designed and built to provide spatially resolved ion signals, mass-resolved images of analytes revealing the spatial distribution on sample surfaces could be obtained using this instrument. Based on this technique, the details of ion generation on specific sites with sub-micrometer resolution could be investigated, which will be helpful in examining the mechanisms of SALDI or catalytic reactions on different substrates. The imaging TOF can also be used for analysis of biological samples (i.e. cell or tissue) to observe the molecular images of different species on or within the sample. This will significantly facilitate numerous important applications such as the understanding of cell metabolism and the search for various biomarkers.

With the advantages of simple, fast, and sensitive analysis, stimulated desorption photoionization mass spectrometry (SD/PI MS) can be applied to many biological or pharmaceutical studies involving small molecules such as metabolite analysis and neurotransmitter detection in physical fluids or cells. By coupling SD/PI with high resolution mass spectrometry, the elemental composition and chemical structure could be obtained for faster and easier identification of unknown biological molecules from complicated samples. This new technology will be highly beneficial to the advances of biological sciences.

Stimulated desorption/photoionization (SD/PI) usually utilizes specific substrate such as graphite and porous silicon. This platform offers an endless range of functionalization options. By derivatizing or modifying the surface with functional groups such as receptors, antigens, or specific ligands, the SD/PI MS can provide precise and rapid detection of many different analytes in a relative simple assay format. It has a broad market in various applications (i.e. drug candidate screening, protein digest mapping and metabolite identification). The chip-based format of SD/PI is also compatible with microfluidics and microdevices. It indicates that this technology in the micrometer range or less can be fully used in the next generation of instruments.

To improve the detection efficiency of LD/SPI MS, phase matching of VUV generation can be further utilized by mixing xenon with argon in a partial pressure ratio of ~ 1:10. The flux of 118 nm photons will be increased by ~ 10 times and the detection limit of LD/SPI MS will be extended to 100 attomole range for sensitive analysis of target molecules. The high flux of VUV photons is also helpful to improve the imaging detection of neutral molecules desorbed from the sample surface by photons or electrons. The use of an ultra-fast laser with high spectral purity will also increase the VUV conversion efficiency and enhance the overall detection sensitivity.

A set of LD/SPI MS and HPLC-MS/MS method has been established for the analysis of organoselenium compounds in human urine. Using this method, the characterization and quantitative detection of known and unknown selenium metabolites should be further studied to understand the pharmacokinetics and metabolic pathway of selenium supplements in the human body.

The DNA damage should be further studied by performing more experiments as a function of incident electron energy. Negative ions and neutrals could be monitored simultaneously by using two mass spectrometers to provide a complete picture of the formation of TNI and other intermediate species. This work will offer direct understanding to the interaction between DNA molecules and low-energy electrons. A

FTIR spectroscopy method should also be developed to report the DNA damage during the electron bombardment. This method will precisely provide *in situ* strand break information and greatly reduce the analyzing time by replacing the post-ionization gel electrophoresis.

REFERENCES

(1) Cooper, M. A. *Curr. Opin. Pharmacol.* **2003**, *3*, 557-562.

(2) Lawrence, N. S.; Beckett, E. L.; Davis, J.; Compton, R. G. *Anal. Biochem.* **2002**, *303*, 1-16.

(3) Schwille, P. *Cell Biochem. Biophys.* **2001**, *34*, 383-408.

(4) Altria, K. D.; Elder, D. *J. of Chromatogr., A* **2004**, *1023*, 1-14.

(5) Berna, M. J.; Ackermann, B. L.; Murphy, A. T. *Anal. Chim. Acta* **2004**, *509*, 1-9.

(6) Kuhara, T. *Mass Spectrom. Rev.* **2005**, *24*, 814-827.

(7) Tanaka, K.; Waki, H.; Ido, Y.; Akita, S.; Yoshida, Y.; Yohida, T. *Rapid Commun. Mass Spectrom.* **1988**, *2*, 151-153.

(8) Karas, M.; Bahr, U.; Giessmann, U. *Mass Spectrom. Rev.* **1991**, *10*, 335-357.

(9) Stults, J. T. *Curr. Opin. Struct. Biol.* **1995**, *5*, 691-698.

(10) Schriemer, D. C.; Li, L. *Anal. Chem.* **1996**, *68*, 2721-2725.

(11) Griesser, H. J.; Kingshott, P.; McArthur, S. L.; McLean, K. M.; Kinsel, G. R.; Timmons, R. B. *Biomaterials* **2004**, *25*, 4861-4875.

(12) Marvin, L. F.; Roberts, M. A.; Fay, L. B. *Clin. Chim. Acta* **2003**, *337*, 11-21.

(13) Stump, M. J.; Fleming, R. C.; Gong, W. H.; Jaber, A. J.; Jones, J. J.; Surber, C. W.; Wilkins, C. L. *Appl. Spectroscop. Rev.* **2002**, *37*, 275-303.

(14) Laiko, V. V.; Taranenko, N. I.; Berkout, V. D.; Musselman, B. D.; Doroshenko, V. M. *Rapid Commun. Mass Spectrom.* **2002**, *16*, 1737-1742.

(15) Dale, M. J.; Knochenmuss, R.; Zenobi, R. *Anal. Chem.* **1996**, *68*, 3321-3329.

(16) Cohen, L. H.; Gusev, A. I. *Anal. Bioanal. Chem.* **2002**, *373*, 571-586.

(17) Chen, H.; Chen, Y.; Aleksandrov, A.; Dong, J.; Liu, M.; Orlando, T. M. *Appl. Surf. Sci.* **2005**, *243*, 166-177.

(18) Chen, H.; Aleksandrov, A.; Chen, Y.; Zha, S.; Liu, M.; Orlando, T. M. *J. Phys. Chem. B* **2005**, *109*, 11257-11262.

(19) Lhuillier, A.; Schafer, K. J.; Kulander, K. C. *J. of Phys. B* **1991**, *24*, 3315-3341.

(20) Lockyer, N. P.; Vickerman, J. C. *Laser Chem.* **1997**, *17*, 139-159.

(21) Ferge, T.; Muehlberger, F.; Zimmermann, R. *Anal. Chem.* **2005**, *77*, 4528-4538.

(22) Kung, A. H. *Opt. Lett.* **1983**, *8*, 24-26.

(23) Kobayashi, Y.; Ogra, Y.; Ishiwata, K.; Takayama, H.; Aimi, N.; Suzuki, K. T. *Proc. Natl. Acad. Sci. U. S. A.* **2002**, *99*, 15932-15936.

(24) Karas, M.; Bachmann, D.; Bahr, U.; Hillenkamp, F. *Int. J. Mass Spectrom. Ion Processes* **1987**, *78*, 53-68.

(25) Vastola, F. J.; Mumma, R. O.; Pirone, A. J. *Org. Mass Spectrom.* **1970**, *3*, 101-&.

(26) Zaluzec, E. J.; Gage, D. A.; Watson, J. T. *Protein Expression Purif.* **1995**, *6*, 109-123.

(27) Beavis, R. C.; Chait, B. T. In *High Resolution Separation and Analysis of Biological Macromolecules, Pt A*, 1996; Vol. 270, pp 519-551.

(28) Cramer, R.; Gobom, J.; Nordhoff, E. *Expt. Rev. of Proteom.* **2005**, *2*, 407-420.

(29) Feistner, G. J.; Faull, K. F.; Barofsky, D. F.; Roepstorff, P. *J. Mass Spectrom.* **1995**, *30*, 519-530.

(30) Harvey, D. J. *Mass Spectrom. Rev.* **1999**, *18*, 349-450.

(31) Harvey, D. J. *Int. J. Mass Spectrom.* **2003**, *226*, 1-35.

(32) Limbach, P. A. *Mass Spectrom. Rev.* **1996**, *15*, 297-336.

(33) Crain, P. F.; McCloskey, J. A. *Curr. Opin. Biotechnol.* **1998**, *9*, 25-34.

(34) Edwards, J. R.; Ruparel, H.; Ju, J. Y. *Mutat. Res.* **2005**, *573*, 3-12.

(35) Jurinke, C.; Oeth, P.; van den Boom, D. *Mol. Biotechnol.* **2004**, *26*, 147-163.

(36) Charlwood, J.; Bryant, D.; Skehel, J. M.; Camilleri, P. *Biomol. Eng.* **2001**, *18*, 229-240.

(37) Fujita, T.; Itagaki, Y.; Hisaka, M.; Naoki, H.; Nakajima, T.; Andriantsiferana, M. *Rapid Commun. Mass Spectrom.* **1997**, *11*, 1115-1119.

(38) Sleno, L.; Volmer, D. A. *Anal. Chem.* **2005**, *77*, 1509-1517.

(39) Rader, H. J.; Schrepp, W. *Acta Polym.* **1998**, *49*, 272-293.

(40) Nielen, M. W. F. *Mass Spectrom. Rev.* **1999**, *18*, 309-344.

(41) Macha, S. F.; Limbach, P. A. *Curr. Opin. Solid State Mater. Sci.* **2002**, *6*, 213-220.

(42) Murgasova, R.; Hercules, D. M. *Anal. Bioanal. Chem.* **2002**, *373*, 481-489.

(43) Sunner, J.; Dratz, E.; Chen, Y. C. *Anal. Chem.* **1995**, *67*, 4335-4342.

(44) Xu, S. Y.; Li, Y. F.; Zou, H. F.; Qiu, J. S.; Guo, Z.; Guo, B. C. *Anal. Chem.* **2003**, *75*, 6191-6195.

(45) Chen, W. Y.; Wang, L. S.; Chiu, H. T.; Chen, Y. C.; Lee, C. Y. *J. Am. Soc. Mass Spectrom.* **2004**, *15*, 1629-1635.

(46) Kim, H. J.; Lee, J. K.; Park, S. J.; Ro, H. W.; Yoo, D. Y.; Yoon, D. Y. *Anal. Chem.* **2000**, *72*, 5673-5678.

(47) Wei, J.; Buriak, J. M.; Siuzdak, G. *Nature (London)* **1999**, *399*, 243-246.

(48) Thomas, J. J.; Shen, Z.; Crowell, J. E.; Finn, M. G.; Siuzdak, G. *Proc. Natl. Acad. Sci. U. S. A.* **2001**, *98*, 4932-4937.

(49) Dattelbaum Andrew, M.; Iyer, S. *Expt. Rev. of Proteom.* **2006**, *3*, 153-161.

(50) Moore, S.; Stein, W. H. *J. Biol. Chem.* **1951**, *192*, 663-681.

(51) Alterman, M. A.; Gogichayeva, N. V.; Kornilayev, B. A. *Anal. Biochem.* **2004**, *335*, 184-191.

(52) Husek, P.; Simek, P. *Lc Gc North America* **2001**, *19*, 986-990.

(53) May, S. W. *Expert Opin. Invest. Drugs* **2002**, *11*, 1261-1269.

(54) Aaseth, J.; Haugen, M.; Forre, O. *Analyst* **1998**, *123*, 3-6.

(55) Kose, K.; Dogan, P.; Kardas, Y.; Saraymen, R. *Biol. Trace Elem. Res.* **1996**, *53*, 51-56.

(56) Beck, M. A. *Biomed. Enviro. Sci.* **1997**, *10*, 307-315.

(57) Huttunen, J. K. *Biomed. Enviro. Sci.* **1997**, *10*, 220-226.

(58) Ip, C. *J. Nutr.* **1998**, *128*, 1845-1854.

(59) Schrauzer, G. N. *Cell. Mol. Life Sci.* **2000**, *57*, 1864-1873.

(60) Clark, L. C.; Combs, G. F., Jr.; Turnbull, B. W.; Slate, E. H.; Chalker, D. K.; Chow, J.; Davis, L. S.; Glover, R. A.; Graham, G. F.; Gross, E. G.; Krongrad, A.; Lesher, J. L., Jr.; Park, H. K.; Sanders, B. B., Jr.; Smith, C. L.; Taylor, J. R. *JAMA, J. Am. Med. Assoc.* **1996**, *276*, 1957-1963.

(61) Yoshizawa, K.; Willett, W. C.; Morris, S. J.; Stampfer, M. J.; Spiegelman, D.; Rimm, E. B.; Giovannucci, E. *J. Natl. Cancer Inst.* **1998**, *90*, 1219-1224.

(62) Baum, M. K.; Shor-Posner, G.; Lai, S.; Zhang, G.; Lai, H.; Fletcher, M. A.; Sauberlich, H.; Page, J. B. *J. of Acquired Immune Defic. Syndr. Hum. Retrovirol.* **1997**, *15*, 370-374.

(63) Shih, S.; Jung, K. H.; Qian, R. Z.; Kwong, D. L. *Appl. Phys. Lett.* **1993**, *62*, 467-469.

(64) Han, M.; Sunner, J. *J. Am. Soc. Mass Spectrom.* **2000**, *11*, 644-649.

(65) Lewis, W. G.; Shen, Z.; Finn, M. G.; Siuzdak, G. *Int. J. Mass Spectrom.* **2003**, *226*, 107-116.

(66) Shen, Z.; Thomas, J. J.; Averbuj, C.; Broo, K. M.; Engelhard, M.; Crowell, J. E.; Finn, M. G.; Siuzdak, G. *Anal. Chem.* **2001**, *73*, 612-619.

(67) Koster, C.; Grotemeyer, J. *Org. Mass Spectrom.* **1992**, *27*, 463-471.

(68) Lockyer, N. P.; Vickerman, J. C. *Int. J. Mass Spectrom.* **2000**, *197*, 197-209.

(69) Francesconi, K. A.; Pannier, F. *Clin. Chem.* **2004**, *50*, 2240-2253.

(70) Hoang, T. T.; Chen, Y.; May, S. W.; Browner, R. F. *Anal. Chem.* **2004**, *76*, 2062-2070.

(71) Park, K. H.; Kim, H. J. *Rapid Commun. Mass Spectrom.* **2001**, *15*, 1494-1499.

(72) Hoang Tiffany, T.; Chen, Y.; May Sheldon, W.; Browner Richard, F. *Anal. Chem.* **2004**, *76*, 2062-2070.

(73) Li, Q.; Ricardo, A.; Benner, S. A.; Winefordner, J. D.; Powell, D. H. *Anal. Chem.* **2005**, *77*, 4503-4508.

(74) Kinumi, T.; Shimomae, Y.; Arakawa, R.; Tatsu, Y.; Shigeri, Y.; Yumoto, N.; Niki, E. *J. Mass Spectrom.* **2006**, *41*, 103-112.

(75) Zhang, R.; Colbran, S.; Fisher, K.; Willett, G. *Adv. Mass Spectrom.* **2001**, *15*, 757-758.

(76) Chen, Y. C.; Sun, M. C. *Rapid commun. in mass spectrom.* **2001**, *15*, 2521-2525.

(77) Bhattacharya, S. H.; Raiford, T. J.; Murray, K. K. *Anal. Chem.* **2002**, *74*, 2228-2231.

(78) Chen, C.-T.; Chen, Y.-C. *Anal. Chem.* **2005**, *77*, 5912-5919.

(79) Lin, Y. S.; Chen, Y. C. *Anal. Chem.* **2002**, *74*, 5793-5798.

(80) Zhan, Q.; Wright, S. J.; Zenobi, R. *J. Am. Soc. Mass Spectrom.* **1997**, *8*, 525-531.

(81) Kruse, R. A.; Li, X.; Bohn, P. W.; Sweedler, J. V. *Anal. Chem.* **2001**, *73*, 3639-3645.

(82) Alimpiev, S.; Nikiforov, S.; Karavanskii, V.; Minton, T.; Sunner, J. *J. Chem. Phys.* **2001**, *115*, 1891-1901.

(83) Luo, G.; Chen, Y.; Siuzdak, G.; Vertes, A. *J. Phys. Chem. B* **2005**, *109*, 24450-24456.

(84) Chen, Y.; Chen, H.; Aleksandrov, A.; Orlando, T. *Anal. Chem.* in prep.

(85) Li, X.; Bohn, P. W. *Appl. Phys. Lett.* **2000**, *77*, 2572-2574.

(86) Finkel, N. H.; Prevo, B. G.; Velev, O. D.; He, L. *Anal. Chem.* **2005**, *77*, 1088-1095.

(87) Dejong, A. M.; Niemantsverdriet, J. W. *Surf. Sci.* **1990**, *233*, 355-365.

(88) King, D. A. *Surf. Sci.* **1975**, *47*, 384-402.

(89) Sunner, J.; Dratz, E.; Chen, Y.-C. *Anal. Chem.* **1995**, *67*, 4335-4342.

(90) Taylor, D. P.; Simpson, W. C.; Knutsen, K.; Henderson, M. A.; Orlando, T. M. *Appl. Surf. Sci.* **1998**, *127-129*, 101-104.

(91) Gorman, G. S.; Speir, J. P.; Turner, C. A.; Amster, I. J. *J. Am. Chem. Soc.* **1992**, *114*, 3986-3988.

(92) Gotoh, T.; Kotake, S.; Ishikawa, K.; Kanasaki, J.; Tanimura, K. *Phys. Rev. Lett.* **2004**, *93*, 117401-117401.

(93) Kanasaki, J.; Nakamura, M.; Ishikawa, K.; Tanimura, K. *Phys. Rev. Lett.* **2002**, *89*, 257601-257604.

(94) Alexandrov, A.; Piacentini, M.; Zema, N.; Felici, A. C.; Orlando, T. M. *Phys. Rev. Lett.* **2001**, *86*, 536-539.

(95) Knutsen, K.; Orlando, T. M. *Phys. Rev. B* **1997**, *55*, 13246-13252.

(96) Trevor, J. L.; Lykke, K. R.; Pellin, M. J.; Hanley, L. *Langmuir* **1998**, *14*, 1664-1673.

(97) Karas, M.; Hillenkamp, F. *Anal. Chem.* **1988**, *60*, 2299-2301.

(98) Villas-Boas, S. G.; Mas, S.; Akesson, M.; Smedsgaard, J.; Nielsen, J. *Mass Spectrom. Rev.* **2005**, *24*, 613-646.

(99) Friess, S. D.; Daniel, J. M.; Zenobi, R. *Phys. Chem. Chem. Phys.* **2004**, *6*, 2664-2675.

(100) Muddiman, D. C.; Gusev, A. I.; Hercules, D. M. *Mass Spectrom. Rev.* **1995**, *14*, 383-429.

(101) Kraft, P.; Alimpiev, S.; Dratz, E.; Sunner, J. *J. Am. Soc. Mass Spectrom.* **1998**, *9*, 912-924.

(102) Chen, Y. C.; Shiea, J.; Sunner, J. *J. of Chromatogr. A* **1998**, *826*, 77-86.

(103) Chen, Y.; Chen, H.; Aleksandrov, A.; Orlando, T. *J. Phys. Chem. B* in prep.

(104) Adam, T.; Streibel, T.; Mitschke, S.; Muehlberger, F.; Baker, R. R.; Zimmermann, R. *J. Anal. Appl. Pyrolysis* **2005**, *74*, 454-464.

(105) Becker, C. H.; Jusinski, L. E.; Moro, L. *Int. J. Mass Spectrom. Ion Processes* **1990**, *95*, R1-R4.

(106) Cuiffi, J. D.; Hayes, D. J.; Fonash, S. J.; Brown, K. N.; Jones, A. D. *Anal. Chem.* **2001**, *73*, 1292-1295.

(107) Duan, H. L.; Zaharias, G. A.; Bent, S. F. *Appl. Phys. Lett.* **2001**, *78*, 1784-1786.

(108) Edirisinghe, P. D.; Lateef, S. S.; Crot, C. A.; Hanley, L.; Pellin, M. J.; Calaway, W. F.; Moore, J. F. *Anal. Chem.* **2004**, *76*, 4267-4270.

(109) Koester, C.; Lindner, J.; Kinsel, G. R.; Grotemeyer, J. *Lect. Notes Phys.* **1991**, *389*, 139-148.

(110) Matsuda, Y.; Bernstein, E. R. *J. Phys. Chem. A* **2005**, *109*, 314-319.

(111) Cao, L.; Muehlberger, F.; Adam, T.; Streibel, T.; Wang, H. Z.; Kettrup, A.; Zimmermann, R. *Anal. Chem.* **2003**, *75*, 5639-5645.

(112) Kimmel, G. A.; Orlando, T. M. *Phys. Rev. Lett.* **1995**, *75*, 2606-2609.

(113) Haefliger, O. P.; Zenobi, R. *Anal. Chem.* **1998**, *70*, 2660-2665.

(114) Butcher, D. J.; Goeringer, D. E.; Hurst, G. B. *Anal. Chem.* **1999**, *71*, 489-496.

(115) Ayre, C. R.; Moro, L.; Becker, C. H. *Anal. Chem.* **1994**, *66*, 1610-1619.

(116) Terhorst, M.; Kampwerth, G.; Niehuis, E.; Benninghoven, A. *J. Vac. Sci. Technol., A* **1992**, *10*, 3210-3215.

(117) Zhang, Y.; Frankenberger, W. T. *Sci. Total Environ.* **2000**, *257*, 111-119.

(118) Engelke, F.; Hahn, J. H.; Henke, W.; Zare, R. N. *Anal. Chem.* **1987**, *59*, 909-912.

(119) Tembreull, R.; Lubman, D. M. *Anal. Chem.* **1987**, *59*, 1003-1006.

(120) Pallix, J. B.; Schuhle, U.; Becker, C. H.; Huestis, D. L. *Anal. Chem.* **1989**, *61*, 805-811.

(121) Ens, W.; Mao, Y.; Mayer, F.; Standing, K. G. *Rapid Commun. Mass Spectrom.* **1991**, *5*, 117-123.

(122) Sundqvist, B. U. R. *Int. J. Mass Spectrom. Ion Processes* **1992**, *118*, 265-287.

(123) Oektem, B.; Tolocka, M. P.; Johnston, M. V. *Anal. Chem.* **2004**, *76*, 253-261.

(124) Goenaga-Infante, H.; Sargent, M. *Spectrosc. Europ.* **2005**, *17*, 6,8,10,12,14.

(125) Lawrence, T. S.; Davis, M. A.; Maybaum, J.; Stetson, P. L.; Ensminger, W. D. *Radiat. Res.* **1990**, *123*, 192-198.

(126) Aaseth, J.; Haugen, M.; Forre, O. *Analyst* **1998**, *123*, 3-6.

(127) King, B. V.; Pellin, M. J.; Moore, J. F.; Veryovkin, I. V.; Savina, M. R.; Tripa, C. E. *Appl. Surf. Sci.* **2003**, *203*, 244-247.

(128) Klein, E. A.; Lippman, S. M.; Thompson, I. M.; Goodman, P. J.; Albanes, D.; Taylor, P. R.; Coltman, C. *World J. Urol.* **2003**, *21*, 21-27.

(129) De Silva, V.; Woznichak, M. M.; Burns, K. L.; Grant, K. B.; May, S. W. *J. Am. Chem. Soc.* **2004**, *126*, 2409-2413.

(130) Gammelgaard, B.; Jessen, K. D.; Kristensen, F. H.; Jons, O. *Anal. Chim. Acta* **2000**, *404*, 47-54.

(131) Shibata, Y.; Morita, M.; Fuwa, K. *Adv. Biophys.* **1992**, *28*, 31-80.

(132) Riederer, D. E.; Chatterjee, R.; Rosencrance, S. W.; Postawa, Z.; Dunbar, T. D.; Allara, D. L.; Winograd, N. *J. Am. Chem. Soc.* **1997**, *119*, 8089-8094.

(133) Cao, T. H.; Cooney, R. A.; Woznichak, M. M.; May, S. W.; Browner, R. F. *Anal. Chem.* **2001**, *73*, 2898-2902.

(134) Wucher, A.; Heinrich, R.; Braun, R. M.; Willey, K. F.; Winograd, N. *Rapid Commun. Mass Spectrom.* **1998**, *12*, 1241-1245.

(135) Bendahl, L.; Gammelgaard, B. *J. Anal. At. Spectrom.* **2004**, *19*, 950-957.

(136) Herring, J.; Aleksandrov, A.; Orlando Thomas, M. *Phys. Rev. Lett.* **2004**, *92*, 187602-187605.

(137) Orlando, T. M.; Kimmel, G. A.; Simpson, W. C. *Nucl. Instrum. Methods Phys. Res., Sect. B* **1999**, *157*, 183-190.

(138) Vestal, M. L.; Campbell, J. M. In *Biol. Mass Spectrom.*, 2005; Vol. 402, pp 79-108.

(139) Spengler, B.; Karas, M.; Bahr, U.; Hillenkamp, F. *J. Phys. Chem.* **1987**, *91*, 6502-6506.

(140) Preisler, J.; Yeung, E. S. *Anal. Chem.* **1997**, *69*, 4390-4398.

(141) Birringer, M.; Pilawa, S.; Flohe, L. *Nat. Prod. Rep.* **2002**, *19*, 693-718.

(142) Munoz Olivas, R.; Quevauviller, P.; Donard, O. F. X. *Fresenius. J. Anal. Chem.* **1998**, *360*, 512-519.

(143) Hope, H. *Acta Crystallographica* **1966**, *20*, 610-615.

(144) Zenobi, R.; Knochenmuss, R. *Mass Spectrom. Rev.* **1999**, *17*, 337-366.

(145) Petrik, N. G.; Knutsen, K.; Paparazzo, E.; Lea, S.; Camaioni, D. M.; Orlando, T. M. *J. Phys. Chem. B* **2000**, *104*, 1563-1571.

(146) Nemes, P.; Schlosser, G.; Vekey, K. *J. Mass Spectrom.* **2005**, *40*, 43-49.

(147) Peurrung, A. J.; Cowin, J. P.; Teeter, G.; Barlow, S. E.; Orlando, T. M. *J. Appl. Phys.* **1995**, *78*, 481-488.

(148) Herring-Captain, J.; Grieves, G. A.; Alexandrov, A.; Sieger, M. T.; Chen, H.; Orlando, T. M. *Phys. Rev. B* **2005**, *72*, 035431/035431-035431/035410.

(149) Hoang, T. T.; Chen, Y. F.; May, S. W.; Browner, R. F. *Anal. Chem.* **2004**, *76*, 2062-2070.

(150) Gammelgaard, B.; Bendahl, L.; Wessel Jacobsen, N.; Stuerup, S. *J. Anal. At. Spectrom.* **2005**, *20*, 889-893.

(151) Zlatkis, A.; Bertsch, W.; Lichtenstein, H. A.; Tishbee, A.; Shunbo, F.; Liebich, H. M.; Coscia, A. M.; Fleischer, N. *Anal. Chem.* **1973**, *45*, 763-767.

(152) Madubunyi, L. C.; Hassanali, A.; Ouma, W.; Nyarango, D.; Kabii, J. *J. Chem. Ecol.* **1996**, *22*, 1187-1199.

(153) Hunt, D. F.; Giordani, A. B.; Rhodes, G.; Herold, D. A. *Clin. Chem.* **1982**, *28*, 2387-2392.

(154) Yi, D.; Ingelse, B. A.; Duncan, M. W.; Smythe, G. A. *J. Am. Soc. Mass Spectrom.* **2000**, *11*, 578-586.

(155) Mottaleb, M. A.; Brumley, W. C.; Sovocool, G. W. *Int. J. Environ. Anal. Chem.* **2004**, *84*, 1069-1078.

(156) Zamenhof, S.; De Giovanni, R.; Greer, S. *Nature* **1958**, *181*, 827-829.

(157) Ahnstrom, G. *Mutat. Res.* **1974**, *26*, 99-103.

(158) Van der Schans, G. P.; Van Loon, A. A. W. M.; Groenendijk, R. H.; Baan, R. A. *Int. J. Radiat. Biol.* **1989**, *55*, 747-760.

(159) Sognier, M. A.; Eberle, R. L.; Zhang, Y.; Belli, J. A. *Radiat. Res.* **1991**, *126*, 80-87.

(160) Ahmed, F. E. *Anal. Biochem.* **1993**, *210*, 253-257.

(161) Beach, C.; Fuciarelli, A. F.; Zimbrick, J. D. *Radiat. Res.* **1994**, *137*, 385-393.

(162) Banath, J. P.; Wallace, S. S.; Thompson, J.; Olive, P. L. *Radiat. Res.* **1999**, *151*, 550-558.

(163) Chen, H.-Y.; Chao, I. *ChemPhysChem* **2004**, *5*, 1855-1863.

(164) deLara, C. M.; Jenner, T. L.; Stewart, K. M.; Townsend, K. M. S.; Marsden, S. J.; O'Neill, P. *Radiat. Res.* **1995**, *144*, 43-49.

(165) Purkayastha, S.; Bernhard, W. A. *J. Phys. Chem. B* **2004**, *108*, 18377-18382.

(166) Michael, B. D.; O'Neill, P. *Science* **2000**, *287*, 1603-1604.

(167) Sonntag, C. V. *The Chemical Basis for Radiation Biology*, 1987.

(168) *International Commision on Radiation Units and Measurements, IRCU Report 31*, 1979.

(169) Cobut, V.; Frongillo, Y.; Patau, J. P.; Goulet, T.; Fraser, M. J.; Jay-Gerin, J. P. *Radiat. Phys. Chem.* **1998**, *51*, 229-243.

(170) Boudaiffa, B.; Cloutier, P.; Hunting, D.; Huels, M. A.; Sanche, L. *Science* **2000**, *287*, 1658-1660.

(171) Huels, M. A.; Boudaiffa, B.; Cloutier, P.; Hunting, D.; Sanche, L. *J. Am. Chem. Soc.* **2003**, *125*, 4467-4477.

(172) Sieger, M. T.; Simpson, W. C.; Orlando, T. M. *Nature* **1998**, *394*, 554-556.

(173) Abdoul-Carime, H.; Cloutier, P.; Sanche, L. *Radiat. Res.* **2001**, *155*, 625-633.

(174) Antic, D.; Parenteau, L.; Lepage, M.; Sanche, L. *J. Phys. Chem. B* **1999**, *103*, 6611-6619.

(175) Zheng, Y.; Cloutier, P.; Hunting, D. J.; Sanche, L.; Wagner, J. R. *J. Am. Chem. Soc.* **2005**, *127*, 16592-16598.

(176) Pan, X.; Cloutier, P.; Hunting, D.; Sanche, L. *Phys. Rev. Lett.* **2003**, *90*, 208101-208104.

(177) Tao, N. J.; Lindsay, S. M. *Biopolymers* **1989**, *28*, 1019-1030.

(178) Swarts, S. G.; Sevilla, M. D.; Becker, D.; Tokar, C. J.; Wheeler, K. T. *Radiat. Res.* **1992**, *129*, 333-344.

(179) Sanche, L. *Eur. Phys. J. D* **2005**, *35*, 367-390.

(180) Meesungnoen, J.; Jay-Gerin, J. P.; Filali-Mouhim, A.; Mankhetkorn, S. *Radiat. Res.* **2002**, *158*, 657-660.

(181) Chen, B. I., I. ; Klein, M. L; Parrinello M. *Phys. Rev. Lett.* **2003**, 215503.

(182) Mann, M.; Hendrickson, R. C.; Pandey, A. *Annu. Rev. Biochem.* **2001**, *70*, 437-473.

(183) Zheng, Y.; Dextraze, M.-E.; Cloutier, P.; Hunting, D. J.; Sanche, L. *J. Chem. Phys.* **2006**, *124*, 024705-024714.

(184) Kimmel, G. A.; Orlando, T. M. *Phys. Rev. Lett.* **1996**, *77*, 3983-3986.

(185) Sieger, M. T.; Simpson, W. C.; Orlando, T. M. *Phys. Rev. B* **1997**, *56*, 4925-4937.